A HOLOGRAPHIC SYSTEM THAT RECORDS FRONT-SURFACE DETAIL OF A SCENE MOVING AT HIGH VELOCITY

by

Robert L. Kurtz

Thesis submitted to the Graduate Faculty of the

Virginia Polytechnic Institute and State University

in partial fulfillment of the requirements for the degree of

DOCTOR OF PHILOSOPHY

in

Physics

APPROVED: _____

Chairman, Dr. H. Y. Loh

_____ _____

Dr. J. A. Jacobs Dr. R. F. Tipsword

_____ _____

Dr. T. E. Gilmer Dr. R. L. Bowden

June 1971

Blacksburg, Virginia

ACKNOWLEDGMENTS

The author would like to express his appreciation to his advisor, Dr. H. Y. Loh, of the Virginia Polytechnic Institute and State University for his sustained interest, guidance, and cooperation. Appreciation is also expressed to Mr. John R. Williams of the Space Sciences Laboratory, George C. Marshall Space Flight Center, National Aeronautics and Space Administration, Huntsville, Alabama, for his interest and helpful discussions of the project and to Mr. Geoffrey Hintze and Mr. Wesley Darbro for their mathematical assistance, and computer programs.

The author wishes to thank Mrs. Anita Underwood for her contributions in the typing of this manuscript.

The author offers an expression of gratitude to his wife, Ann, and his daughters, Lee Ann and Nancy, for their cooperation and understanding during the preparation of this manuscript.

TABLE OF CONTENTS

TABLE OF CONTENTS (Concluded)

LIST OF TABLES

LIST OF ILLUSTRATIONS

LIST OF ILLUSTRATIONS (Concluded)

LIST OF SYMBOLS

a	Semimajor axis of ellipse
$a(x, y)$	Amplitude function of reference field
b	Semiminor axis of ellipse
$b(x, y)$	Amplitude function of scene field
d	Separation distance from foci to origin of ellipse
E_r	Reference field
E_s	Scene field
E_t	Transmitted field
$\mathcal{E}$	Exposure
I	Intensity or irradiance $\equiv m E^2$
m	A constant $\equiv \frac{1}{2Z}$
$\overline{S}_i$	Average measurement of length of image resolved
$\overline{S}_{0_i}$	Relative average length = $\frac{\overline{S}_i \text{ (motion case)}}{\overline{S}_i \text{ (stationary case)}}$
T	Transmission Coefficient
T_a	Transmission amplitude coefficient
v	Magnitude of velocity
$\vec{V}$	Velocity vector
Z	Impedance $= \sqrt{\frac{\mu}{\epsilon}}$
α	Phase function of reference field
β	Phase function of scene field

LIST OF SYMBOLS (Concluded)

γ	Contrast of photographic film or plate
ΔL	Total change in optical pathlength of front illumination beam
τ	Time

CHAPTER I. INTRODUCTION

In 1947 Dr. Dennis Gabor of the University of London coined the word "hologram," which means entire word or whole picture. Holography is a two-step imaging process that involves the recording of an interference pattern usually between two beams from a common origin and the subsequent use of this recorded pattern to construct an image of the original object.

From the physical arrangement of the separated light beams, (the modulated signal beam and the unmodulated reference beam), one is able to record not only the amplitude but also the phase of the light beam as well. The medium normally used for the recording is conventional photographic emulsions. Herein lies the primary difference between holography and conventional photography — the ability to record phase of the light as well as amplitude while using essentially the same type of square law detector.

The light intensity recorded by the photographic film or spectroscopic plate is a function of the amplitude of the wave from the object or signal beam and the amplitude of the unmodulated or reference beam. Since we have interference between these two waves at the film plane, the two waves interact here and provide a maximum intensity where the crests of both waves meet and a minimum where the crest of one meets the trough of the other. This interaction of the two light waves forms lines of exposure on the photographic emulsion. As each point on the object contributes its share of lines or fringes, all of the optical information about the object is stored on the plate.

Remembering that the fringes dictate the position of each object point as it relates to the unmodulated reference beam, illumination of the processed film with the reference beam alone will reconstruct the original signal beam and an image of the original object will appear in the same position as the original object; it will be quite authentic but slightly reduced in brightness. Since forming the hologram record is essentially a two-beam interference experiment, it is important that the phase difference between the two beams remain essentially constant during the exposure. A change in the phase difference at the recording plane of $\lambda/2$ (λ is the wavelength of illumination being used) will shift the fringe position by one-half of one fringe spacing. If this shift occurs during the exposure, the recorded fringe modulation will fall to essentially zero and possibly no hologram will be recorded. Such phase shifts can be caused by numerous situations, for example, vibration of the optical components, creep or vibration of the emulsion of the film plane, or motion of the object under test. However, it is suggested that object motion with any time dependence and any magnitude will be recorded by the hologram if the location and orientation of the holographic system are properly chosen.

It is the purpose of this paper to discuss one such proper location. It is a new holographic technique that offers promise for the holographic recording of front-surface detail from an object traveling in an essentially straight line with constant velocity of very high magnitude. A simple analysis, given in Chapter IV, shows that this technique is capable of recording front-surface

detail from a moving scene traveling at very high velocities, depending upon the pulse duration of the laser source, its power output, and the tolerance of the optical path difference.

This subject of motion holography has covered scenes from microscopic particles and aerosol sprays to seeded gas flow and bullet-type projectiles. The bullet or macroscopic projectiles have received considerable attention recently. A reasonable search of the literature by the author shows that the highest target velocity for which a hologram was successfully recorded to date was 375 m/sec (15). No report of the resolution of front-surface detail from targets at high speeds was found, however. According to the calculations made in Chapter IV, section (1), the technique offered there will allow resolution of front-surface detail from a moving scene having a velocity of 9×10^5 cm/sec using a 25-nsec pulse-length ruby laser and still not cause the phase shift of the signal beam to be greater than $\lambda/8$. As will be shown later, this small phase shift cannot be accounted for on the basis of the pulse length or exposure time alone, i. e., the resultant shift is also system dependent.

This paper defines a variety of different types of holography, first and then derives detailed theory of one type of holography in particular — Fresnel sideband holography — since this is the type of holography utilized in the experimental testing of the present technique. This paper also shows that holographic recording of the resolution of front-surface detail for scenes moving at high velocities is possible; it presents experimental evidence of

this for a given total scene travel, Δx, since the primary parameter is just the total motion, Δx, that the scene undergoes during the exposure. The appendix gives the role of photography in the holographic process.

Furthermore, since the effect of scene motion on a hologram and its reconstructed image is the summation of the effects resulting from each point of the scene contributing individually, we will consider such motion induced effects of a single point of the scene; then one may obtain the complete field by the principle of superposition.

CHAPTER II. LITERATURE REVIEW

An extensive computerized literature search of the general area of holography was performed that yielded more than 400 reference sources for holography. Many of these sources are on specialized applications and varied types of holography. Those pertinent to this application have been included in the Reference and Bibliography sections.

In this literature review, emphasis will be given to those reference sources dealing primarily with motion holography (either motion of the scene or of the components). It is worthy of note that no reference has been found where the resolution of front-surface detail was experimentally obtained from a moving scene at velocities higher than a few centimeters per second. However, as indicated in the introduction, a number of researchers agree that this type of resolution can theoretically be obtained if proper system orientation is found for a given type of motion.

It is the first purpose of this review to present the four basic types of holography from which additional variations can be, and have been, made and the essential requirements of each. They are as follows:

1. The Gabor in-line type of holography is shown in Figure 1a. A divergent beam from source S is incident on an object, or scene, O on the optical axis and also passes around the object on all sides to form the unmodulated reference beam for this arrangement. Obviously the first limitation of this system is on the object size. The next limitation is on the

resolving power since the reference waves and the scattered rays cross at a small angle to give coarse fringes (appendix). The next and perhaps primary limitation is caused by the fact that the object and source both fall on the optic axis and, hence, the term "in line"; therefore, in the reconstruction (Fig. 1b) when a real image R and a virtual image V are produced, they are essentially in a straight line. For this reason it is almost impossible to separate them except by complex procedures. The advantages of this arrangement are the following: Because of the low resolution requirement of the system, coarse-grained and therefore fast film can be used. Furthermore, this system shows greater tolerance to a lack of mechanical stability.

2. Direct-transmission holography or dark-field holography is quite applicable to the aerodynamic study of the behavior of fluid or gas flow fields. An example of this type of holographic arrangement is shown in Figure 2, which utilizes a modified Mach-Zender interferometer (28).

3. Diffuse-transmission holography is very similar to the direct-transmission method except that now a diffusing screen is placed in the signal beam upstream of the object (see Fig. 3). If direct transmission is called dark-field holography, diffuse transmission is called light-field holography. This is so because this type of holography recreates the diffuse screen, which acts as a luminous background against which the object appears in silhouette. Viewing can thus be done with the unaided eye instead of with an eyepiece or screen as is necessary for the first two methods. The main advantage of this method is to avoid the high sensitivity to disturbance by

dust particles inherent in the previous methods (28). This method is most adaptable to the holography of moving targets and allows a black silhouette of the traveling target against a lighted diffuser background. This method has been used almost unanimously for motion holography studies (2), (5), (10), (19), (20), (23), (24), (28), (30), (31).

4. Reflection holography has many of the characteristics of diffuse-transmission holography with the advantage that the object is illuminated from the front or from one side, rather than from behind, and consequently provides resolution of front-surface detail. An arrangement for both producing and reconstructing the reflection-type hologram is shown in Figure 4. The requirements of this system for mechanical stability are quite severe. The resolution requirement is strictly a function of the angle between the signal and reference beam at the holographic plate (see appendix).

With the exception of the Gabor type, all the other arrangements may be grouped into the Fresnel sideband holographic category. There is a category called the Fourier Transform Holography (7), (12), (14), (21), (24), (25), (28), whose component arrangement is given in Figure 5. This type provides a means of storing the information in an assembly of straight-line fringes lying at different angles across the plate and having different spacings. This has such applications as information storage and pattern recognition. The present system described in Chapter IV is basically a Fresnel sideband form of holography and utilizes type 4 in a modified version.

Many experimenters have produced holograms of high-speed phenomena using either type 3, the diffuse-transmission arrangement where the scene appears in silhouette against some lighted background, or type 2, the direct-transmission or dark-field holography, (2), (3), (4), (5), (10), (19), (20), (23), (24), (28), (30), (31). Some success has been accomplished using the far-field or Fraunhofer-type holography, (6) whereas some experimenters have applied the Fourier transform holography to velocity determination of scenes (7). Although the preceding references demonstrate the ability to holograph motion quite successfully,[1] none to date have achieved front-surface resolution from these moving scenes. Some measure of success has been shown in obtaining front-surface resolution from moving targets but only at extremely low velocities or at apparent velocities, i.e., animation (15), (23). The ability to holographically achieve resolution of front-surface detail from fast-moving scenes has been demonstrated in Chapter IV of this paper; it is the final purpose of this paper to produce a means of demonstrating this feat experimentally.

---

[1]See also References 1, 9, 11, 13, 16, 17, 22, and 27.

CHAPTER III. THEORY OF HOLOGRAPHY

(1) A General Description of Fresnel Sideband Holography for a Stationary Scene

Let the plane of the hologram lie in the xy plane of the coordinate system as given in Figure 6. The amplitude in this plane can be described by the radiation from the scene,

$$E_s = b(x,y) \exp \{i[\beta(x,y) - \omega t]\} \quad , \tag{3.1}$$

and by that of the reference beam,

$$E_r = a(x,y) \exp \{i[\alpha(x,y) - \omega t]\} \quad . \tag{3.2}$$

We here consider the amplitude functions $b(x,y)$ and $a(x,y)$ and the phase functions $\alpha(x,y)$ and $\beta(x,y)$ to be real functions. This, then, is a scalar treatment that does not take account of polarization effects. However, it is always possible to split the scene wave into two components, one with the electric vector in the plane containing the electric vector and the direction of propagation of the reference ray and the other with the electric vector perpendicular to this plane. Only the parallel component contributes to the interference pattern on the hologram and hence to the reconstruction. Furthermore, $a(x,y)$ is a slowly variable function (it is a constant for a plane reference wave, but for a spherical wave it varies as the reciprocal of distance from the reference source to different points on the hologram). The reference wave may also be a distorted spherical wave, as formed by a lens

with geometrical aberrations. The amplitude function of the scene (object) wave $b(x,y)$, is materially smaller than $a(x,y)$, since the ratio of intensity of the reference beam to that of the scene beam is usually required to be 10 to 1. The exposure on the hologram plate is given by the product of intensity at the plate times the time of exposure, or pulse length.

In general, from the definition of Poynting's vector in the rationalized mks system

$$\vec{S} \equiv \vec{E} \times \vec{H} \quad ,$$

one can see that its time average is

$$\langle \vec{S} \rangle = \langle \vec{E} \times \vec{H} \rangle = 1/2 \sqrt{\frac{\epsilon}{\mu}}\ EE^* \hat{n} \tag{3.3}$$

where E^* is the complex conjugate of E and $\hat{n}$ is a unit vector, mutually perpendicular to $\vec{E}$ and $\vec{H}$. Since the intensity, i.e., irradiance, of electromagnetic radiation is the energy crossing normal to a unit area per unit time,

$$I = \langle S \rangle = 1/2 \sqrt{\frac{\epsilon}{\mu}}\ EE^* = 1/2Z\ EE^* \equiv m\ EE^* \tag{3.4}$$

where $Z = \sqrt{\frac{\mu}{\epsilon}}$ is the impedance of the medium and m is a constant for simplification. For a hologram

$$I = m\ EE^* = m(E_r + E_s)\ (E_r^* + E_s^*) \tag{3.5}$$

and from (3.1) and (3.2)

$$I = m\Big[\, b(x,y)\; e^{i[\beta(x,y) - \omega t]} + a(x,y)\; e^{i[\alpha(x,y) - \omega t]} \,\Big]$$
$$\cdot \Big[b(x,y)\; e^{-i[\beta(x,y) - \omega t]} + a(x,y)\; e^{-i[\alpha(x,y) - \omega t]} \Big] \qquad (3.6)$$

or

$$I = m\Big[b^2(x,y) + a^2(x,y) + a(x,y)\, b(x,y) \left(e^{i[\beta(x,y) - \alpha(x,y)]} + e^{-i[\beta(x,y) - \alpha(x,y)]} \right) \Big] \qquad (3.7)$$

where equation (3.7) for the intensity recorded at the plate is generally called the Recording Equation.

Now substitution of equation (3.7) into the equation for the exposure produces

$$\mathcal{E} = \int_0^\tau I\, dt = m \int_0^\tau b^2(x,y) + a^2(x,y) + 2a(xy)\, b(xy)\, \cos(\beta - \alpha)\, dt$$

or

$$It = m\tau \Big[b^2(x,y) + a^2(x,y) + 2a(xy)\, b(xy)\, \cos(\beta - \alpha) \Big] \qquad (3.8)$$

but τ is just some constant exposure time, τ_0, for a given hologram; therefore, the exposure may be simply written as

$$It = m\tau_0 \Big[a^2 + b^2 + 2ab \cos(\beta - \alpha) \Big]$$

where a, b, α, and β are coordinate dependent, or

$$It = m\tau_0 \Big[a^2 + b^2 + ab \left(e^{i(\beta - \alpha)} + e^{-i(\beta - \alpha)} \right) \Big] \quad . \qquad (3.9)$$

It is well known in photography (32) that the Heurter-Driffield characteristic curve, as plotted on a semilog plate (see appendix, Fig. A-3), is linear for most of its length and can be represented, in this linear region, by the equation

$$D = \gamma \log \frac{I\tau}{g}$$

where D is the density of the image on the film, γ is the contrast, and g is the inertia of the emulsion. Since

$$D \equiv -\log T$$

$$T = g^{\gamma}(I\tau)^{-\gamma} \tag{3.10}$$

where T is the transmission coefficient. The amplitude transmission coefficient, T_a, is the square root of the transmission; consequently,

$$T_a = g^{\gamma/2}(I\tau_0)^{-\gamma/2} = k\, I^{-\gamma/2} \tag{3.11}$$

where $k \equiv (g/\tau_0)^{\gamma/2}$ is a constant and

$$T_a = k\left[a^2 + b^2 + ab\left(e^{i(\beta-\alpha)} + e^{-i(\beta-\alpha)}\right)\right]^{-\gamma/2} \tag{3.12}$$

factoring

$$T_a = (k)\,(a^2 + b^2)^{-\gamma/2}\left[1 + \frac{a\,b}{a^2+b^2}\left(e^{i(\beta-\alpha)} + e^{-i(\beta-\alpha)}\right)\right]^{-\gamma/2}. \tag{3.13}$$

We may use binomial expansion to get

$$T_a = k(a^2 + b^2)^{-\gamma/2}\left[1 - \frac{\gamma}{2}\,\frac{a\,b}{a^2+b^2}\left(e^{i(\beta-\alpha)} + e^{-i(\beta-\alpha)}\right) + \text{higher-order terms}\right]. \tag{3.14}$$

However, by careful development of the exposed plate, one obtains a positive transparency with an overall gamma of $(\gamma = -2)$, and then we have

$$T_a = k(a^2 + b^2)\left[1 + \frac{a\,b}{a^2+b^2}\left(e^{i(\beta-\alpha)} + e^{-i(\beta-\alpha)}\right)\right] \tag{3.15}$$

and the higher-order terms are omitted because they are negligibly small compared to 1.

Consider the usual case where the reference beam during reconstruction is essentially identical with that during recording. We let this reference wave be incident on the developed hologram. Just beyond the hologram the wave amplitude is then

$$E_t = T_a\, E_r \quad . \tag{3.16}$$

Then from equations (3.2) and (3.15) we have

$$E_t = \left[ka(a^2 + b^2)\right]\left[e^{i(\alpha-\omega t)} + \frac{a\,b}{a^2+b^2}\left(e^{i(\beta-\omega t)} + e^{-i(\beta-2\alpha+\omega t)}\right)\right] \quad . \tag{3.17}$$

The first term,

$$ka(a^2 + b^2)\,e^{i(\alpha-\omega t)} \quad , \tag{3.18}$$

is then simply the reference beam attenuated by a term proportional to $(a^2 + b^2)$. Therefore, the first term is

$$k(a^2 + b^2)\; E_r \tag{3.19a}$$

The second term

$$\left[ka(a^2 + b^2)\right]\left[\frac{a\,b}{a^2+b^2}\, e^{i(\beta-\omega t)}\right]$$

becomes

$$ka^2\left(b\, e^{i(\beta-\omega t)}\right) = k a^2 E_s \qquad (3.19b)$$

which corresponds to the original object wave, equation 3.1 multiplied by the same shading factor as for the reference beam. We may infer from the form of this second term than on viewing through the hologram, illuminated by the reference beam, we should see this virtual image of the object in the precise position previously occupied by the object with reference to the original position of the hologram. If the hologram is placed back in its same position after reconstruction, the image of the object will be precisely superimposed on the actual object. The brightness of the image, however, will be slightly reduced.

The third term,

$$k\, a^2\, b\, e^{-i(\beta-2\alpha+\omega t)} = k\, a^2\, b\, e^{i2(\alpha-\beta)+i(\beta-\omega t)} \quad ,$$

becomes

$$k\, a^2\, e^{i2(\alpha-\beta)}\, E_s \quad ; \qquad (3.19c)$$

and corresponds to the real image of the object and is located on the opposite side of the hologram plate from the virtual image. This real image is not aberration-free and is therefore termed "pseudoscopic."

(2) The Effect of Linear Scene Motion During the Hologram Exposure

The effect of scene motion during the exposure of a hologram is a spatial modulation of the recorded fringe contrast. This in turn causes a spatial amplitude modulation of the reconstructed wavefront that blurs the reconstructed image in the same way that it would blur a conventional photograph having the same exposure time. In addition, this modulation reduces the brightness of even that part of the image that is reconstructed. The amount of object motion that can be successfully tolerated during the hologram exposure is certainly dependent on the geometry of the holographic configuration with respect to the velocity vector of the motion. One such chosen geometry is discussed in detail in Chapter IV.

We will present two different theoretical approaches to the time-dependent theory of motion holography. We closely follow the presently existing methods presented by Dr. Don B. Neumann (25). Both approaches serve a purpose. The first uses a coordinate system with origin at the scene point of interest. This is a vector approach and allows a more intuitive feeling for the physics of the problem. It is primarily valid only for those cases where the allowed motion is small compared with the distance from the scene to the hologram. This particular approach is applied to the present system under investigation in Chapter IV. The second approach uses a coordinate system with the origin at the hologram. It is the most general derivation and if a sufficient number of terms are taken in the infinite series

that occur, it will cover all geometries. It suffers, however, from the mathematical complexity that results from these expansions.

(a) Scene-Oriented Coordinates

Following Neumann we assume some basic holographic configuration (Fig. 7).

The radiation from the laser is split into two beams. As usual, we consider these to be the reference beam and the signal beam. Let the point R of Figure 7 serve as the reference position for the system and S be some point of the scene. Light scattered from this point S is made incident at the point P of the hologram, where it now interferes with light from the reference point.

Let the field at point P be given by

$$\vec{E}(P) = \vec{E}_r(P) + \vec{E}_s(P)$$

or

$$E(P) = E_r(P)\, e^{i[\omega t - kr(P)]} + E_s(P)\, e^{i[\omega t - ks(P)]} \qquad (3.20)$$

where $\vec{E}_r(P)$ is that contribution from the reference point and is considered to be plane polarized, $\vec{E}_s(P)$ is that contribution at P due to the scene point S and is that component of the scene field parallel to the reference polarization, and r and s represent the corresponding pathlengths from the laser to the point P.

Now the intensity is given by

$$I = m|E|^2 \quad .$$

Therefore,

$$I = m\left[E_r^2 + E_s^2 + 2E_rE_s \cos k(r-s)\right] \quad . \tag{3.21}$$

If we allow the point S to move with some velocity, then s becomes a function of time. But we consider that the field amplitude does not change appreciably over the time, τ, of the exposure. Then the interference pattern remains approximately constant except for the motion of the fringes.

Then, as before, we can write the exposure as

$$\mathcal{E}(P) = m\int_{-\tau/2}^{\tau/2}\left[E_r^2 + E_s^2 + 2E_rE_s \cos k(s(t)-r)\right]dt \quad ,$$

and

$$\mathcal{E}(P) = m\tau\left[E_r^2 + E_s^2 + \frac{2E_rE_s}{\tau}\int_{-\tau/2}^{\tau/2}\cos k(s(t)-r)\,dt\right] \quad .$$

Let

$$K_C = E_r^2 + E_s^2$$

$$\mathcal{E}(P) = m\tau\left\{K_C + \frac{2E_rE_s}{\tau}\int_{-\tau/2}^{\tau/2}\cos k[s(t)-r]dt\right\} \quad . \tag{3.22}$$

In order to proceed we must state the time dependence of s. In general, $s = s_0 + f(t)$ where $f(t)$ may be any function of time where the midpoint of the exposure is at $\tau = 0$.

In particular, if we assume that s varies linearly with time, we have

$$s = s_0 + vt \quad ;$$

then equation (3.22) becomes

$$\mathcal{E}(P) = m\tau \left\{ K_C + \frac{E_r E_s}{\tau/2} \int_{-\tau/2}^{\tau/2} \cos\left[kvt + k(s_0 - r)\right] dt \right\} \quad . \tag{3.23}$$

Let $\Phi = k(s_o - r)$ be the time invariant portion; then

$$\mathcal{E}(P) = m\tau \left[K_C + \frac{E_r E_s}{\tau/2} \int_{-\tau/2}^{\tau/2} \cos\,(kvt + \Phi)\, dt \right] \tag{3.24}$$

becomes after integration:

$$\mathcal{E}(P) = m\tau \left(K_C + E_r E_s \, \frac{\sin kv\,\tau/2}{kv\,\tau/2} \cos\Phi \right) \quad . \tag{3.25}$$

Then, since $\frac{\sin x}{x} = \operatorname{sinc} x$, we obtain for the exposure

$$\mathcal{E}(P) = m\tau \left[K_C + E_r E_s \operatorname{sinc}\,(kv\,\tau/2) \cos\Phi \right] \quad . \tag{3.26}$$

In the case that $v = 0$, we have no motion, i.e., the stationary case, and the sinc function becomes unity. This is the most desired case for most holographic experiments, i.e., that the argument of the sinc function be zero.

It is observed that if v is constant over the hologram, the resulting fringe contrast of the exposure will be poor for large values of the sinc argument and the resulting fringe contrast will be zero whenever the argument is $n\pi$ $(n = \pm 1, 2 \ldots)$. Consider, for example, $n = 1$, where the first

zero occurs; then

$$\frac{kv\tau}{2} = \pi \tag{3.27}$$

or

$$v\tau = \lambda \quad . \tag{3.28}$$

Now, since $v\tau$ is the change in the distance s during the exposure, the possibility exists that motions of the scene as small as a wavelength may totally destroy the fringes or result in a poor hologram at best.

Fortunately, v is not the same for all points of the hologram and the fringe contrast is spatially modulated rather than destroyed (26).

This special case of the linear time variation of s has served to demonstrate the sinc function modulation of the recorded fringes. We may now discuss the problem more generally in terms of the geometry of the holographic configuration with respect to the velocity vector of the motion. Consider the diagram in Figure 8, where R is the reference point and, as before, S is the scene point. Let L be a point on some reference phase front from the laser, which will be common to both beams. Let $\hat{a}_k$ be the unit vector along the direction of propagation of the incident laser radiation at the scene point S, $\hat{a}_p$ be a unit vector along the line from scene point S to hologram point P, and $\hat{a}_v$ be a unit vector indicating the velocity of point S.

The reference beam is constant in length and composed of two parts, LR + RP. The front illumination beam or scene beam is composed of the two parts, LS + SP. The rate of change of the path length LS from the laser to the scene point S is given by

$$\vec{V} \cdot \hat{a}_k = v \cos \gamma \quad . \tag{3.29}$$

The rate at which the path length, SP, from the scene point to the hologram point, P, changes is given by

$$\vec{V} \cdot \hat{a}_p = v \cos \delta \quad . \tag{3.30}$$

Therefore, the path length from the laser to the point P through scene point S is increasing at the rate

$$\frac{ds}{dt} = (\vec{V} \cdot \hat{a}_k - \vec{V} \cdot \hat{a}_p) \tag{3.31}$$

and

$$\int_{s_0}^{s} ds = \int_{-\tau/2}^{\tau/2} \vec{V} \cdot (\hat{a}_k - \hat{a}_p)\, dt \tag{3.32}$$

and

$$s = s_0 + \vec{V} \cdot (\hat{a}_k - \hat{a}_p)\tau \quad . \tag{3.33}$$

We recall, however, that, in general,

$$s = s_0 + f(t) \tag{3.34}$$

and in the special case considered previously,

$$s = s_o + vt \quad ; \tag{3.35}$$

therefore,

$$v = \vec{V} \cdot (\hat{a}_k - \hat{a}_p) \quad .$$

We may write the sinc function for this case as

$$\text{sinc}\left[\frac{k\tau v}{2}\,\hat{a}_v \cdot (\hat{a}_k - \hat{a}_p)\right] \tag{3.36}$$

and the exposure at point P for this case becomes,

$$\mathcal{E}(P) = m\tau\left\{K_C + E_r E_s\,\text{sinc}\left[\left(\frac{k\tau v}{2}\right)\hat{a}_v \cdot (\hat{a}_k - \hat{a}_p)\right]\cos\Phi\right\} \quad . \tag{3.37}$$

Looking again at the sinc function of equation (3.36) and performing the indicated scalar products we see that

$$\text{sinc}\left[\frac{k\tau v}{2}\,a_v \cdot (a_k - a_p)\right] = \text{sinc}\left[\left(\frac{k\tau v}{2}\right)(\cos\gamma - \cos\delta)\right] \quad . \tag{3.38}$$

In this form the modifying function allows several facts to be noted by inspection:

1. Except for the case of $\tau v = 0$, i.e., stationary scene, because sinc $0 = 1$, the sinc function has a maximum for only two other conditions:

2. $\hat{a}_k$ parallel to $\hat{a}_p$

3. $\vec{V}$ perpendicular to the vector $(\hat{a}_k - \hat{a}_p)$.

Consider that the vector $\hat{a}_p$ always points toward the hologram plane (whatever its position); then, the condition that $\hat{a}_k$ and $\hat{a}_p$ be parallel can only

be met if $\hat{a}_k$ also points toward the hologram. It is seen that this condition is equivalent to the arrangement for the direct- and diffuse-type holography described earlier. This maximum occurs at the point where the incident laser radiation intersects the hologram plane when projected through the scene point. It is noted that the sinc function is a maximum there for all orientations of the motion vector $\vec{V}$.

The second condition for a maximum, that $(\hat{a}_k - \hat{a}_p)$ always be perpendicular to the motion vector $\vec{V}$, is satisfied for all vectors $(\hat{a}_k - \hat{a}_p)$ lying in a plane perpendicular to $\hat{a}_v$. Since for that condition

$$\vec{V} \cdot (\hat{a}_k - \hat{a}_p) = 0 \quad . \tag{3.39}$$

But

$$\vec{V} \cdot (\hat{a}_k - \hat{a}_p) = v(\cos\gamma - \cos\delta) = 0 \tag{3.40}$$

and this condition is satisfied whenever $\delta = \pm\gamma$. (It should be noted that this condition is precisely satisfied by the system described in Chapter IV, Section 1, of this paper). This condition is met by any vector, $\hat{a}_{p_0}$, making an angle γ with the vector $\hat{a}_v$. The locus of these vectors $\hat{a}_p$ forms a circular cone with half angle equal to γ about the motion vector and contains $\hat{a}_k$ as an element (Fig. 9).

The zeroes of the sinc function, equation (3.38), occur for

$$\text{sinc}\left[\frac{\tau k\vec{V}}{2}\cdot(\hat{a}_k-\hat{a}_p)\right]=\text{sinc}\,n\pi \qquad n=\pm 1,\ 2\ldots \tag{3.41}$$

Therefore, the zeroes occur for

$$\frac{\tau k\vec{V}}{2}\cdot(\hat{a}_k-\hat{a}_p)=n\pi \quad , \tag{3.42}$$

i.e.,

$$\vec{V}\cdot(\hat{a}_k-\hat{a}_p)=\frac{2n\pi}{\tau k} \tag{3.43}$$

or

$$\hat{a}_v\cdot(\hat{a}_k-\hat{a}_p)=\frac{n\lambda}{v\tau} \tag{3.44}$$

and

$$\cos\gamma-\cos\delta_{n\pi}=\frac{n\lambda}{v\tau} \tag{3.45}$$

or

$$\cos\delta_{n\pi}=\cos\gamma-\frac{n\lambda}{v\tau} \quad , \tag{3.46}$$

where $\delta_{n\pi}$ is that angle between vectors $\hat{a}_{p_0}$ and $\hat{a}_v$ that produces a zero value for the sinc function, i.e., that angle where no fringes will be recorded.

From the above and Figure 9, it is then obvious that if a hologram is formed at any point in space, regions of the hologram having constant fringe contrast will form a conic section, since they represent the intersection of

the hologram plane and the conical loci mentioned above. If we allow the vector $\hat{a}_p$ to take on various values δ in the range

$$\gamma \leq \delta \leq \gamma + 2\pi \tag{3.47}$$

for a constant $\hat{a}_k$ with angle γ, we can then construct all possible orientations of $\hat{a}_p$ about the motion vector $\vec{V}$. If for each specific value of δ we allow it to rotate about the velocity vector $\vec{V}$, we then are able to construct all possible conical loci for $\hat{a}_p$. We show the results of this in Figure 10 where we take 3 possible values of γ for $\hat{a}_k$, and all possible values of δ for $\hat{a}_p$, for the specific γ. We plot the values of the argument of the sinc function for $\gamma = 0$, $\pi/4$, and $\pi/2$.

(b) Hologram-Oriented Coordinates

In the development of Section (a) the exposure is given by

$$\mathcal{E}(P) = m\tau \left\{ K_c + \frac{2E_r E_s}{\tau} \int_{-\tau/2}^{\tau/2} \cos k\,[s(t) - r]\, dt \right\} \tag{3.48}$$

As before we now must determine the form of $s(t)$ but now as a function of position on the hologram.

For this development we use a fixed-coordinate system having its origin at the center of the hologram and the Z-axis normal to the plane of the hologram. This approach or development is the most generalized derivation since it may be used for the region near the hologram as well as in the region far from the hologram by simply taking a sufficient number of terms in the

series expansions that are developed. Its primary malady is that these very expansions tend to obscure the physical significance of the various steps.

We call attention to the diagram in Figure 11. Let it be assumed that a hologram is to be formed in the xy plane of Figure 11, the coordinate system with the origin at the center of the hologram. In analogy to the previous development, let

$$s = s' + S''$$

where s' is the distance from the scene point $P(x, y)$ of the hologram and S'' is the distance from the laser source to the scene point S. (This is just the total length of illumination called $LQ + QP$ of the previous development.) Then, as before, the rate at which S'' changes, because of the motion of S, is

$$\frac{d(S'')}{dt} = \vec{V} \cdot \hat{a}_k = v \cos \gamma \quad .$$

The coordinates for the point source may be found from inspection of the previous diagram (Fig. 11), and are given by

$$\begin{aligned} x_s &= r \sin \theta \cos \Psi \ , \\ y_s &= r \sin \theta \sin \Psi \ , \end{aligned} \tag{3.49}$$

and

$$z_s = r \cos \theta \quad .$$

Therefore, the distance, s', from the scene point S to a point $P(x, y)$ of the hologram is

$$s' = \left[(x-x_s)^2 + (y-y_s)^2 + Z_s^2 \right]^{1/2} \quad , \tag{3.50}$$

which becomes

$$s' = r\left(\frac{x^2}{r^2} + \frac{y^2}{r^2} + 1 - \frac{2x}{r} \sin\theta \cos\Psi - \frac{2y}{r} \sin\theta \sin\Psi \right)^{1/2} \quad .$$

Expanding this, we have

$$\begin{aligned} s' = r\Big(& 1 - \frac{x}{r} \sin\theta \cos\Psi - \frac{y}{r} \sin\theta \sin\Psi \Big) \\ & + \frac{x_2}{2r^2} \Big(1 - \sin^2\theta \cos^2\Psi \Big) + \frac{y^2}{2r^2} \Big(1 - \sin^2\theta \sin^2\Psi \Big) \\ & - \frac{xy}{r^2} \sin^2\theta \sin\Psi \cos\Psi + \frac{x^3}{2r^2} \Big(\sin\theta \cos\Psi - \sin^3\theta \cos^3\Psi \Big) \\ & + \frac{x^2 y}{2r^2} \Big(\sin\theta \sin\Psi - \sin^3\theta \sin\Psi \cos^2\Psi \Big) \\ & + \frac{xy^2}{2r^3} \Big(\sin\theta \cos\Psi - \sin^3\theta \sin^2\Psi \cos\Psi \Big) \\ & + \frac{y^3}{2r^2} \Big(\sin\theta \sin\Psi - \sin^3\theta \sin^3\Psi \Big) + (\text{higher-order terms}) \quad . \end{aligned} \tag{3.51}$$

If we assume that x/r and y/r are sufficiently small that only the first-order terms are needed, we obtain

$$s' = r\left(1 - \frac{x}{r} \sin\theta \cos\Psi - \frac{y}{r} \sin\theta \sin\Psi \right) \quad . \tag{3.52}$$

In order to proceed it becomes necessary to make some assumptions and then investigate some specific examples of the three orthogonal components of motion involved.

Following are derivations of the exposures for linear motions of a constant phase laser source, ϕ_s, along each of three orthogonal directions.

For a linear transverse motion (θ), consider the point source, S, to be moving with a constant radius r_0 and in a constant Ψ plane, called Ψ_0, such that

$$\theta = \theta_0 + \dot{\theta}t \quad ;$$

then

$$\sin\theta = \sin(\theta_0 + \dot{\theta}t)$$

and

$$\sin\theta = \sin\theta_0 \cos\dot{\theta}t + \cos\theta_0 \sin\dot{\theta}t \quad .$$

However,

$$\sin\dot{\theta}t = \dot{\theta}t - \frac{(\dot{\theta}t)^3}{6} + \frac{(\dot{\theta}t)^5}{120} - \ldots$$

and

$$\cos\dot{\theta}t = 1 - \frac{(\dot{\theta}t)^2}{2} + \frac{(\dot{\theta}t)^4}{24} - \ldots \quad .$$

If we now assume that $\dot{\theta}t$ is small enough so that only the first term in each series need be used, then we can write

$$\sin\theta = \sin\theta_0 + \dot{\theta}t\cos\theta_0 \quad ;$$

then

$$\sin^2\theta = \sin^2\theta_0 + 2\dot{\theta}t\sin\theta_0\cos\theta_0$$

and

$$\sin^3\theta = \sin^3\theta_0 + 3\,\dot{\theta}t\,\sin^2\theta_0\cos\theta_0 \quad .$$

If we now substitute these conditions into equation (3.51) for the distance s', we obtain

$$\begin{aligned}
s' = r_0\Bigg[& 1 - \frac{x}{r_0}(\sin\theta_0 + \dot{\theta}t\cos\theta_0)\cos\Psi_0 \\
& - \frac{y}{r_0}(\sin\theta_0 + \dot{\theta}t\cos\theta_0)\sin\Psi_0\Bigg] \\
& + \frac{x^2}{2r_0^2}\Big[1 - (\sin^2\theta_0 + 2\,\dot{\theta}t\sin\theta_0\cos\theta_0)\cos^2\Psi_0\Big] \\
& + \frac{y^2}{2r_0^2}\Big[1 - (\sin^2\theta_0 + 2\,\dot{\theta}t\sin\theta_0\cos\theta_0)\sin^2\Psi_0\Big] \\
& - \frac{xy}{r_0^2}\Big[(\sin^2\theta_0 + 2\,\dot{\theta}t\sin\theta_0\cos\theta_0)\sin\Psi_0\cos\Psi_0\Big] \\
& + \frac{x^3}{2r_0^3}\Big[(\sin\theta_0 + \dot{\theta}t\cos\theta_0)\cos\Psi_0 \\
& \qquad - (\sin^3\theta_0 + 3\,\dot{\theta}t\sin^2\theta_0\cos\theta_0)\cos^3\Psi_0\Big] \\
& + \frac{x^2y}{2r_0^3}\Big[(\sin\theta_0 + \dot{\theta}t\cos\theta_0)\sin\Psi_0 \\
& \qquad - (\sin^3\theta_0 + 3\,\theta t\sin^2\theta_0\cos\theta_0)\sin\Psi_0\cos^2\Psi_0\Big] \\
& + \frac{y^3}{2r_0^3}\Big[(\sin\theta_0 + \dot{\theta}t\cos\theta_0)\sin\Psi_0 \\
& \qquad - (\sin^3\theta_0 + 3\,\dot{\theta}t\sin^2\theta_0\cos\theta_0)\sin^3\Psi_0\Big] + (\text{higher-order terms}) \quad .
\end{aligned} \tag{3.53}$$

Again, if we take only the first-order terms, equation (3.53) becomes

$$s' = r_0\left[1 - \frac{x}{r_0}\,(\sin\theta_0 + \dot{\theta}t\cos\theta_0)\cos\Psi_0 - \frac{y}{r_0}\,(\sin\theta_0 + \dot{\theta}_s t\cos\theta_0)\sin\Psi_0\right] ,$$

or

$$s' = r_0 - (x\cos\Psi_0 + y\sin\Psi_0)\sin\theta_0 - \dot{\theta}t\,(x\cos\Psi_0 + y\sin\Psi_0)\cos\theta_0 .$$

Now for simplicity define

$$s_0' \equiv r_0 - (x\cos\Psi_0 + y\sin\Psi_0)\sin\theta_0$$

and we have

$$s' = s_0' - \dot{\theta}t\,(x\cos\Psi_0 + y\sin\Psi_0)\cos\theta_0 . \qquad (3.54)$$

Then the rate of change of phase between S and P due to that motion in the θ direction is

$$\Omega_\theta = k\left(\frac{\partial s'}{\partial t}\right)_\theta = -k\,V_\theta\left[(x\cos\Psi_0 + y\sin\Psi_0)\,\frac{\cos\theta_0}{r}\right] \qquad (3.55)$$

where

$$V_\theta = \dot{\theta}r .$$

Proceeding in a similar fashion, the derivations for small motions in the r and Ψ directions may be obtained.

For linear radial motion (r), assume that the point source S moves with constant angles θ_r and such that Ψ_r

$$r = r_0 + \dot{r}t \quad ;$$

then

$$\frac{1}{r} = \frac{1}{r_0 + \dot{r}t}$$

or

$$\frac{1}{r} = \frac{1}{r_0}\left[1 - \frac{\dot{r}t}{r_0} + \frac{(\dot{r}t)^2}{r_0^2} - \frac{(\dot{r}t)^3}{r_0^3} + \ldots\right] \quad ,$$

and for $\dot{r}t < r_0$

$$\frac{1}{r^2} = \frac{1}{r_0^2}\left[1 - \frac{2\dot{r}t}{r_0} + \frac{3\,\dot{r}^2 t^2}{r_0^2} - \ldots\right] \quad .$$

If the motion $\dot{r}t$ is small compared with r_0, we may again neglect higher-order terms and using the above expressions in equation (3.51), s', becomes

$$\begin{aligned} s' = {} & r_0 + \dot{r}t - x \sin\theta_r \cos\Psi_r - y \sin\theta_r \sin\Psi_r \\ & + \left[\frac{x^2}{2r_0}\left(1 - \sin^2\theta_r \cos^2\Psi_r\right) + \frac{y^2}{2r_0}\left(1 - \sin^2\theta_r \sin^2\Psi_r\right)\right. \\ & \left. - \frac{xy}{r_0}\sin^2\theta_r \sin\Psi_r \cos\Psi_r\right]\left(1 - \frac{\dot{r}t}{r_0}\right) \\ & + \left[\frac{x^3}{2r_0^2}\left(\sin\theta_r \cos\Psi_r - \sin^3\theta_r \cos^3\Psi_r\right)\right. \\ & \left. + \frac{x^2 y}{2r_0^2}\left(\sin\theta_r \sin\Psi_r - \sin^3\theta_r \sin\Psi_r \cos^2\Psi_r\right)\right. \end{aligned}$$

$$+ \frac{xy^2}{2r_0^2} (\sin\theta_r \cos\Psi_r - \sin^3\theta_r \sin^2\Psi_r \cos\Psi_r)$$

$$+ \frac{y^3}{2r_0^2} (\sin\theta_r \sin\Psi_r - \sin^3\theta_r \sin^3\Psi_r) \Big]\left(1 - \frac{2\dot{r}t}{r_0}\right) \quad .$$

Now, as before, taking only the first-order terms, we get

$$s' = r_0 + \dot{r}t - x \sin\theta_r \cos\Psi_r - y \sin\theta_r \sin\Psi_r$$

and considering the direction of k, we obtain the phase rate

$$\Omega_r = -k \left(\frac{\partial s'}{\partial t}\right)_r$$

$$\Omega_r = -k V_r \qquad (3.56)$$

where

$$V_r = \dot{r} \quad .$$

For linear transverse motion (Ψ), the third orthogonal component, we assume that the point source, S, moves with constant radius r_0 and angle θ_0 such that

$$\Psi = \Psi_0 + \dot{\Psi}t \quad ;$$

then

$$\sin\Psi = \sin\Psi_0 \cos\dot{\Psi}t + \cos\Psi_0 \sin\dot{\Psi}t$$

and

$$\cos\Psi = \cos\Psi_0 \cos\dot{\Psi}t - \sin\Psi_0 \sin\dot{\Psi}t \quad ;$$

further

$$\sin \dot{\Psi} t = \dot{\Psi} t - \frac{(\dot{\Psi} t)^3}{6} + \frac{(\dot{\Psi} t)^5}{120} - \ldots$$

and

$$\cos \dot{\Psi} t = 1 - \frac{(\dot{\Psi} t)^2}{2} + \frac{(\dot{\Psi} t)^4}{24} - \ldots \quad .$$

Again, for small motion, $\dot{\Psi} t < \Psi_0$,

$$\sin \dot{\Psi} t \approx \dot{\Psi} t$$

and

$$\cos \dot{\Psi} t \approx 1 \quad .$$

Using the proper substitution of these relations back in equation (3.51) we obtain for s'

$$\begin{aligned} s' = r_0 \Bigg\{ & 1 - \frac{x}{r_0} \sin \theta_0 \cos \Psi_0 - \frac{y}{r} \sin \theta_0 \sin \Psi_0 \\ & + \frac{x}{r_0} \sin \theta_0 \dot{\Psi} t \sin \Psi_0 - \frac{y}{r_0} \sin \theta_0 \dot{\Psi} t \cos \Psi_0 \\ & + \frac{x^2}{2r_0^2} (1 - \sin^2 \theta_0 \cos^2 \Psi_0) + \frac{x^2}{2r^2} \sin^2 \theta_0 \dot{\Psi} t \sin \Psi_0 \cos \Psi_0 \\ & + \frac{y^2}{2r_0^2} (1 - \sin^2 \theta_0 \sin^2 \Psi_0) - \frac{y^2}{r^2} \sin^2 \theta_0 \dot{\Psi} t \sin \Psi_0 \cos \Psi_0 \\ & - \frac{xy}{r_0^2} \sin^2 \theta_0 \sin \Psi_0 \cos \Psi_0 - \frac{xy}{r^2} \sin^2 \theta_0 \dot{\Psi} t (\cos^2 \Psi_0 - \sin^2 \Psi_0) \\ & + \frac{x^3}{2r_0^3} (\sin \theta_0 \cos \Psi_0 - \dot{\Psi} t \sin \theta_0 \sin \Psi_0 - \sin^3 \theta_0 \cos^3 \Psi_0 \\ & \qquad + 3 \dot{\Psi} t \sin^3 \theta_0 \sin \Psi_0 \cos^2 \Psi_0) \end{aligned}$$

$$+ \frac{x^2 y}{2r_0^3} [\sin\theta \sin\Psi_0 \quad \dot{\Psi} t \sin\theta \cos\Psi_0$$

$$- \sin^3\theta \sin\Psi_0 \cos^2\Psi_0 + \dot{\Psi} t \sin^3\theta (2\sin^2\Psi_0 \cos\Psi_0$$

$$- \cos^3\Psi_0)]$$

$$+ \frac{xy^2}{2r_0^3} [\sin\theta \cos\Psi_0 - \dot{\Psi} t \sin\theta \sin\Psi_0$$

$$- \sin^3\theta \sin^2\Psi_0 \cos\Psi_0 - \dot{\Psi} t \sin^3\theta (2 \sin\Psi_0 \cos^2\Psi_0$$

$$- \sin^3\Psi_0)]$$

$$+ \frac{y^3}{2r_0^3} (\sin\theta \sin\Psi_0 + \dot{\Psi} t \sin\theta \cos\Psi_0$$

$$- \sin^3\theta \sin^3\Psi_0 - 3 \dot{\Psi} t \sin^3\theta \sin^2\Psi_0 \cos\Psi_0) \Bigg\} \quad .$$

Again, taking only first-order terms, we get

$$s' = r_0 - x \sin\theta_0 \cos\Psi_0 - y \sin\theta_0 \sin\Psi_0 + \sin\theta_0 \dot{\Psi} t \sin\Psi_0$$

$$- y \sin\theta \dot{\Psi} t \cos\Psi_0 \quad ,$$

and again noting the direction of k,

$$\Omega_\Psi = - k V_\Psi \frac{(x \sin\Psi_0 - y \cos\Psi_0)}{r} \tag{3.57}$$

where

$$V_\Psi = \dot{\Psi} r_0 \sin\theta_0 \quad .$$

Any general linear motion may be resolved into the three orthogonal components used in the above development, i.e., (V_r, V_θ, V_Ψ). The constant portion will be a sum of the separate contributions to the phase

shifts and the time-variant portions will be formed by summing the time variant phases found for the three orthogonal components. The recorded fringe amplitude will then be modified by a sinc function whose argument is

$$\frac{\Omega\tau}{2} = (\Omega_r + \Omega_\theta + \Omega_\Psi)\ \frac{\tau}{2} \quad .$$

Therefore, combining the time-variant and the constant portions of the phase shifts, the total phase retardation from the laser to the hologram by way of the scene is

$$ks(t) = k\left[S_0'' + (\vec{V} \cdot \hat{a}_k)\tau\right] + k\, s_0' + (\Omega_r + \Omega_\theta + \Omega_\Psi)\tau$$

$$ks(t) = k[s_0' + S_0''] + (kv \cos\gamma + \Omega)\tau$$

$$ks(t) = k\, s_0 + (kv \cos\gamma + \Omega)\tau$$

where

$$\Omega = \Omega_r + \Omega_\theta + \Omega_\Psi \quad . \tag{3.58}$$

The exposure for this case of linear motion may be found by analogy with the exposure for the linear case represented by equation (3.26), where we note by analogy that

$$kv \rightarrow kv \cos\gamma + \Omega \quad . \tag{3.59}$$

The exposure for this hologram-oriented coordinate case then becomes

$$\mathcal{E}(P) = m\tau \left\{ K_c + E_r\, E_s\, \text{sinc}\left[\frac{k\tau}{2}\ (v \cos\gamma + \Omega)\right] \cos\phi \right\} \tag{3.60}$$

where the constants m and K_c are as defined earlier.

Then the fringes are modulated by

$$\text{sinc}\left[\frac{k\tau}{2}\,(v\cos\gamma+\Omega)\right] = \text{sinc}\;\frac{k\tau}{2}\Bigg[v\cos\gamma - \frac{V_\theta}{r}\,(x\cos\Psi_0 + y\sin\Psi_0)\cos\theta_0 - V_r - \frac{V_\Psi}{r}\,(x\sin\Psi_0 - y\cos\Psi_0)\Bigg]. \tag{3.61}$$

This is then the form of the cosine fringe modulation function in terms of the hologram-oriented coordinates.

If we let $r \to \infty$, the sinc function of equation (3.61) becomes

$$\text{sinc}\left[\frac{k\tau}{2}\,(v\cos\gamma+\Omega)\right]_\infty = \text{sinc}\left[\frac{k\tau}{2}\,(v\cos\gamma - V_r)\right] . \tag{3.62}$$

We recall that δ is the angle between the velocity vector and a unit vector in the radial direction of the previous vector analysis development; then, by analogy,

$$V_r = \vec{V}\cdot\hat{a}_p = v\cos\delta \tag{3.63}$$

and equation (3.62) becomes

$$\text{since}\left[\frac{k\tau}{2}\,(v\cos\gamma+\Omega)\right]_\infty = \text{sinc}\left[\frac{k\tau v}{2}\,(\cos\gamma - \cos\delta)\right] \tag{3.64}$$

and we have the identical result obtained earlier in Section (a).

(3) The Resultant Effects of Linear Scene Motion on the Reconstructed Wavefront

In Sections (2) and (3) of this chapter it has been shown that the effect of motion of a point source scene during the formation of a hologram is a modification of the recorded fringe contrast at various points of the hologram. Furthermore, it was stated that the effects on the hologram's recorded fringes caused by scene motion may be derived by considering the motion of only a single point of a rigid moving scene.

We now will investigate the characteristics of the image reconstructed from a hologram having such motion-modified fringes. Comparison of this image with the original object will give a point-spread function for the motion holography case. The approach we will follow is that of the currently existing method presented in Reference 29.

Consider Figure 12, where we assume a particular source distribution in the vicinity of the scene. We desire then to find the resulting amplitude and phase distribution on the hologram at the point Q. If we can then show that this matches the amplitude and phase distribution of the reconstructed field, we will know that the assumed source will describe the reconstructed virtual image. We choose as the assumed source, in Figure 12, a uniform line source lying along the motion vector, i.e., the Z-axis in this diagram. The uniform line source of length $\Delta\ell$ is centered at the $t = 0$ scene point, s_0, and has a linear phase variation, kbz, where b is some proportionality constant. The resulting field will be symmetrical with respect to

revolution about the Z-axis. Then it is desired to know the field at a point Q on the hologram, a distance, $q_0 >> \Delta\ell$, from the source and at an angle δ from the Z-axis.

We consider that the field dE at the point Q is due to the contributions of point sources in the infinitesimal length dZ at a distance Z from the origin. Then $d\vec{E}$ is given by

$$d\vec{E} = \frac{A}{q_0} \exp\left[i(\omega t + kbZ - kq) \quad dZ\right] \quad . \tag{3.65}$$

From the diagram

$$q_0 = q + Z \cos \delta \quad , \tag{3.66}$$

so

$$q = q_0 - Z \cos \delta$$

and then,

$$d\vec{E} = \frac{A}{q_0} \exp\left[i(\omega t + kbZ - kq_0 + kZ \cos \delta)\right] dZ \tag{3.67}$$

where A is a constant involving amplitude.

Now, integrating we find the total field at Q.

$$\vec{E}(Q) = \frac{A}{q_0} \exp i(\omega t - kq_0) \int_{\Delta\ell/2}^{\Delta\ell/2} \exp ik(b - \cos \delta)\, Z dZ \quad . \tag{3.68}$$

Applying Euler's formula to the integral and setting in the limits of integration,

$$\overline{E}(Q) = \frac{A}{q_0} \exp i(\omega t - kq_0) \left\{ \frac{2 \sin\left[k(b - \cos \delta)\Delta\ell/2\right]}{k(b - \cos \delta)} \right\} \quad . \tag{3.69}$$

On multiplying the parenthesis by $\Delta\ell/\Delta\ell = 1$, we find

$$\vec{E}(Q) = \frac{A}{q_0} \exp i(\omega t - kq_0)\Delta\ell \ \text{sinc}\left[k(b - \cos\delta)\Delta\ell/2\right] \quad . \tag{3.70}$$

Therefore, $\vec{E}(Q)$ represents a homocentric wave, centered at the origin point, 0, with an amplitude weighting given by

$$\text{sinc}\left[\frac{k\Delta\ell}{2}(b - \cos\delta)\right] \quad . \tag{3.71}$$

Equation (3.70) is the description of the field at the point Q of the hologram plane resulting from the assumed source of a uniform line.

We now address ourselves to the hologram to determine the amplitude and phase distribution of its reconstructed field. We will then compare the reconstructed (virtual image) field with that of the assumed source. If the two fields match, we will know that the assumed source will describe the reconstructed virtual image.

For the reconstructed hologram the amplitude transmission factor, may be written (see the appendix) as:

$$T_a = T_0 - k_f \mathcal{E} \tag{3.72a}$$

The exposure $\mathcal{E}$ is given by equation (3.37)

$$\mathcal{E} = m\tau\left\{K_c + E_r E_s \ \text{sinc}\left[\frac{k\tau v}{2}(\hat{a}_k - \hat{a}_p)\right]\cos(\phi_r - \phi_s)\right\}$$

or

$$\mathcal{E} = K_1 + K_2 \ \text{sinc}\left[\frac{k\tau v}{2}(\hat{a}_k - \hat{a}_p)\right]\cos(\phi_r - \phi_s) \quad . \tag{3.72b}$$

Then from the amplitude transmission factor we can write

$$T_a = T_0 - k_f \left\{ K_1 + K_2 \operatorname{sinc} \left[\frac{k\tau v}{2} \left(\hat{a}_k - \hat{a}_p \right) \cos \left(\phi_r - \phi_s \right) \right] \right\}$$

or

$$T_a = T_0 - K_1' + K_2' \operatorname{sinc} \left[\frac{k\tau v}{2} \left(\hat{a}_k - \hat{a}_p \right) \cos \left(\phi_r - \phi_s \right) \right] . \qquad (3.73)$$

Now since equations (3.72) and (3.73) describe the exposure and development of the field resulting from a motion scene, the reconstructed virtual image field (first-order diffraction) has an amplitude proportional to the magnitude of the spatial variations in the amplitude transmission factor and is therefore proportional to

$$\operatorname{sinc} \left[\frac{k\tau \vec{V}}{2} \cdot \left(\hat{a}_k - \hat{a}_p \right) \right] = \operatorname{sinc} \left[\frac{kv\tau}{2} \left(\cos \gamma - \cos \delta \right) \right] . \qquad (3.74)$$

Therefore, since the fringe phase $(\Phi_r - \Phi_s)$ is independent of the motion, $\vec{V}$, the hologram will reconstruct a homocentric wave with the center at the $t = 0$ position of the scene point.

Then on comparison of equations (3.71) and (3.74) we see that if $\Delta \ell = v\tau$ and $b = \cos \gamma$, the phase fronts and amplitude distributions are identical for the field of the assumed source and the reconstructed (virtual image) field of the hologram. Therefore, the virtual image will be a line source of length $v\tau$ and with a phase equal to $KZ \cos \gamma$, where Z is the distance from the center of the source. In other words, the image will have the same blur as results from any detector (such as a conventional

photograph) having an integrating time of τ. Furthermore, the phase relationships between the impulses that sequentially formed the hologram are preserved.

CHAPTER IV. ANALYTICAL AND EXPERIMENTAL RESULTS

(1) A Unique Holographic Technique That Allows Resolution of Front-Surface Detail From Scenes Moving Linearly at High Velocities

Front-surface resolution, from targets moving with a velocity of the order of 9×10^5 cm/sec, will be obtainable if one uses a specific orientation of the holographic system (18). With this specific orientation, described below, the path length of the reflection arm is constrained to change by an amount equal to $\lambda/8$ and thereby should allow front-surface resolution, heretofore unobtainable for moving targets, by conventional methods. (The choice of $\lambda/8$ was arbitrary and simply satisfied the need to be smaller than $\lambda/2$.)

The specific orientation of a holographic system, referred to above, also involves the use of a hypothetical ellipse oriented with its major axis parallel to the line of motion defined by the moving projectile.[2] This line of motion must be made tangent to the hypothetical ellipse at a certain point Q. One possible configuration of a holographic system[3] positioned in this

---

[2] In this section we discuss a projectile target, while the actual target tested was a rotating disc whose tangential velocity approximated linear motion (see section 4a of this chapter). The concept of projectile target or scene facilitates the understanding of this section.

[3] This specific system is termed a hybrid system (17) and has been patented by the U. S. Government for its inherent advantages for holography of moving targets.

preferred orientation, inside the hypothetical ellipse, is shown in Figure 13. The specific orientation is defined by the following conditions: a thin film beam-splitter (b/s) centered at the focus f_2 of the hypothetical ellipse; a film plane centered at the other focus f_2, and the major axis of this ellipse, defined by XX' in Figure 13, being parallel to the tangent line, PP' of Figure 13. This tangent line PP' of Figure 13 may be identified as the line of motion of the high-speed projectile referred to above; similarly, it may be defined as a tangent to the rim of a spinning wheel whose tangential velocity may be very high. More generally, PP' may be defined as a line coincident with the linear velocity vector of the moving scene under investigation.

The system may be described as follows, again considering Figure 13. Laser radiation is incident on the first thin film beam-splitter (b/s), centered at the focus f_1. The transmitted beam from here is made incident on the projectile that is moving along the tangent line PP', and is momentarily at the point Q on the perpendicular bisector of XX'. The beam is then reflected from the projectile and made incident on the film, centered at the focus f_2. The reflected beam, from the beam-splitter at f_1, is made incident on a second beam splitter (b/s), just slightly displaced from f_1, where it is again split into two beams. This transmitted beam constitutes the reference beam for the system and after a reflection from a mirror, M, (Fig. 13) this reference beam is made incident on the film at focus f_2. The reflected beam, from this last beam-splitter, is used as a second signal

beam that backlights the target via a diffuser plate (Fig. 13). After being incident on a mirror, M_2, this signal beam passes through a diffuser plate in the region of the projectile, where it then is incident on the film at focus f_2, after being reflected by another mirror, M_3.

From the use of the backlighting arm, one is reasonably assured of a backlighted hologram, i.e., a silhouette of the moving projectile (see holographic type 3, Chapter II). With this information one has more freedom to manipulate the hypothetical ellipse until one obtains front-surface resolution of the silhouetted projectile.

The exact matching of the length of the three arms is of no real concern if one has a source with sufficient coherence length. The source being used in this experiment has a coherent length greater than 3 m, operates at the 6943-Å ruby line, and has a pulse length as short as 25 nsec.

Consider Figure 14a; the general equations of such an ellipse are given by

$$b^2x^2 + a^2y^2 = a^2b^2 \quad . \tag{4.1}$$

The line segment PP' is considered to be tangent to this ellipse at the point Q, which lies on the perpendicular bisector of XX'. This line PP' in Figure 14a is identical to the tangent line PP' of Figure 13. It is the line of motion of the high-speed projectile; it is parallel to the major axis XX' of the ellipse and may be considered perfectly straight. The projectile travels along PP' of Figure 14a and reaches the point Q at some time t_0. The radiation incident at this point at t_0 will be reflected to the film, which

is positioned at focus f_2. At this particular moment the hypothetical ellipse passes through the point Q, with a beam-splitter at f_1 and a film at f_2, and we have the situation depicted earlier in Figure 13.

As the projectile moves some incremental distance Δx, along PP', past the point Q, it moves off this initial ellipse, but it can be considered to move immediately onto another ellipse, just slightly larger than the initial one. If the elliptic constant of the initial ellipse was 2a, the elliptic constant of this new ellispe will be $2(a + \Delta a)$. The radiation reflected from this moving projectile will then be incident on the film at f_2 and will interfere there with the reference beam as long as $2\Delta a$ is less than $\lambda/2$.
long as $2\Delta a$ is less then $\lambda/2$.

In Figure 14b, we construct a family of such ellipses, each successive ellipse being intercepted by the line segment PP' as one moves from Q to the right along PP' parallel to the x-axis of the coordinate system. We see that the separation of the foci remains constant and equal to 2d for the entire family of curves. Figure 14c is a convenient enlargement of the first quadrant of Figure 14b. The points of interception of PP' with each successive member of the family of ellipses are given by P_1, P_2, P_3, etc., respectively. We maintain that as PP' is traversed to the right, the original ellipse can be considered to grow successively to the next larger member of its family, while the foci separation distance 2d remains constant.

If we consider that the ellipse is to enlarge during the time t, then expanding to a larger ellipse, equation (4.1) becomes

$$b^2 x \Delta x + b \Delta b x^2 + a^2 y \Delta y + a \Delta a y^2 = a^2 b \Delta b + b^2 a \Delta a \quad . \qquad (4.2)$$

Since the direction of projectile motion is parallel to the x-axis, $\Delta y \equiv 0$ and we have

$$b^2 x \Delta x = a \Delta a (b^2 - y^2) + b \Delta b (a^2 - x^2) \quad . \qquad (4.3)$$

However, from Figure 14a

$$a^2 - b^2 = d^2 \qquad (4.4)$$

where d is a constant; therefore,

$$a \Delta a = b \Delta b \qquad (4.5)$$

and equation (4.3) becomes

$$b^2 x \Delta x = a \Delta a \, [a^2 + b^2 - (x^2 + y^2)] \quad . \qquad (4.6)$$

From the basic equation for our ellipse, equation (4.1), we may easily obtain

$$x^2 + y^2 = b^2 + x^2 \, [\, 1 - (b^2/a^2)\,] \quad . \qquad (4.7)$$

By substituting equation (4.7) into equation (4.6), we obtain

$$x \Delta x = (\Delta a / a b^2) \, (a^4 - d^2 x^2) \quad . \qquad (4.8)$$

For any ellipse, $2a = L$, where L is a constant and at present is the optical path length of the front illumination signal arm. When the ellipse expands because of projectile travel along PP', $2a = L$ changes by $2\Delta a = \Delta L$. Therefore, since $\Delta a = \Delta L/2$, equation (4.8) becomes

$$x \Delta x = (\Delta L/2) \, (1/ab^2) \, (a^4 - d^2 x^2) \quad . \qquad (4.9)$$

Since we have taken the point Q as the reference point for x (i. e., x is zero when the projectile is at the point Q), therefore, as measurement of the projectile motion starts from point Q and traverse to some point P, $x = \Delta x$ and equation (4. 9) becomes

$$(\Delta x)^2 = (\Delta L/2)\ (1/ab^2)\ [a^4 - d^2(\Delta x)^2] \tag{4.10}$$

or

$$(\Delta x)^2 = \frac{\Delta L\, a^3/2b^2}{1 + \dfrac{\Delta L d^2}{2a\, b^2}} \quad . \tag{4.11}$$

Making the assumption that d^2 is not drastically different from b^2 and $\Delta L/2 << a$, we have that

$$\frac{\Delta L d^2}{2a\, b^2} << 1$$

and equation (4. 11) becomes

$$(\Delta x)^2 \approx (\Delta L/2)\ (a^3/b^2) \tag{4.12}$$

where $\Delta L = 2\Delta a$ is the variation in the original elliptic constant 2a caused by the travel Δx of the projectile along PP'. At a given velocity v for a time τ,

$$\Delta x = v\tau \tag{4.13}$$

where τ is the pulse length of the laser and thereby the exposure time.

Equation (4. 12) is therefore an expression that relates the distance Δx, traveled by the projectile along PP', to the total change in elliptic constant, $\Delta L = 2\Delta a$; i. e., ΔL is the change in optical path length of the front-surface illumination arm of the holographic system. Substituting

equation (4.13) into equation (4.12) and solving for the projectile velocity, we have

$$v = (\Delta L/2)^{1/2} a^{3/2}/b\tau \quad . \tag{4.14}$$

We may use this relation to determine the permissible projectile velocities allowed by the specific configuration having a set of elliptic parameters and a specified tolerance ΔL. For illustration we arbitrarily set ΔL equal to $\lambda/8$ ($\lambda = 6943\,\text{Å}$) and let the distance of separation between the center of the first beam-splitter, at f_1, and the center of the photographic film, at f_2, be a constant value 2d. By varying the semimajor axis a, which in turn varies the semininor axis b, we may obtain a set of allowed distances of travel, $\Delta x = v\tau$. This set of Δx values is graphically shown in Figure 15, where we have used the allowed Δx values as ordinate and the arbitrarily chosen values of semimajor axis a as abscissa. Each separate curve corresponds to a specific value of d and the elliptic parameters are related by $a^2 = d^2 + b^2$.

It may be interesting to note the following:

1. For this fixed value of $\Delta L = \lambda/8$ and each assigned value of d, the curve approaches the vertical line $a = d$ asymtotically. This seems to indicate that the projectile velocity can be any high value without limit if $a = d$. Obviously this is not practical, since at $a = d$, $b \equiv 0$ and the projectile would have to pass directly through the beam-splitter and film. However, picking the smallest practical value of b allows the highest possible velocity

for a given value of d. As the assigned value of d increases (bounded by some practical value of d), the curve rises and thereby raises the allowed value of velocity, although, because of the steepness of the curve, this region (of the asymtotic limit for a given curve where $a > d$) may be somewhat unstable with respect to changes in a or b.

2. As the assigned value of d decreases, the respective curve lowers. The lower bound for these curves occurs at d equal to zero, the hypothetical ellipse becomes a circle. This is again impractical since the beam-splitter would be located at the photographic plate.

3. Differentiation of equation (4. 14) shows that each curve has a minimum at the value of $a = \sqrt{3}d$. Substitution of this result back into equation (4. 14) produces

$$v_{min} = \frac{3}{2}^{3/4} \left(d \frac{\Delta L}{\tau^2}\right)^{1/2} . \qquad (4.15)$$

This v_{min} is the minimum permissible value of the velocity that falls on the curve for each specific value of d. (Obviously all values of velocity lower than v_{min} are still permissible since lower velocities will cause even less shift in path length than the arbitrarily chosen $\lambda/8$.) Because each curve has a zero slope at this point, the region about this point is the most stable (for a given curve, i. e. , value of d) with regard to possible changes in the value of the elliptic parameters a or b. (Changes in b and, therefore, a might occur because of the projectile varying slightly off path as it travels along the line of motion).

The system description above has been for a moving point only; however the contribution of a point in the rigid moving scene to the total reconstructed wave is independent of other points in the scene; i. e. , the principle of superposition applies to the holography of moving rigid scenes.

(2) Application of the Theory of Motion Holography to the Holographic Technique Under Investigation

Two theoretical approaches to the motion holography problem were developed in Chapter III, Sections 3a and b. They both were equivalent to first order. For application here we shall use the "scene-oriented coordinate" approach, since it allows more physical insight into the problem.

Consider the diagram, Figure 16, which represents a typical elliptical configuration such as that investigated in Section I of this chapter and subsequently tested experimentally.

We consider a single point of the scene, Q having a linear velocity $\vec{V}$ parallel to the x-axis. As before, we consider the point R on the reference arm as our reference point. Let L be a point on some reference phase front from the laser, which is common to both beams, because of the presence of a beam-splitter. Let Q represent a single point of the scene having the coordinates (o, b), i. e. , lying on the y-axis. Let $\hat{a}_p$ be a unit vector along the line from the scene point, Q, to the hologram point P. Let $\hat{a}_k$ be a unit vector along the direction of propagation of the incident laser radiation at the scene point. Let $\hat{a}_v$ be a unit vector indicating the velocity of point

Q. Then the angle, γ, between $\hat{a}_k$ and $\hat{a}_v$ is equal to the angle, δ, between $\hat{a}_p$ and $\hat{a}_v$.

We allow that the reference beam is constant in its length. The scene illumination beam is composed of two parts, LQ + QP. The rate of change of the partial path length, LQ, from the laser to the scene point, Q, is

$$\vec{V} \cdot \hat{a}_k = v \cos \gamma \quad . \tag{4.16}$$

The rate of change of the path length, QP, from the scene point, Q, to the hologram point P is given by

$$\vec{V} \cdot \hat{a}_p = v \cos \delta = v \cos \gamma \quad . \tag{4.17}$$

Following identically the procedure of Section 3a, we find the expression for the exposure, because of the motion of this point, from equation (3.37), i.e.,

$$\mathcal{E}(P) = m\tau \left\{ K_c + E_r E_s \operatorname{sinc} \left[\frac{kv\tau}{2} (\cos \gamma - \cos \delta) \right] \cos \Phi \right\} \tag{4.18}$$

where $K_c = E_r^2 + E_s^2 =$ constant and $\Phi = k(s_0 - r)$ is the time-invariant portion of the phase and m is the constant due to the intensity defined earlier.

Using equation (4.17),

$$\mathcal{E}(P) = m\tau \left\{ K_c + E_r E_s \operatorname{sinc} \left[\frac{kv\tau}{2} (\cos \gamma - \cos \gamma) \right] \cos \Phi \right\} . \tag{4.19}$$

Therefore, the sinc function for the scene point at Q is

$$\text{sinc}\left[\frac{kv\tau}{2}\right](0) = \text{sinc}\,(0) = 1 \quad . \tag{4.20}$$

Then we see that the reconstruction of this scene point, Q, will be a maximum. It will still be a bright reconstruction as long as its travel along $\hat{a}_v$ is some small quantity $\Delta x << QP$ — in other words, as long as the motion, Δx, of the scene point, Q, is small enough that $\delta \approx \gamma$.

To place some value on the allowed magnitude of Δx, such that $\delta \approx \gamma$, we direct our attention to a plot of the sinc function (Fig. 17). We see that if we restrict the change in the total path length

$$S = LQ + QP$$

due to the motion, Δx, to be equal to or less than $\lambda/2$, we will obtain a hologram. If we further restrict this change to $\lambda/8$, we will obtain a reasonably bright hologram.

In Section 1 of this chapter, we derived an expression for the total allowed scene travel Δx along the direction of $\hat{a}_v$ in terms of the parameters of an ellipse and quantity ΔL, which was the total change in path length, S. This expression is from equation (4.12):

$$v = \left(\frac{\Delta L}{2}\right)^{1/2} \frac{a^{3/2}}{b\tau}$$

and from equation (4.13), this becomes

$$\Delta x = \left(\frac{\Delta L}{2}\right)^{1/2} \frac{a^{3/2}}{b} \quad . \tag{4.21}$$

The magnitude of Δx, sufficient to cause a change in total path length, S, of $\lambda/8$ and $\lambda/2$ has been tabulated in Table I for various ellipses and a wavelength, λ, equal to 6943 Å.

If we choose $\Delta L = \lambda/8$, then

$$\Delta x = \left(\frac{\lambda}{16}\right)^{1/2} \frac{a^{3/2}}{b} \tag{4.22}$$

and since

$$\Delta x = v\tau \tag{4.23}$$

is the total allowed travel of the scene during exposure, then from equation (4.18) the expression for the scene exposure for the elliptical configuration is

$$\mathcal{E}(P) = m\tau \left\{ K_c + E_r E_s \operatorname{sinc} \left[\frac{k\Delta x}{2} (\cos\gamma - \cos\delta) \right] \cos\Phi \right\} \tag{4.24}$$

and, specifically, the sinc function for this symmetrical scene point Q is, upon substitution of equation (4.22),

$$\operatorname{sinc} \left[\frac{k\lambda^{1/2} a^{3/2}}{8b} (\cos\gamma - \cos\delta) \right] \tag{4.25}$$

where for this point Q

$$\delta \approx \gamma \quad .$$

(3) Comparison of Vector Analysis Approach to the Description in Terms of Elliptic Parameters

We will now pursue a discussion intended to provide an intuitive insight into the motion holography problem. Again the approach is based on the vector analysis of Chapter III and therefore considers only first-order effects. It is further based on the results of the use of the elliptical configuration holographic technique of Section 1 of this chapter. The resulting facts will prove most useful for the experimentalist, whether he desires to minimize the effect of motion (resolution of front-surface detail) or maximize the effects of motion (vibration analysis).

Consider the diagram of Figure 18, where all the parameters shown have the definitions given previously.

Assume that the scene moves with a velocity $\vec{V}$ which is referenced to the bisector line OQ, the y-axis. Then

$$\vec{V} = \vec{V}_{||} + \vec{V}_{\perp} \tag{4.26}$$

where $\vec{V}_{||}$ is the velocity component parallel to the bisector OQ and $\vec{V}_{\perp}$ is that velocity component perpendicular to OQ.

As before let the total path length from the laser to the hologram point P be given by

$$S = LQ + QP \quad .$$

Then the rate of change of the total path length is

$$\frac{dS}{dt} = k\vec{V} \cdot (\hat{a}_k - \hat{a}_p) \quad ,$$

or

$$\frac{dS}{dt} = k\left(\vec{V}_{||} + \vec{V}_{\perp}\right) \cdot (\hat{a}_k - \hat{a}_p) \quad . \tag{4.27}$$

However, since $(\hat{a}_k - \hat{a}_p)$ lies along the bisector OQ and since $\vec{V}_{\perp}$ is normal to OQ, $\cos \pi/2 = 0$ and

$$\vec{V}_{\perp} \quad (\hat{a}_k - \hat{a}_p) = 0 \quad .$$

Therefore,

$$\frac{dS}{dt} = k\,\vec{V}_{||} \cdot (\hat{a}_k - \hat{a}_p) \tag{4.28}$$

and only motion along the bisector OQ (i.e., the y-axis for the elliptical configuration) contributes to hologram degradation (to first order).

For general linear motion (not necessarily parallel to the x-axis of our ellipse), the modifying function in equation (4.18) may be written as

$$\begin{aligned}
\operatorname{sinc}\left[\frac{k\tau\vec{V}}{2} \cdot (\hat{a}_k - \hat{a}_p)\right] &= \operatorname{sinc}\left[\frac{k\tau}{2}\left(\vec{V}_{||} + \vec{V}_{\perp}\right) \cdot (\hat{a}_k - \hat{a}_k)\right] \\
&= \operatorname{sinc}\left\{\frac{k\tau}{2}\left[\vec{V}_{||} \cdot (\hat{a}_k - \hat{a}_p) + \vec{V}_{\perp} \cdot (\hat{a}_k - \hat{a}_p)\right]\right\} \\
&= \operatorname{sinc}\left\{\frac{k\tau}{2}\left(\left|\vec{V}_{||}\right| \left|\hat{a}_k\right| \cos\theta \right.\right. \\
&\qquad \left.\left. + \left|\vec{V}_{||}\right| \left|-\hat{a}_p\right| \cos\theta\right)\right\}
\end{aligned}$$

$$= \text{sinc}\left[\frac{k\tau}{2}\, v_{||}\, 2\cos\theta\right]$$

$$\text{sinc}\left[\frac{k\tau\vec{V}}{2}\cdot(a_k - a_p)\right] = \text{sinc}\left[k\tau v_{||}\cos\theta\right] \quad . \qquad (4.29)$$

We appeal once more to the plot of the sinc function given in Figure 17. We see that a good (bright reconstruction) hologram may be obtained if the argument of the sinc function is kept $\leq \pi/2$ (this means an allowed change in the total path length, S, of $\lambda/4$).

Then from equation (4.29) we may write

$$k\tau v_{||}\cos\theta \leq \pi/2 \quad .$$

Since $k = \frac{2\pi}{\lambda}$ we then have

$$\Delta y = \tau v_{||} \leq \frac{\lambda}{4\cos\theta} \qquad (4.30)$$

where θ is the half angle shown in Figure 18.

Therefore, the total allowed motion along the y direction, i.e., in the direction of $\vec{V}_{||}$, must be less than or equal to $\frac{\lambda}{4\cos\theta}$.

In Section 1 of this chapter, we described the allowed motion of the typical elliptical system just discussed but in an entirely different language, that of the parameters of an ellipse. In that section we considered the value of d to be constant where d is the distance of separation of each foci from the origin. Now, with the fact that for any ellipse

$$a^2 = b^2 + d^2 \quad , \qquad (4.31)$$

we may write

$$\Delta b = \frac{a}{b} \Delta a \quad . \tag{4.32}$$

From the diagram of Figure 18 we may make the observation that Δb is just the total allowed motion along the y direction; then

$$\Delta b = \Delta y = v_{||} \tau \quad .$$

Now combining the last two equations and observing that $a/b = \sec \theta$,

$$\Delta y = \Delta a \sec \theta \quad . \tag{4.33}$$

Since Δa is just that change in the total path length, S, caused by motion, Δy, along the y direction, which will allow a bright reconstruction of the hologram, we use $\Delta a \leq \lambda/4$ and equation (4.33) to obtain

$$\Delta y \leq \frac{\lambda}{4} \sec \theta \tag{4.34}$$

or

$$v_{||} \tau \leq \frac{\lambda}{4 \cos \theta} \quad . \tag{4.35}$$

A comparison of equations (4.35) and (4.30) shows the necessary agreement between the description in terms of elliptic parameters and that of "scene-oriented coordinates." This expression will be of considerable interest in the next section.

We observe that for a silhouette hologram (backlighted, diffuse or direct type), $\theta = \pi/2$ and any motion is acceptable. If the direction of motion is known and resolution of front-surface detail is desired, the elliptic

configuration investigated is highly desirable since here the hologram is placed such that the bisector OQ is normal to the velocity vector. This makes $v_{||} = 0$ and maximizes the hologram quality. This is strictly true, of course, only for straight-line motion of v.

(4) Experimental Results of the Elliptical Configuration

In the following paragraphs the systems tested are identified.

(a) System Identification and Description

During the experimental investigation of the elliptical configuration technique, many elliptical configurations were tested. In each case the linear target velocity along the x direction was approximated by the tangential rim velocity of a wheel of radius r, centered at the symmetrical point, (o,b), of the respective elliptical configuration. The reason for this choice and the degree of approximation will be presented later.

Of the systems tested, five different configurations were selected that will now be described. Consider Figure 19, where we diagramatically describe a general configuration. Radiation from the ruby laser, $\lambda = 6943\text{Å}$, is made incident on beam-splitter, BS, at foci, f_1, by mirror, M_1. Here the beam is split into two beams, the object wave and the reference wave. The object wave is incident on the rim of the target wheel of radius r after passing through the diffuser. Radiation then scattered by the wheel's edge is made incident on the hologram, H, at the second foci, f_2. The diffuser in the path of the object beam serves to uniformly illuminate the target. The

reference wave, reflected from the beam-splitter, passes through a single positive lens plus a 25-μ pinhole, which constitutes a spatial filter. This was necessary because of the inhomogeneity of the intensity of the normal-mode pulse from the laser. It, of course, then provides a uniformly intense divergent beam that is made incident on the film plane at H by mirror, M_2.

All the parameters necessary for the description of the configuration are also labeled on this diagram. Using Figure 19 and Table II of system parameters, we will now identify the various systems investigated. By system we mean the particular configuration including the wheel radius. We have shown a total of six systems in Table II. The definition of systems 1 through 6, identified by Table II, will be used throughout this discussion. Figure 20 is a photograph of one of the configurations used, in which the location of the wheel is clearly visible.

Figure 21 is a photograph of the ruby laser showing the oscillator and amplifier cavity, with the limiting aperture between them. This limiting aperture, when properly aligned, serves two purposes. It produces a marked increase in the coherence length of the radiation, at the expense of intensity, and it provides a more uniformly intense source. However, the homogeneity of the intensity is still unacceptable without the use of the spatial filter described earlier. Two pulses of different pulse lengths were obtained from this source, using the two available mode selections, normal and Q spoiled. Both of these pulses were detected and measured at the output of the spatial filter. Photographs and schematics of each are shown in Figures 22 and 23.

The pulse length of the normal mode pulse was 2.5×10^{-4} sec while that of the Q-spoiled pulse was four orders of magnitude shorter, 25×10^{-9} sec. These values were monitored and stayed essentially constant for each shot. (This constancy was assured by the control of the water coolant temperature and the period of flash-tube firing.)

A photograph of the two different radii wheels used as the target for systems 1 through 6 is shown in Figure 24. On the surface of the large wheel, r = 20.32 cm, it will be observed that a cross-hatched tape covers its entire periphery. This served two purposes: (1) it provided some definite markings whose detail could hopefully be resolved after motion, and (2) it provided a dielectric-type surface as a reflector or scatterer instead of a metallic surface. A similar coating is found on the small wheel, r = 10.16 cm, except that here the white surface is a flat, diffuse white paint with vertical lines hand-painted on it. This serves the same two purposes described above; the reason for the painted surface will be explained later.

Close inspection of Figure 24 will show that the tape on the periphery of the large wheel appears to have a slight curvature along its height. This is because the height of this taped surface is greater than the thickness of the wheel; consequently, the tape on either side of the disc tends to bend back toward the center of the disc. For the painted surface of the small wheel this curvature does not exist. To ascertain the influence of this surface curvature of the tape, refer to Figure 25. The angle β is the total angle into which both wheels scatter the radiation originally incident at some point Q.

(Actually, this will be a solid angle, not a plane β, but the hologram was 4 by 5 in. and it suffices to speak of an angle β in the xy plane for this argument.) Now the hologram in both cases intercepts an angle $\epsilon < \beta$, i.e., the radiation is scattered over an angle β, greater then the angle ϵ, so the curvature of the surface is immaterial from this point of view. Of course, the magnitude of the angle ϵ will vary, depending on the magnitude of d or a, but ϵ is always less than β. The energy density at point, P, caused by radiation scattered from Q is probably less for the curved surface disc since β for this disc was slightly greater than β for the flat wheel. This, however, had little or no effect since the ratio of the beams at point P was controlled throught the use of neutral-density filters. More will be said about this angle ϵ from a different point of view later.

The original plan for this investigation was to use the hybrid system described in Figure 13 with the back diffuser arm (see Section 1 of this chapter) and to record one hologram of a single projectile showing the resolution of front-surface detail. This approach was not pursued for the following reasons:

(1) This approach would involve the engineering problem of designing a fairly complicated synchronization circuit to synchronize a nanosecond-type pulse with a high-speed event, namely, a projectile with v = 40,000 cm/sec.

(2) It was felt that the accomplishment of the above single shot really provided very little insofar as the physics of the elliptical technique were concerned.

Therefore, in lieu of the above approach, it was decided that for this project we would use a continuous-type target to obviate the need for a synchronization circuit and use a variety of slower velocities to better investigate the physics of the elliptical configuration, i.e., the influence of such parameters as d, a, θ, and δ (see Table II). To achieve fairly high velocities as well as a continuous target, the decision was made to use a rotating disc, a gyroscope-type target. For the slower velocities a, dc continuously variable-speed motor was used to rotate the target disc. For the highest velocity, an ac motor, taken from a Router tool, was used. The upper limit on the angular speed of this motor was $\approx$ 417 revolutions per second. The angular speed of the disc attached to this motor was, of course, less then this because of air resistance.

The decision to use a rotating disc was further strengthened by the fact that the theory shows (as well as experimental evidence; see Section c of this chapter) that the important parameter for motion holography is the total apparent distance, Δx, moved by the target during the exposure time, i.e., $\Delta x = v\tau$. Then the velocity per se is unimportant; its product with exposure time is the important parameter, other things being constant.

(b) Comparison of the Experimental Results of the Systems Identified Above

As mentioned in the last section, edge washout occurs here primarily because all of the illuminated target does not lie along the line parallel and tangent to the chosen ellipse. For this particular problem, then, we are interested in those points of the target that do not satisfy the chosen ellipse by virtue of their geometrical displacement from a line PP' tangent to our chosen ellipse. For simplicity, we represent the disc as a stack of two parallel plates, having a linear velocity $\vec{V}$ directed parallel to PP', as our target (Fig. 26). Points considered are S_1, S_0, and S_2. The angles δ_i, γ_i, are the same as defined in Chapter III, Section 3a, in the discussion of Figure 8. From equation (3.37) we may write the exposure at point P as

$$\mathcal{E}(P) = m\tau \left\{ K_c + E_r E_s \operatorname{sinc} \left[\frac{k\tau}{2} \vec{V} \cdot (\hat{a}_k - \hat{a}_p) \right] \cos \Phi \right\} . \quad (4.36)$$

The sinc function, which was thoroughly discussed in Chapter III, is that function caused by motion, which modifies the cosine fringes. We recall that if the argument of this function is zero we have

$$\operatorname{sinc} [0] \equiv 1 \quad (4.37)$$

and we obtain the brightest hologram. Any other value of the argument presents a degradation of the cosine fringes (see Fig. 10, Chapter III).

We can write

$$\operatorname{sinc} \left[\frac{k\tau}{2} \vec{V} \cdot (\hat{a}_k - \hat{a}_p) \right] = \operatorname{sinc} \left[\frac{k\tau v}{2} (\cos \gamma - \cos \delta) \right] . \quad (4.38)$$

Similarly, we can write the respective sinc functions for the three points of Figure 26:

$$\text{sinc}\left[\frac{k\tau v}{2}\ (\cos\gamma_1 - \cos\delta_1)\right] \quad , \tag{4.39}$$

$$\text{sinc}\left[\frac{k\tau v}{2}\ (\cos\gamma_0 - \cos\delta)\right] \quad , \tag{4.40}$$

and

$$\text{sinc}\left[\frac{k\tau v}{2}\ (\cos\gamma_2 - \cos\delta_2)\right] \quad . \tag{4.41}$$

From the symmetry of point S_0 of Figure 26,

$$\gamma_0 = \delta_0 \quad . \tag{4.42}$$

Furthermore, from the diagram the following relations are clear:

$$\left.\begin{aligned} &\gamma_1 > \gamma_0 > \gamma_2 \\ &\delta_1 < \delta_0 < \delta_2 \\ &\delta_2 > \gamma_0 \\ &\delta_1 < \gamma_0 \end{aligned}\right\} \tag{4.43}$$

Additionally, in all three cases the total angle between $\hat{a}_k$ S $\hat{a}_p = \gamma + \delta$. Then we can write

$$\beta' = \gamma + \delta \quad . \tag{4.44}$$

Let us consider a hypothetical case in order to evaluate the sinc function for the three points, S_1, S_0, and S_2, of the target in Figure 26. As our chosen ellipse we take the parameters of system number 2, Table II, which demand that, at the point of symmetry, i. e, S_0 of our system,

$$\delta_0 = 20 \text{ deg} \quad ,$$

$$\gamma_0 = 20 \text{ deg} \quad , \tag{4.45}$$

and

$$\theta_0 = 70 \text{ deg} \quad .$$

Then let

$$\beta' \equiv \delta_0 + \gamma_0 = 40 \text{ deg} \quad . \tag{4.46}$$

We assume that our target is sufficiently long and displaced from PP' at points S_1 and S_2 such that, for example,

$$\delta_1 = 10 \text{ deg}$$

and (4.47)

$$\delta_2 = 30 \text{ deg} \quad .$$

Then, from equations (4.46) and (4.47),

$$\beta' = 40 \text{ deg} = \gamma_1 + \delta_1 \quad , \tag{4.48}$$

$$\gamma_1 = 40 \text{ deg} - \delta_1 \quad ,$$

or

$$\gamma_1 = 30 \text{ deg} \quad . \tag{4.49}$$

Also, by the same reasoning,

$$\gamma_2 = 10 \text{ deg}$$

and from equations (4.39), (4.40), and (4.41) the respective sinc functions become

$$\text{sinc}\left[\frac{k\tau v}{2}\ (\cos 30\ \text{deg} - \cos 10\ \text{deg})\right] \quad ;\ S_1 \quad , \tag{4.50}$$

$$\text{sinc}\left[\frac{k\tau v}{2}\ (\cos 20\ \text{deg} - \cos 20\ \text{deg})\right] \quad ;\ S_0 \quad , \tag{4.51}$$

and

$$\text{sinc}\left[\frac{k\tau v}{2}\ (\cos 10\ \text{deg} - \cos 30\ \text{deg})\right] \quad ;\ S_2 \quad , \tag{4.52}$$

Therefore, since $v\tau = \Delta x$ for S_1, we have

$$\text{sinc}\left[(-0.019)\ \frac{k\Delta x}{2}\right] \neq 1 \quad ; \tag{4.53}$$

for S_0

$$\text{sinc}\left[(0)\ \frac{k\Delta x}{2}\right] \equiv 1 \quad , \tag{4.54}$$

and for S_2

$$\text{sinc}\left[(0.019)\ \frac{k\Delta x}{2}\right] \neq 1 \quad . \tag{4.55}$$

It is then seen that edge washout occurs because of this variation of the sinc function that modifies the cosine fringes. It is further observed that this degradation occurs in an equally displaced fashion about the symmetrical point of the chosen ellipse (i.e., the S_0 point). This same fact, of course, is implied in Figure 10, where we varied the direction of illumination with respect to the velocity vector and plotted the value of the argument of the sinc function. It is noted here and will be shown later in this section that this is precisely what happens experimentally.

It is further clear from this discussion and Figure 26 that the same type of phenomena would occur even if the target were not displaced, i.e.,

if it were parallel and coincident with the line PP' that is tangent to the chosen ellipse, provided the target were "long enough." But in terms of the elliptical description, we would simply say that the "long" target does not sufficiently approximate the chosen elliptical surface. Then, again, we have agreement between the vectoral description and the elliptical description. However, this phenomenon of edge washout is not so startling since the allowed size of the target is certainly determined by the choice of the parameters or size of the chosen ellipse.

The systems numbered 1 through 6, identified in Section 4a of this chapter, will be compared. Each system has the geometrical parameters displayed in Table II and was tested in the following fashion.

To establish a reference between the condition of a stationary target and that of a moving target, the first hologram taken for each system was that of its respective stationary target. Ultimately the measured value, $\bar{S}_i$, of each hologram was divided by the respective value of $\bar{S}_i$ for its stationary target.

Equation (4.12) was used to calculate the value of $\Delta x_{\lambda/8}$ for each system, sufficient to cause a path-length shift of $\lambda/8$ in the front surface illumination arm (Table II). From equation (4.13),

$$v = \frac{\Delta x}{\tau} \quad , \tag{4.56}$$

we were able to ascertain that velocity, $v_{\lambda/8}$, that was necessary to cause a $\lambda/8$ shift in this path length of each system. Then, using

$$\frac{v}{r} = \omega \quad , \tag{4.57}$$

we were able to determine the rotational speed sufficient to allow the desired tangential velocity that was used to approximate a linear velocity. Of course, the same procedure allows determination of the proper rotational speed sufficient to cause a $\lambda/2$ shift in the front-surface illunimation arm.

Two more holograms then were acquired in which the target moved the distance $\Delta x_{\lambda/8}$ and $\Delta x_{\lambda/2}$, respectively, during the exposure time of 2.5×10^{-4} sec, which was constant for all shots of all systems tested. Two exceptions to this exposure time occurred in systems numbers 2 and 5, which will be explained later. From the value of ω determined above, the frequency of the rotating wheel was accurately set through the use of a strobetachometer, calibrated to within 1 percent of the value being measured. This approach was followed systematically for all systems tested.

Therefore, using a pulse length or exposure time, which was constant for all systems, we obtained the following three holograms of the target wheel for each system:

1. The stationary target wheel.

2. The target wheel while it moved a distance, $\Delta x_{\lambda/8}$, sufficient to shift the path length of $\lambda/8$ for that system.

3. The target wheel while it moved a total distance, $\Delta x_{\lambda/2}$, for that system.

Actually, holograms were taken with a $\Delta x > \Delta x_{\lambda/2}$ for each system, but we will primarily compare only the holograms mentioned above for systems numbers 1, 3, and 4, since these particular holograms have values of path-length shift which are common to all of them. We will, however, discuss a total of eight holograms for system number 2 in an effort to demonstrate the effect of edge washout discussed earlier. Two holograms each of systems numbers 5 and 6 will be discussed separately.

After developing all of the holograms in the manner discussed in the appendix, photographs were taken of the image produced by each hologram during reconstruction. All images were placed in a one-to-one correspondence with their original target and the target was the same for all systems. The resultant negatives, whose development was carefully controlled, were then used to measure the amount of front-surface detail resolved in each case. These measurements were made in the following way.

Since each target wheel had a pattern on its periphery, the resultant negative of the image of this pattern was viewed to determine a position that would be used as the limit of resolved detail for each image on the negatives. A densitometer was then used to determine the density of this point and to locate the position of corresponding density on the opposite side of the image. At these precise positions on the negative, a hair-thin line was drawn with a knife edge. This particular value of the density was found for all the other negatives and, again, a fine line was drawn. It should be pointed out that the

density of all the holograms and photographs was held as constant as possible so that the only influence on the density of each was determined by the reduction in brightness of the image due solely to the motion of the target itself during the exposure time.

Each negative was then aligned on the stage of a spectrum line comparator, where a visual display of the resolved pattern, magnified up 10 times, was present on a screen. The position of the fine line, drawn on the negative, was electronically determined by a trace on the cathode-ray tube of the spectrum line comparator. A photograph of this line comparator is shown in Figure 27. Using this instrument, the length of the image lying between the fine lines was measured several times and an average value taken. We thereby obtained an average quantity, $\bar{S}_i$, for each negative corresponding to each hologram of the specific system tested. The value of $\bar{S}_i$ for each hologram of all six systems tested is listed in Table III and represents the average of the length of the resolved detail of each image.

Since the stationary target of each system is the reference between the condition of motion versus no motion of the target for that system, we define another quantity, $\bar{S}_{0_i}$, for each system,

$$\bar{S}_{0_i} \equiv \frac{\bar{S}_i \text{ (for motion case)}}{\bar{S}_i \text{ (for stationary case)}} \quad ; \tag{4.58}$$

i.e., $\bar{S}_{0_i}$ is just the average length of each resolved image, relative to the average length of the stationary image, for each respective system. This is

necessary since the length of the image resolved is certainly dependent on the length of the image illuminated and this illuminated length was unavoidably different for each system tested. Then $\bar{S}_{0_i}$ just denotes the amount of the original stationary object resolved by each successive hologram of a given system. Again, all of the values of $\bar{S}_{0_i}$ are listed in Table III for each respective system.

From the theory of the elliptical holographic system we know that the total allowed travel, Δx, is definitely a function of the system parameters a, b, and d. That is, for a given specific value of travel, Δx, the effect of this motion in terms of the degradation of image quality will be less for a large ellipse than for a small ellipse, other things being constant. Shortly we will present experimental evidence to support this theoretical contention.

Figure 28 presents eight photographs showing the images resolved for eight successive holograms, taken with system number 2. Each photograph represents successively larger motions, i.e., values of Δx. Photograph number H-5 is of the stationary target. Photographs H-6 through H-11 represent successively larger motions, all with the same constant exposure time of 2.5×10^{-4} sec. These photographs vividly display the effect of edge washout discussed earlier. Photograph number H-12 is a Q-spoil exposure, $\tau = 25 \times 10^{-9}$ sec and is the result of the same motion as for photograph H-11. Because of the difference in the exposure time of four orders of magnitude,

resolved detail is strikingly different. Therefore, it is obvious that the stop action is a function of exposure time, other things being constant. Consequently, in what follows we will recall that the exposure time of 2.5×10^{-4} sec was constant for all systems except in system number 5, which will be discussed separately. Additional information is included in the caption for each photograph of Figure 28.

We now present experimental verification that the stop action is indeed a function of the elliptical system configuration. Consider the following data from Table III:

for H-3 with

Parameters

$$\begin{aligned} d &= 15 \text{ cm} \\ a &= 25.4 \text{ cm} \\ \theta &= 36 \text{ deg} \\ \Delta x &= 257\ \mu \\ v &= 102 \text{ cm/sec} \\ \tau &= 2.5 \times 10^{-4} \text{ sec} \quad , \end{aligned} \tag{4.59}$$

we have

$$\overline{S}_{0_3} = 0.595 \quad .$$

and for H-6 with

Parameters

$$\begin{aligned} d &= 50 \text{ cm} \\ a &= 53.3 \text{ cm} \\ \theta &= 70 \text{ deg} \\ \Delta x &= 257\ \mu \\ v &= 102 \text{ cm/sec} \\ \tau &= 2.5 \times 10^{-4} \text{ sec} \quad , \end{aligned} \tag{4.60}$$

we have

$$\overline{S}_{0_6} = 0.867 \quad . \tag{4.61}$$

Then, since

$$\overline{S}_{0_6} = 1.48\ \overline{S}_{0_3} \tag{4.62}$$

and since the only parameters that differ for these two cases are those defining the different systems, we must conclude that the differences observed in the magnitude of the relative average value of the resolved image must be due to some function of the elliptical system itself, i.e., in the orientation of the holographic system used. We may make a second such comparison using H-4 and H-9, whose parameters and data are found in Table III. We observe that the magnitude of the relative average value for H-4 is

$$\overline{S}_{0_4} = 0.516 \tag{4.63}$$

while that for H-9 is

$$\overline{S}_{0_9} = 0.652 \quad ; \tag{4.64}$$

then, in this case,

$$\bar{S}_{0_9} = 1.26\ \bar{S}_{0_4} \quad . \tag{4.65}$$

From a comparison of parameters of these systems, found in Table III, the total travel, $\Delta x = v\tau$, is the same for both systems in spite of the difference in magnitude of the relative average value for each. We must again conclude that this observed difference is due solely to system dependence. Furthermore, it is observed that the larger the system is, i.e., the larger the value of d, it always allows the larger relative length $\bar{S}_{0_i}$.

As further evidence of this last statement, consider the results for a path-length shift for three successively larger ellipses. For H-2, with d = 15 cm and other parameters as given in Table III, the magnitude of the relative average value of the resolved image is

$$\bar{S}_{0_2} = 0.638 \quad ; \tag{4.66}$$

for H-14, with d = 30 cm,

$$\bar{S}_{0_{14}} = 0.752 \quad , \tag{4.67}$$

and, finally, for H-7, with d = 50 cm,

$$\bar{S}_{0_7} = 0.776 \quad . \tag{4.68}$$

Yet we note from an inspection of parameters that the range of the value of d in centimeters, for these three systems is

$$15 \leq d \leq 50 \tag{4.69}$$

and the allowed range of total travel, $\Delta x_{\lambda/8}$, sufficient to shift the optical path length in each system by a constant amount, $\lambda/8$, is

$$128\,\mu < \Delta x_{\lambda/8} < 438\,\mu \quad , \tag{4.70}$$

respectively, as indicated by equation (4.12). That is, the larger ellipse allows the scene to travel further during the exposure time before the total phase shift of the optical path length changes by $\lambda/8$. Yet, in spite of this increase in the total allowed travel, $\Delta x_{\lambda/8}$, the ability of the larger system to resolve detail from the target, as indicated by the $\bar{S}_{0_i}$ value, increases or at least stays approximately constant for the successively larger ellipses.

If we consider the results of a $\lambda/2$ path-length change for these same systems, we see essentially the same result as note above — the ability of the larger system to resolve detail from the moving scene, as indicated by the quantity $\bar{S}_{0_i}$ of Table III, increases or at least stays approximately constant for the successively larger ellipses. This occurs in spite of the fact that the total travel, $\Delta x_{\lambda/2}$, necessary to cause a $\lambda/2$ path length change is necessarily larger for the larger ellipses.

Having established that the stop action is indeed a function of the system, we ask the question, What is the form of this function? To answer this, we will compare two systems having identical values of the angle, θ, but different values of the length, a. We will also compare two systems having approximately equal values of the length a but different values of the angle, θ.

For the case of two different systems having the same value of the angle, θ, but different values of semimajor axis a, we point out systems 1 and 3 with $\theta = 36$ deg and other parameters given by Table III. Then, on comparing the results for Δx_i and $\bar{S}_{0_i}$ of H-1, H-2, and H-3 of system 1 with those for H-13, H-14, and H-15 of system 3, we see that the allowed increase in total travel, Δx, for a constant value of path-length change is caused primarily by the difference in the values of the parameters d and a for the two systems.

Likewise, for two systems with a semimajor axis of $a \approx 50.81$ cm but different values of the angle, θ, we compare the results for Δx_i and $\bar{S}_{0_i}$ of H-13, H-14, and H-15 of system 3 with these results of H-16, H-17, and H-18 of system 4. We note that now the allowed increase in Δx is due primarily to the difference in the value of the parameters d and θ for these systems. Therefore, our desired functional dependence must be of the form $f(d, a, \theta)$.

Recalling equation (4.12) for Δx, we have

$$\Delta x = \left(\frac{\Delta L}{2}\right)^{1/2} \frac{a^{3/2}}{b} \tag{4.71}$$

and from Chapter IV, Section 1, we know that

$$\Delta L = 2\Delta a \tag{4.72}$$

and

$$\frac{a}{b} = \sec\theta = \frac{1}{\cos\theta} \quad . \tag{4.73}$$

Then, equation (4.71) may be written as

$$\Delta x = (\Delta a)^{1/2} \frac{a^{1/2}}{\cos \theta} \tag{4.74}$$

or

$$\Delta x \propto \frac{a^{1/2}}{\cos \theta} \tag{4.75}$$

where θ is the angle between b and a of our ellipse. Then we see that our analytical equation (4.12) derived for our hypothetical ellipse has the desired functional form that satisfies the results observed experimentally. The value of this function, shown in equation (4.75), for all systems tested, is shown in Table III and is seen to increase for each system having a larger value of the parameter d. Figure 29 presents photographs showing the results of system number 1, which was the smallest system tested. (Figure 28 has already shown the largest system tested, system number 2.)

We now direct attention back to the discussion of Chapter IV, Section 4a, where mention was made of an angle ϵ; Figure 25, and Chapter IV, Section b, where the effect of the variation of the sinc function was discussed. We intend at this point to demonstrate a connection between the parameters a and θ, with this angle ϵ and another effect of the variation of the sinc function (Fig. 30). From this figure we can write

$$\frac{\epsilon}{2} = \tan^{-1}\left(\frac{\frac{h}{2} \cos \delta}{a - \frac{h}{2} \sin \delta} \right) \tag{4.76}$$

where h is the dimension of the hologram plate. From this relation it is readily seen that as a increases, the value of $\epsilon/2$ decreases and the effect caused by the variation of the sinc function is reduced from some maximum — evidence again that the larger system tolerates higher motion.

We now present experimental verification of the theoretical conclusion that the total allowed motion, $\Delta x = v\tau$, is the primary parameter affecting image degradation due to scene motion. Consider systems numbers 5 and 6 whose system parameters are identical in every respect. The sole difference is in the type of surface found on the periphery of the target wheel in each case. The periphery of the wheel of system number 5 is composed of a flat, diffuse, painted background on which vertical bars have been painted. A painted surface had to be used since the tangential velocity of this wheel was so high that any tape that was put on it exploded after a certain velocity was reached. The periphery of the target wheel in system number 6 was composed of white tape with vertical bars inked on it; the vertical bars on this surface are slightly narrower than the painted ones of system number 5. Furthermore, the surface of system number 5 is more diffuse than that of system number 6.

With this sole exception in mind, the otherwise identical parameters of systems 5 and 6 are as presented in Table II and Table III.

Systems numbers 5 and 6 have the following:

Parameters

$r = 10.16$ cm

$\theta = 36$ deg

$\delta = 54$ deg

$a = 50.81$ cm

$b = 41$ cm

$d = 30$ cm

$\Delta x = 4.4\,\mu = v_5\tau_5 = v_6\tau_6$

$$\frac{a^{1/2}}{\cos\theta} = 8.81$$

$\bar{S}_{0_{20}} = 0.667$; $S_{0_{22}} = 0.651$.

Other than the periphery surface, the sole difference between the two systems is found in the individual values of velocity and exposure time or pulse length, i. e.;

System Number	System Number 6
$v_5 = 1.7546 \times 10^4$ cm/sec	$v_6 = 1.76$ cm/sec
$\tau = 25 \times 10^{-9}$ sec	$\tau = 25 \times 10^{-4}$ sec $= \tau_5 \times 10^{-4}$

The value of Δx is identical for both, while the velocity and exposure time of each differ by four orders of magnitude. It is further noted that the respective values of the relative average length parameter, $\bar{S}_{0_i}$, is approximately equal. Photographic evidence of this is shown in Figure 31, where we present the results of the systems 5 and 6. Notice that for this highest

velocity of 17,546 cm/sec, we used the second smallest system tested and therefore one of the worst systems available to us.

Since we have verified that the value of Δx is the important parameter in this study of motion holography, we now find the second highest value of Δx obtained in this study. We, of course, select H-10 of system 2 since here the limit is certainly being approached as evidenced by the blur of the pattern resolved (Fig. 28). For H-10

$$\Delta x = 2,250\,\mu = v\tau \quad .$$

We recall that this value was the result of a velocity equal to 900 cm/sec and an exposure time of 2.5×10^{-4} sec. Suppose we attempted the same shot with an exposure time four orders of magnitude shorter, i. e., 25×10^{-9} sec (a Q-spoil pulse) and retained all parameters identical to those for H-10. In view of the last results, what limiting upper velocity could the system allow such that we would obtain at least the same resolution offered by H-10?

From Table III for H-10

$$\Delta x = 2,250\,\mu = v\tau \tag{4.77}$$

using the Q-spoil pulse length

$$v = \frac{2250 \times 10^{-4}\ \text{cm}}{25 \times 10^{-9}\ \text{sec}} \tag{4.78}$$

and

$$v = 90 \times 10^{5}\ \text{cm/sec} \quad . \tag{4.79}$$

Then, even using a safety factor of one order of magnitude, our limiting upper velocity would be

$$v = 9 \times 10^5 \text{ cm/sec} \quad . \tag{4.80}$$

Therefore, for a system having parameters identical to those of system number 2, this velocity represents the upper limit of velocity using a Q-spoil pulse of 25×10^{-9} sec. The predicted results of such a velocity will be at least as good as the results shown by H-10 of Figure 28 and Table III and probably as good as H-8, in view of the order of magnitude change above.

CHAPTER V. SUMMARY AND CONCLUSIONS

Various types of holography have been presented and discussed, theoretically and experimentally, including the time-variant effects caused by motion. A holographic system, unique in its configuration, has been discussed that allows the resolution of front-surface detail from scenes moving at high velocity. The highest velocity for which front-surface detail was experimentally resolved was 17, 546 cm/sec; however, it has been inferred from the comparison of systems numbers 5 and 6 that front-surface detail could be resolved even for scenes with very high velocities. These very high velocity cases have not actually been accomplished experimentally yet. However, before this work, the highest scene velocity from which front-surface detail was obtained has been a few centimeters per second. For this experiment, the scene velocity was the tangential velocity of the rim of a rotating wheel. The degree to which this approximates linear velocity is denoted by the fact that for the largest total displacement, Δx, of the scene, $\Delta x = 4240\ \mu$, the angle of wheel rotation was only 1.2 deg.

From the experimental results of this investigation, we may conclude the following:

1. That the total scene motion during exposure, $\Delta x = v\tau$, is the parameter of importance for motion holography, i.e., the product of velocity and time.

2. That the degradation of the cosine fringes due to scene motion during exposure causes the scene detail to blur out. Furthermore, this

blurring or edge washout occurs symmetrically about that point of the target that is tangential to the surface of the hypothetical ellipse. (This was also shown theoretically in terms of the sine function.)

3. That the allowed motion or stop action of the moving scene is definitely a function of the elliptical arrangement used that defines the holographic system. The functional form of this system dependence, for travel in the $\vec{x}$-direction, has been shown to be proportional to $a^{1/2}/\cos\theta$; the value of this function for all systems tested has been tabulated.

4. That the ability to allow larger total motion, Δx, for a given optical path length shift, during a constant exposure time is found to increase with the size of the holographic system being used.

Although it was not experimentally concluded, it is believed that we may reasonably infer from comparison of the data of this investigation that one can resolve fairly good front-surface detail from a scene traveling at velocities

$$v = 9 \times 10^5 \text{ cm/sec}$$

if one uses the system configuration similar to that discussed in Chapter IV. It is also believed that the detail obtained from a target having this velocity would probably be as good as that shown by photograph H-8 of Figure 31.

TABLE I. ΔX FOR SYSTEMS INVESTIGATED

d	SEMI-MAJOR AXIS = a		SEMI-MINOR AXIS = b	$\Delta X \frac{\lambda}{8}$	$\Delta X \frac{\lambda}{2}$
15 cm	18 cm		9.95 cm	159.88 μ	319.79 μ
	20		13.23	140.84	281.69
	22		16.09	133.57	267.13
	24		18.74	130.73	261.46
	25.5	(MIN: $a = \sqrt{3d}$)	20.50	128.50	257.00
	26		21.24	130.04	260.09
	50		47.70	154.41	308.82
	100		98.87	210.70	421.34
	200		199.44	295.43	590.86
	300		299.63	361.26	722.52
20 cm	22 cm		9.17 cm	234.54 μ	469.07 μ
	24		13.27	184.62	369.24
	26		16.61	166.23	332.47
	30		22.34	153.08	306.15
	34	(MIN: $a = \sqrt{3d}$)	27.50	150.20	300.40
	40		34.64	152.13	304.26
	50		45.83	160.72	321.23
	100		97.98	212.61	425.21
	200		199.00	296.08	592.16
	300		299.33	361.61	723.22
30 cm	32 cm		11.14 cm	338.63 μ	677.27 μ
	36		19.90	226.11	452.22
	40		26.46	199.18	398.37
	48		37.47	184.88	369.76
	51	(MIN: $a = \sqrt{3d}$)	41.00	182.00	364.00
	70		63.25	192.90	385.80
	100		95.40	218.37	436.74
	150		146.97	260.39	520.78
	200		197.74	297.97	595.94
	300		298.50	362.62	725.25
50 cm	52 cm		14.28 cm	546.89 μ	1093.79 μ
	60		33.17	291.91	583.81
	70		48.99	249.03	498.06
	80		62.45	238.68	477.36
	85	(MIN: $a = \sqrt{3d}$)	69.00	235.72	471.44
	90		74.83	237.68	475.36
	96		81.95	239.09	478.18
	100		86.60	240.54	481.08
	200		193.65	304.26	608.52
	300		295.80	365.92	731.85

TABLE II. PARAMETERS OF SYSTEMS INVESTIGATED

	r	θ	δ_o	a	b	d	$\Delta x \lambda/8$	$\Delta x \lambda/2$
SYSTEM 1	20.32cm	$\approx 36^o$	$\approx 54^o$	25.4cm	20.5cm	15cm	128 μ	257 μ
SYSTEM 2	20.32cm	$\approx 70^o$	$\approx 20^o$	53.3cm	18.5cm	50cm	438 μ	875 μ
SYSTEM 3	20.32cm	$\approx 36^o$	$\approx 54^o$	50.81cm	41cm	30cm	182 μ	364 μ
SYSTEM 4	20.32cm	$\approx 70^o$	$\approx 20^o$	50.79cm	17.9cm	47.5cm	415 μ	830 μ
SYSTEM 5	10.16cm	$\approx 36^o$	$\approx 54^o$	50.81	41cm	30cm	182 μ	364 μ
SYSTEM 6	10.16cm	$\approx 36^o$	$\approx 54^o$	50.81	41cm	30cm	182 μ	364 μ

WHERE:

r = RADIUS OF WHEEL USED AS OBJECT

θ = ANGLE BETWEEN b AND a

δ = ANGLE BETWEEN a AND PERPENDICULAR LINE TO y AXIS (i.e., TANGENT TO ELLIPSE AT POINT Q)

a = SEMI-MAJOR AXIS OF ELLIPSE

b = SEMI-MINOR AXIS OF ELLIPSE

d = SEPARATION DISTANCE FROM ORIGIN TO EITHER FOCI

$\Delta x \lambda/8 = \frac{\lambda}{8}$ PATH LENGTH CHANGE OF FRONT ILLUMINATION ARM FROM LASER TO HOLOGRAM

$\Delta x \lambda/2 = \frac{\lambda}{2}$ PATH LENGTH CHANGE OF FRONT ILLUMINATION ARM FROM LASER TO HOLOGRAM

(SYSTEMS 5 AND 6 IDENTICAL EXCEPT FOR PERIPHERY OF WHEEL, SEE TEXT)

TABLE III. SUMMARY OF EXPERIMENTAL RESULTS AND PARAMETERS

SYSTEM	$\bar{S}_i$(cm)	$\bar{S}_{0_i}$	$\Delta x_{i(\mu)}$	V_i(cm/sec)	θ(o)	δ(o)	d(cm)	a(cm)	$\frac{(cm)^2}{\frac{a1/2}{\cos\theta}}$
H-1	8.955	1							
H-2	5.895	0.658	128	52	36o	54°	15	25.4	6.22
H-3	5.330	0.595	257	102					
H-4	4.625	0.516	715	286					
H-5	6.380	1							
H-6	5.530	0.867	255	102					
H-7	4.950	0.776	438	175					
H-8	3.885	0.609	875	350	70°	20°	50	53.3	21.35
H-9	4.160	0.652	715	286					
H-10	2.120	0.332	2,250	900					
H-11	1.070	0.168	4,240	1696					
H-12	6.320	0.991	0.424	1696					
H-13	11.235	1							
H-14	8.455	0.752	182	73	36°	54°	30	50.81	8.81
H-15	6.030	0.537	364	146					
H-16	6.350	1							
H-17	4.930	0.776	438	174	70°	70°	47.5	50.79	20.89
H-18	3.873	0.609	875	348					
H-19	4.503	1							
H-20	3.003	0.667	4.4	17,546	36°	54°	30	50.81	8.81
H-21	5.230	1							
H-22	3.402	0.651	4.4	1.75	36°	54°	30	50.81	8.81

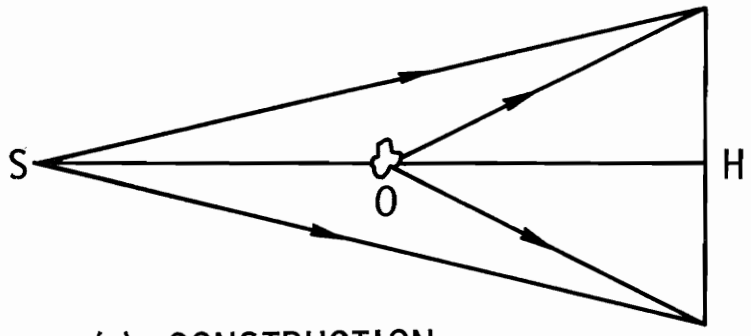

(a) CONSTRUCTION

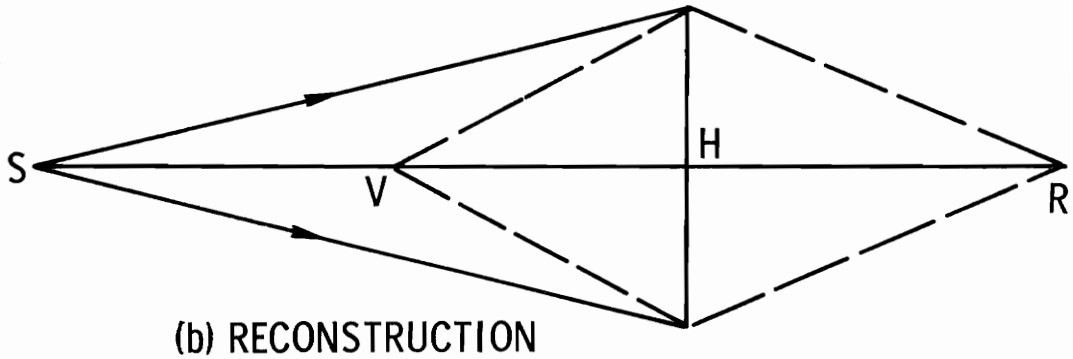

(b) RECONSTRUCTION

FIGURE 1. GABOR IN-LINE HOLOGRAPHY

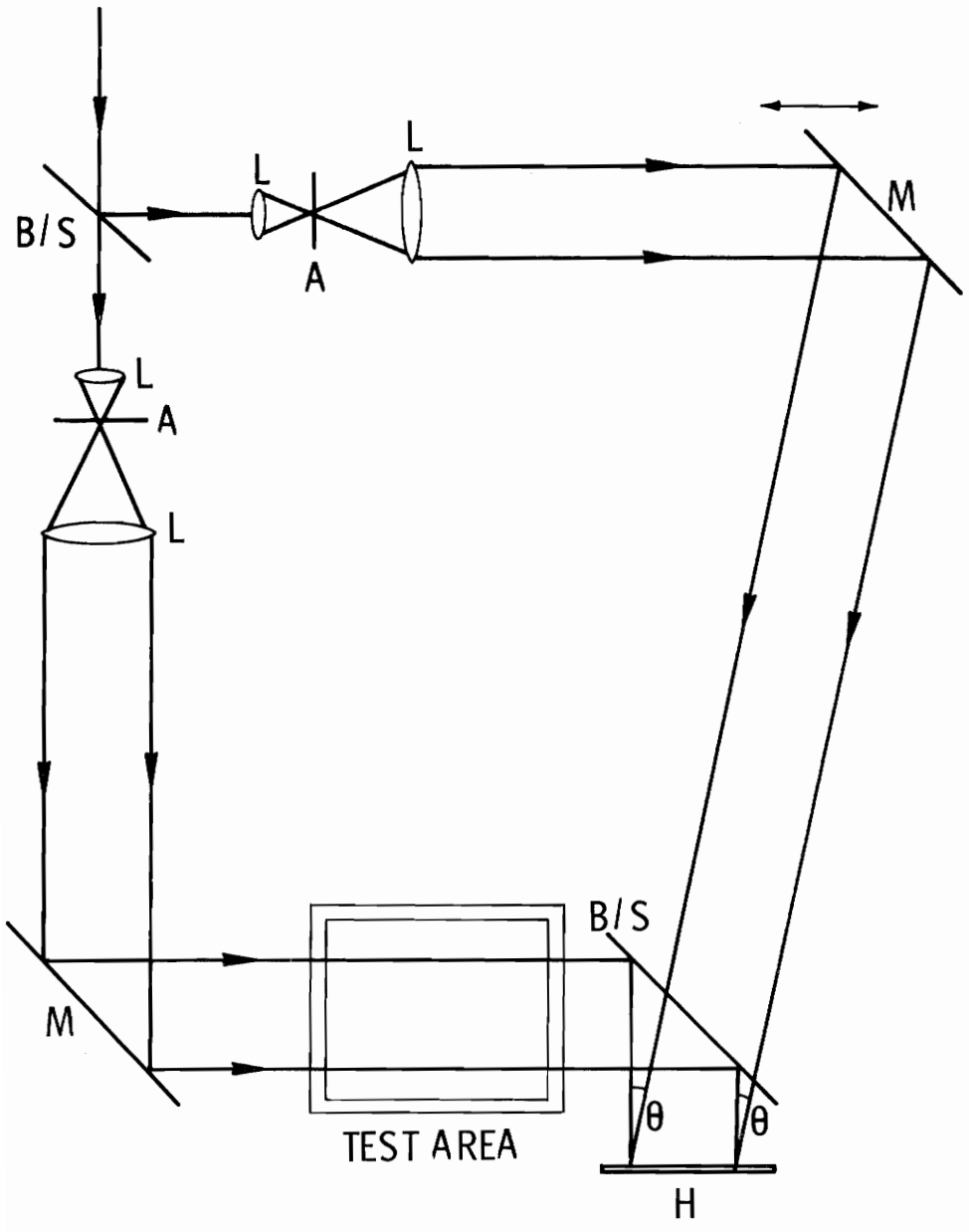

FIGURE 2. DIRECT-TRANSMISSION HOLOGRAPHY

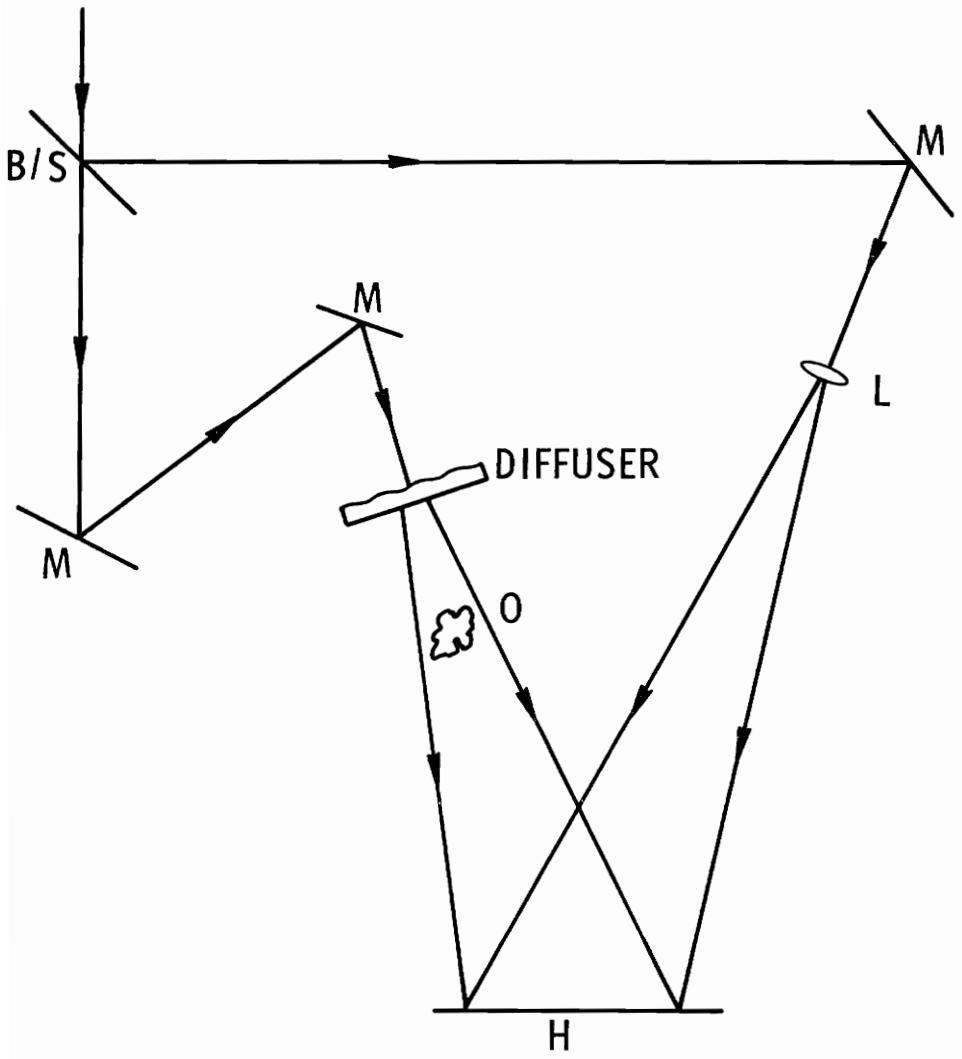

FIGURE 3. DIFFUSE-TRANSMISSION HOLOGRAPHY

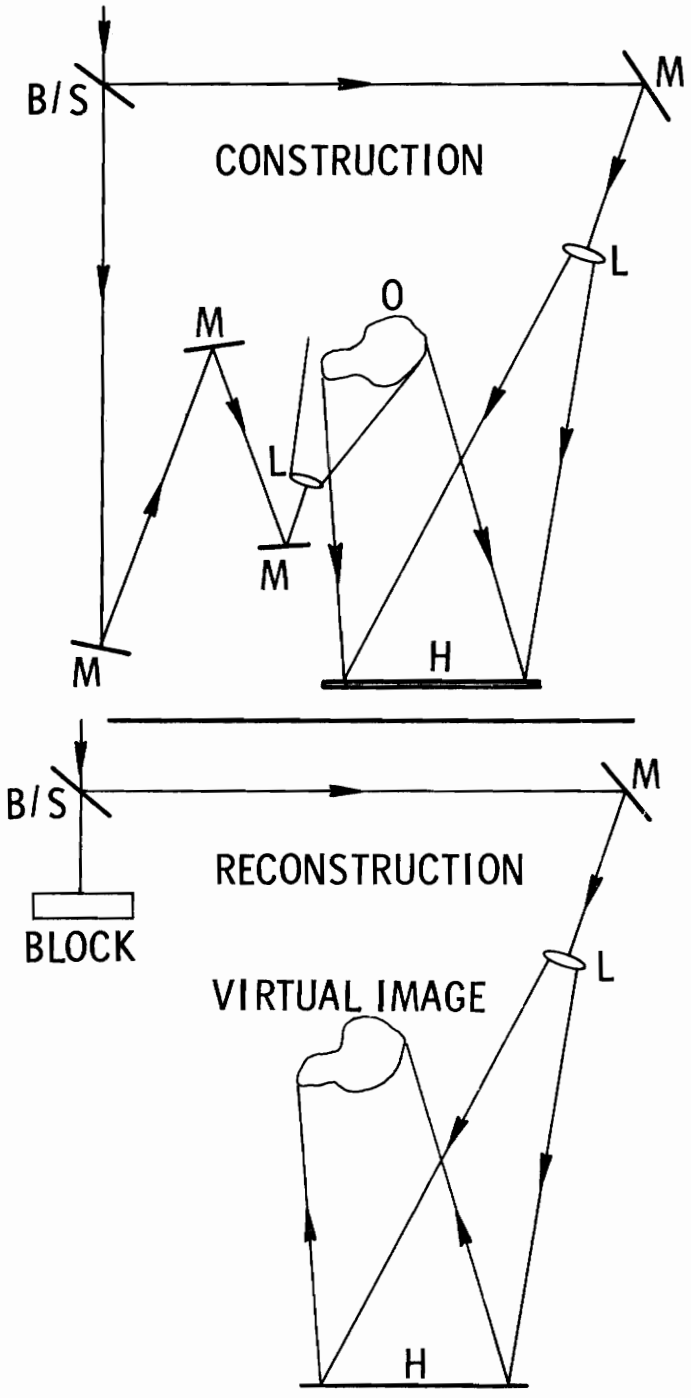

FIGURE 4. FRONT-SURFACE REFLECTION HOLOGRAPHY

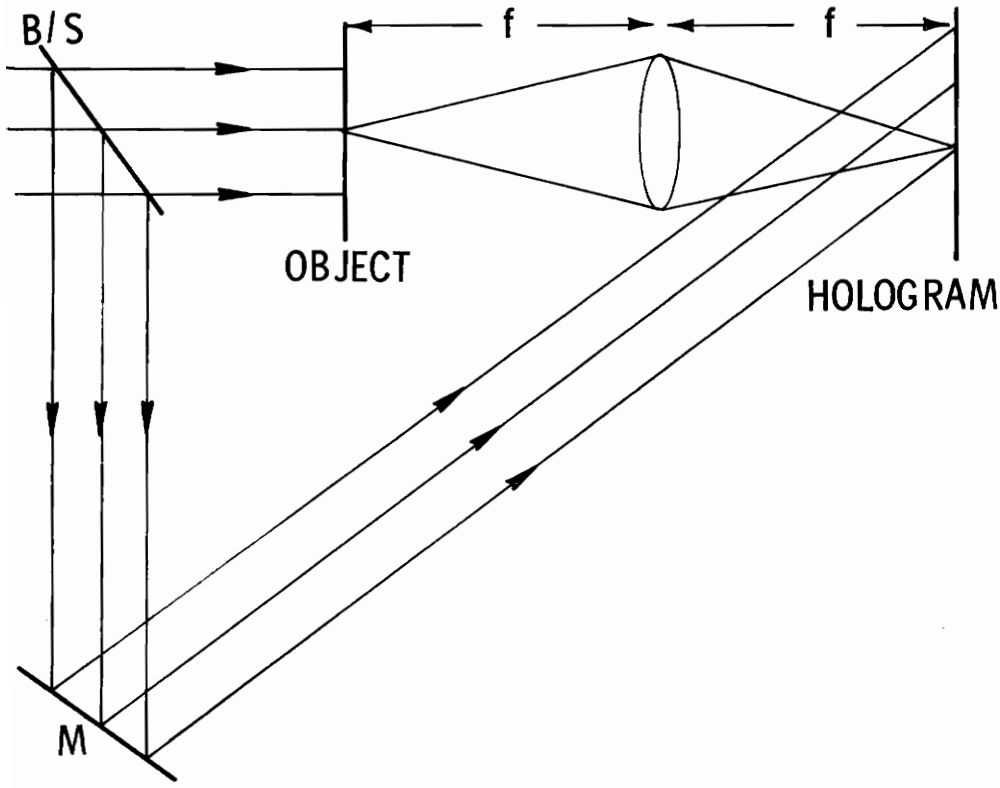

FIGURE 5. FOURIER TRANSFORM HOLOGRAPHY

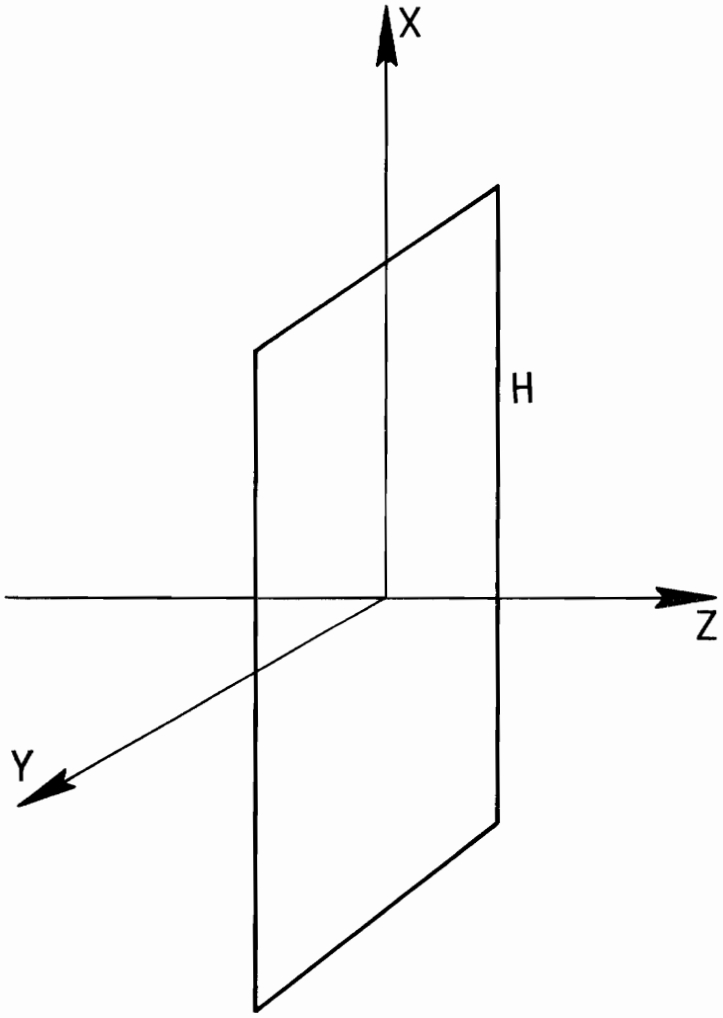

FIGURE 6. HOLOGRAM COORDINATE SYSTEM FOR STATIONARY SCENE

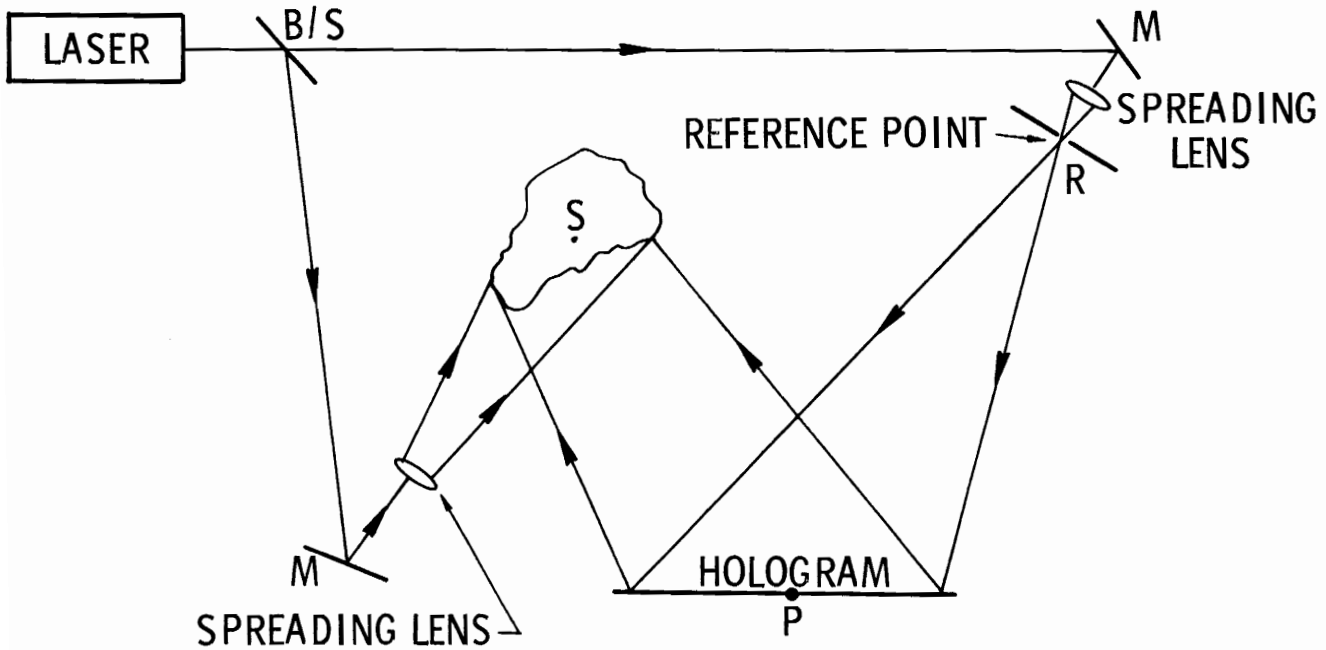

FIGURE 7. TYPICAL CONFIGURATION

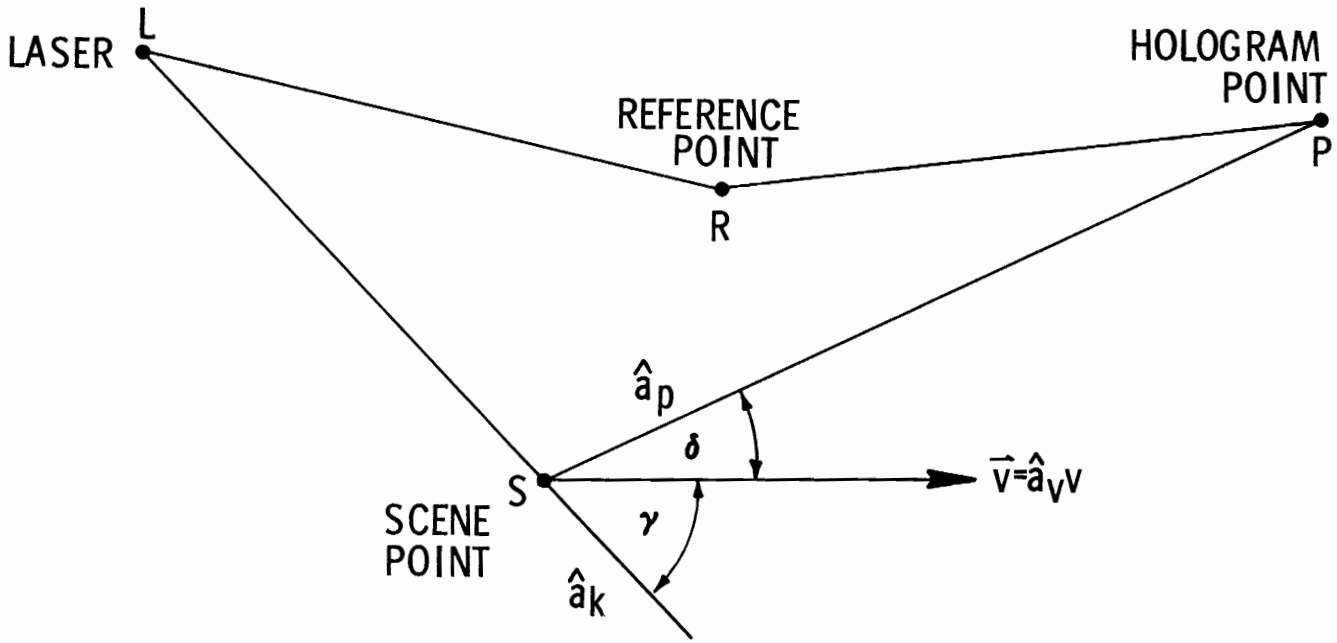

FIGURE 8. GENERAL GEOMETRY FOR SCENE-ORIENTED COORDINATES

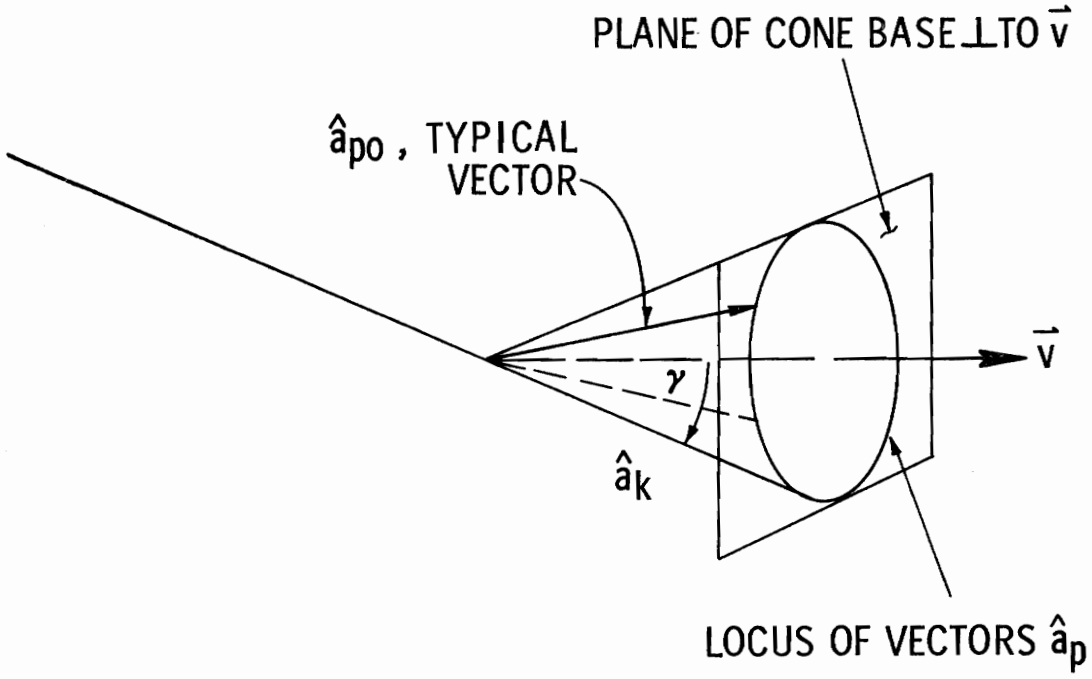

FIGURE 9. CONE OF CONSTANT FRINGE CONTRAST

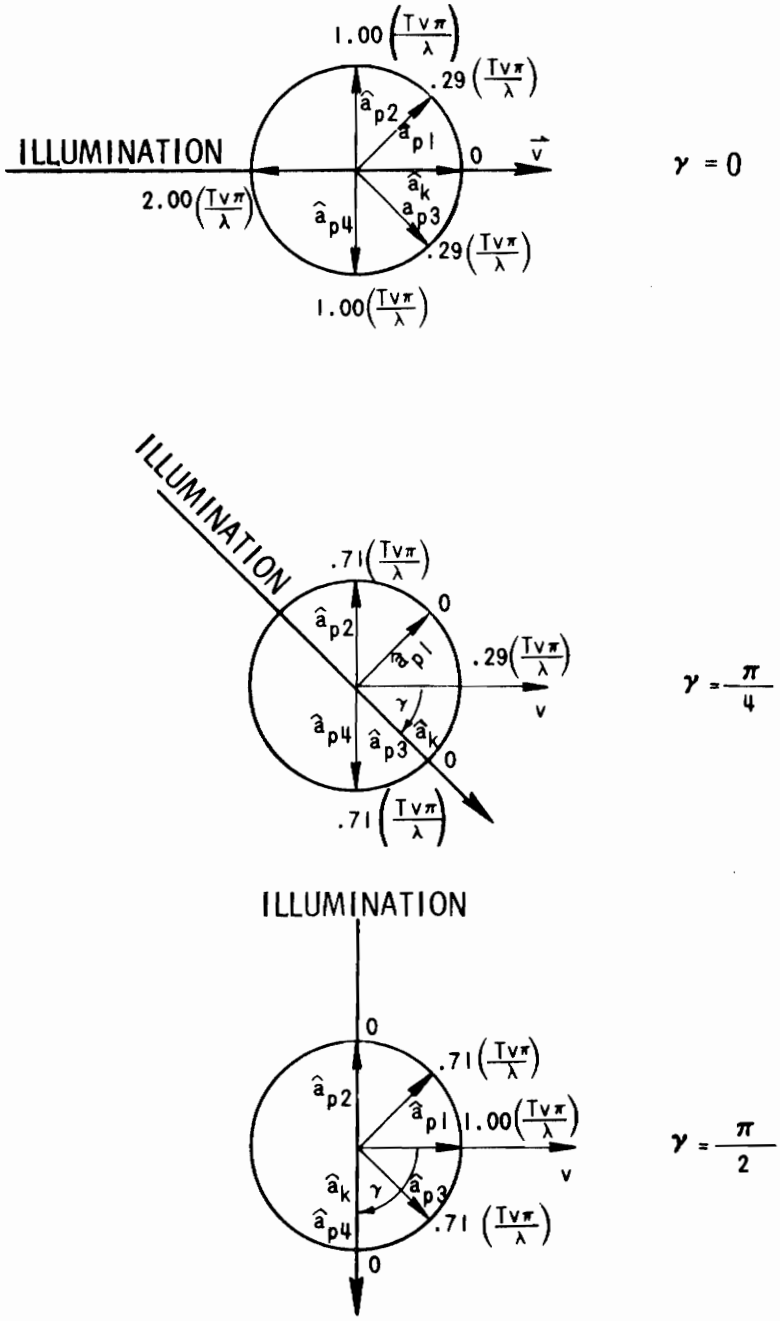

FIGURE 10. VARIATION OF SINC FUNCTION ARGUMENT WITH ILLUMINATION DIRECTION

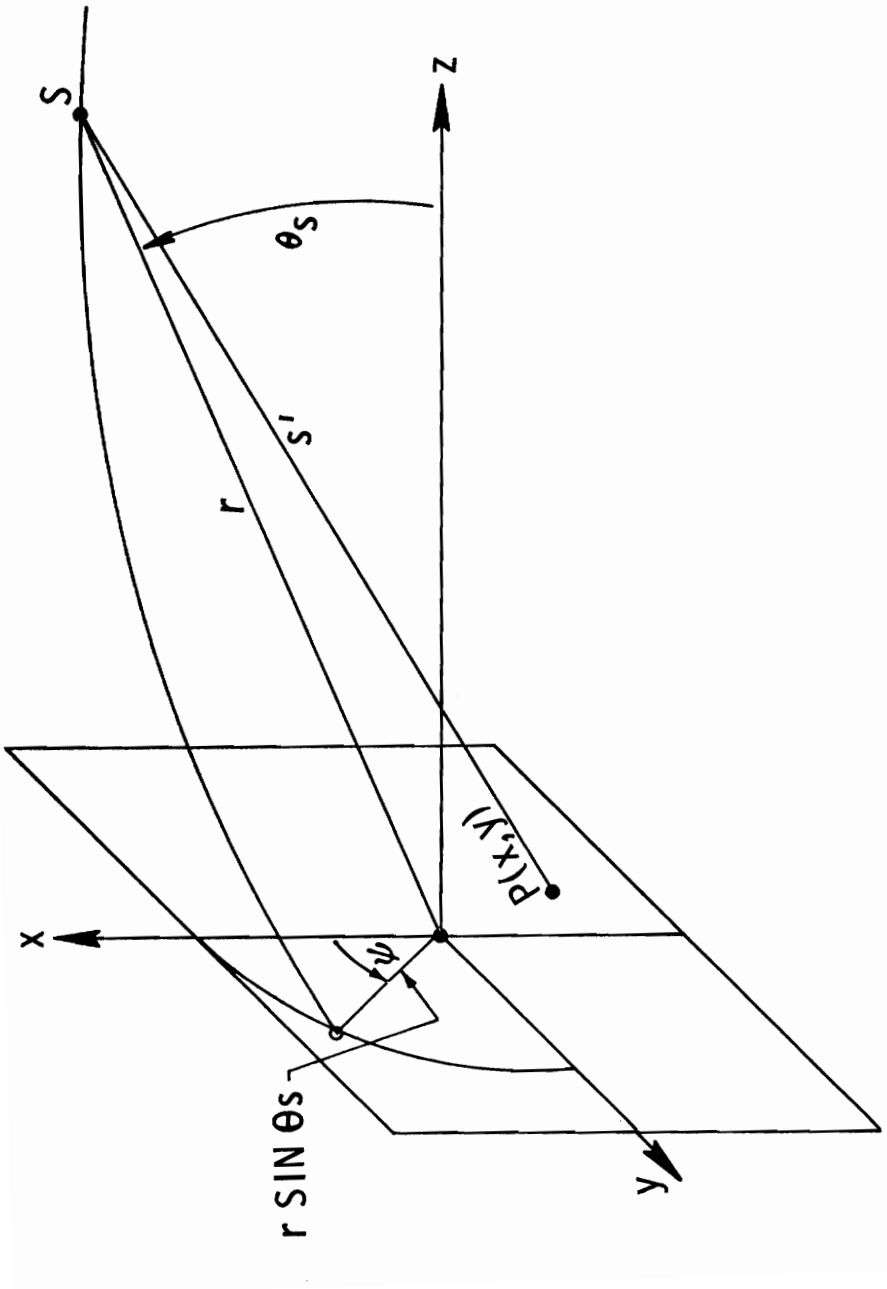

FIGURE 11. HOLOGRAM-ORIENTED COORDINATE SYSTEM

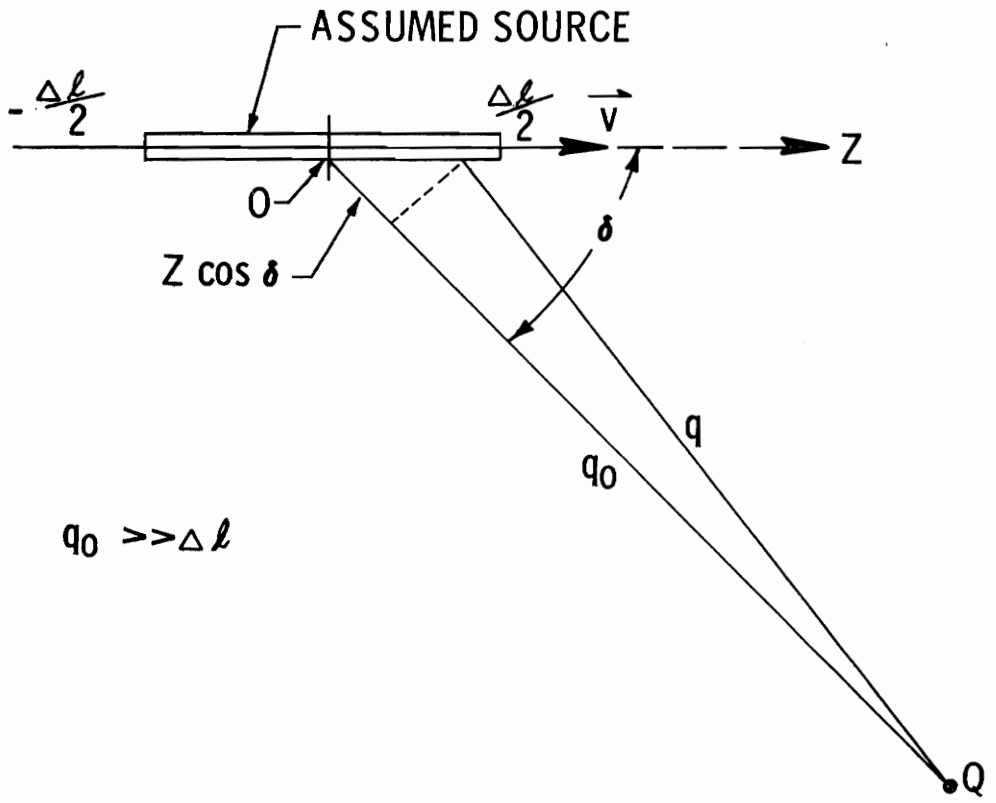

FIGURE 12. GEOMETRY FOR RECONSTRUCTION ANALYSIS

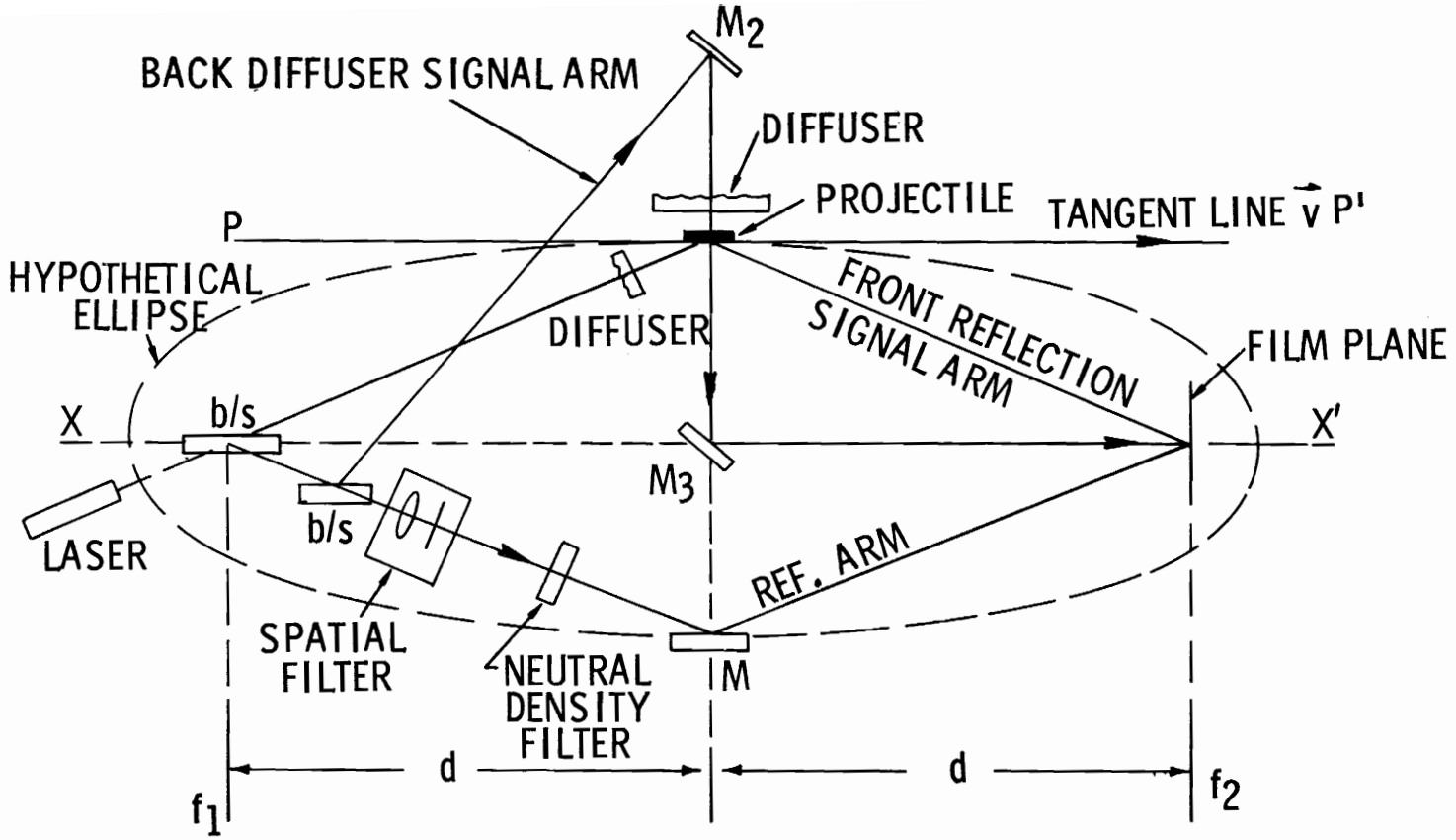

FIGURE 13. HYBRID HOLOGRAPHY SYSTEM WITH AN ELLIPTIC ORIENTATION

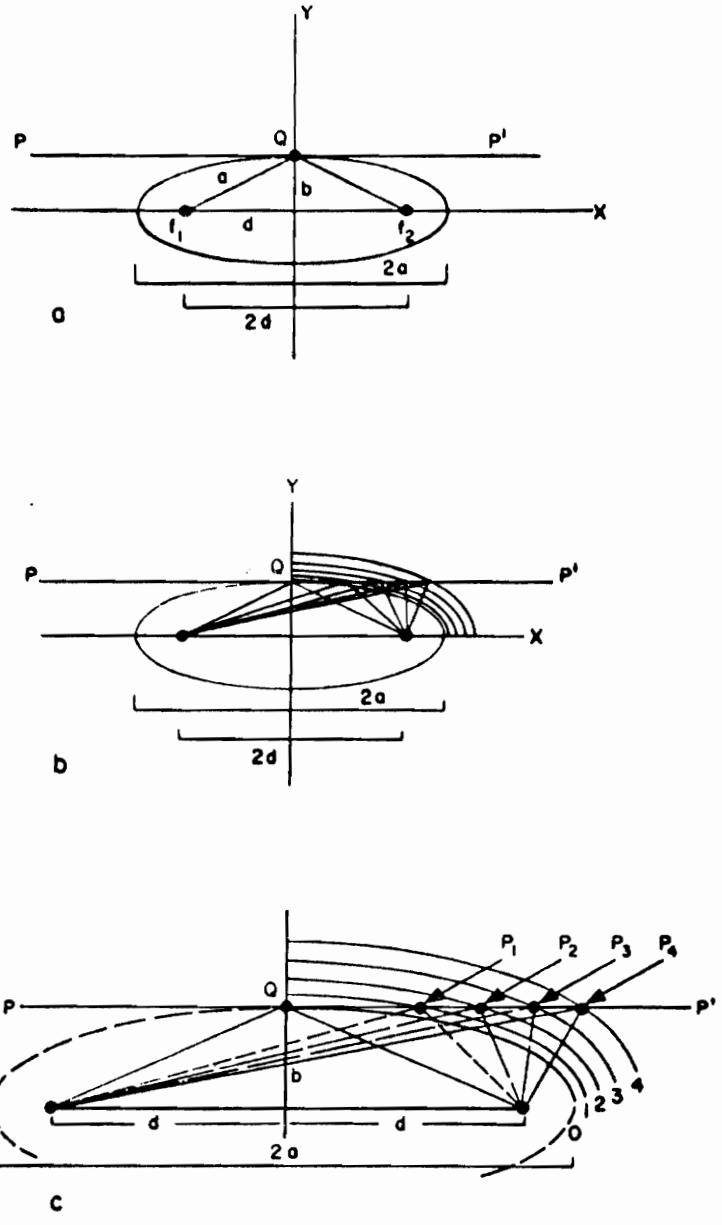

FIGURE 14. FAMILY OF SUCCESSIVE ELLIPSES WITH CONSTANT SEPARATION OF FOCI 2d

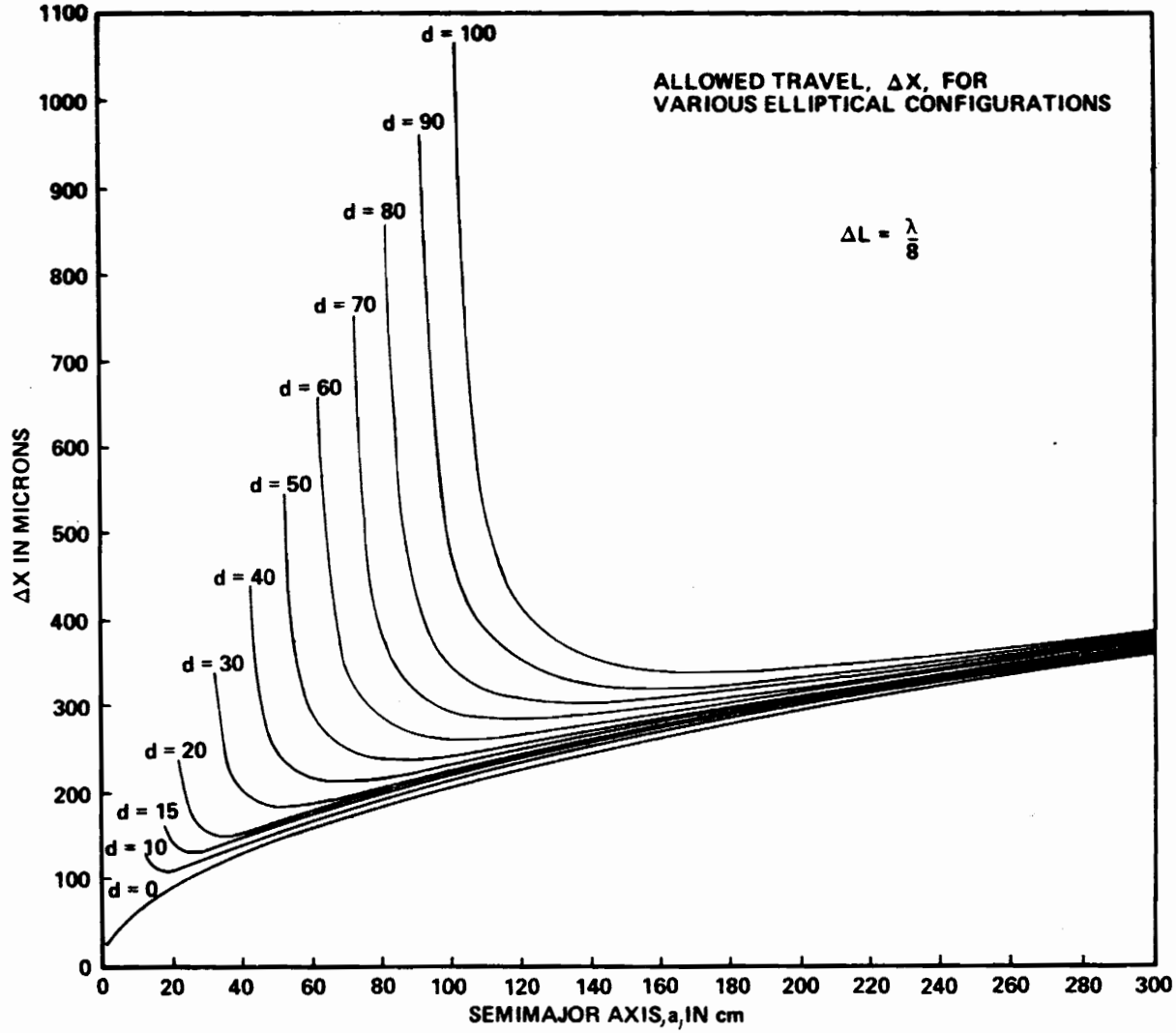

FIGURE 15. ALLOWED TRAVEL, ΔX, FOR VARIOUS ELLIPTICAL CONFIGURATIONS

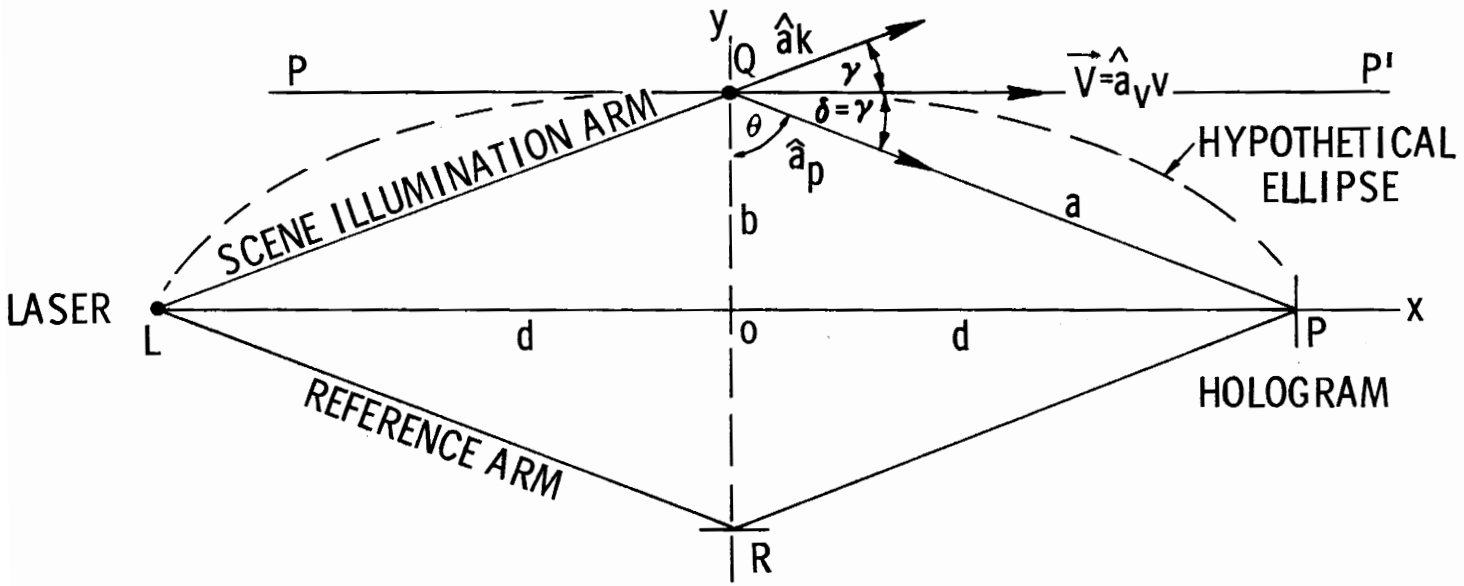

FIGURE 16. TYPICAL ELLIPTICAL CONFIGURATION

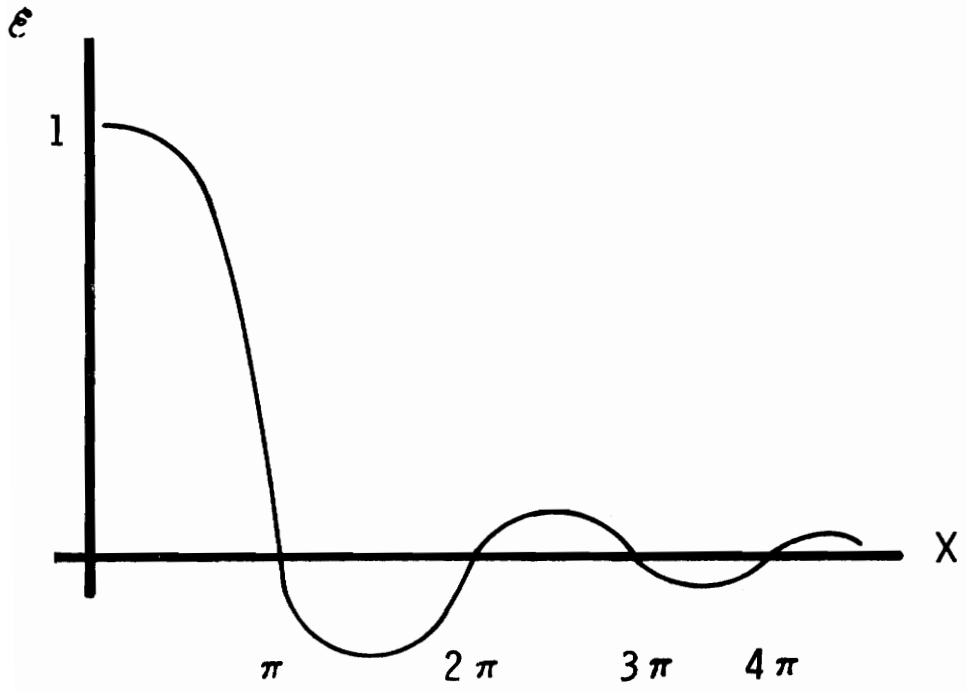

FIGURE 17. PLOT OF SINC $X = \frac{\sin X}{X}$

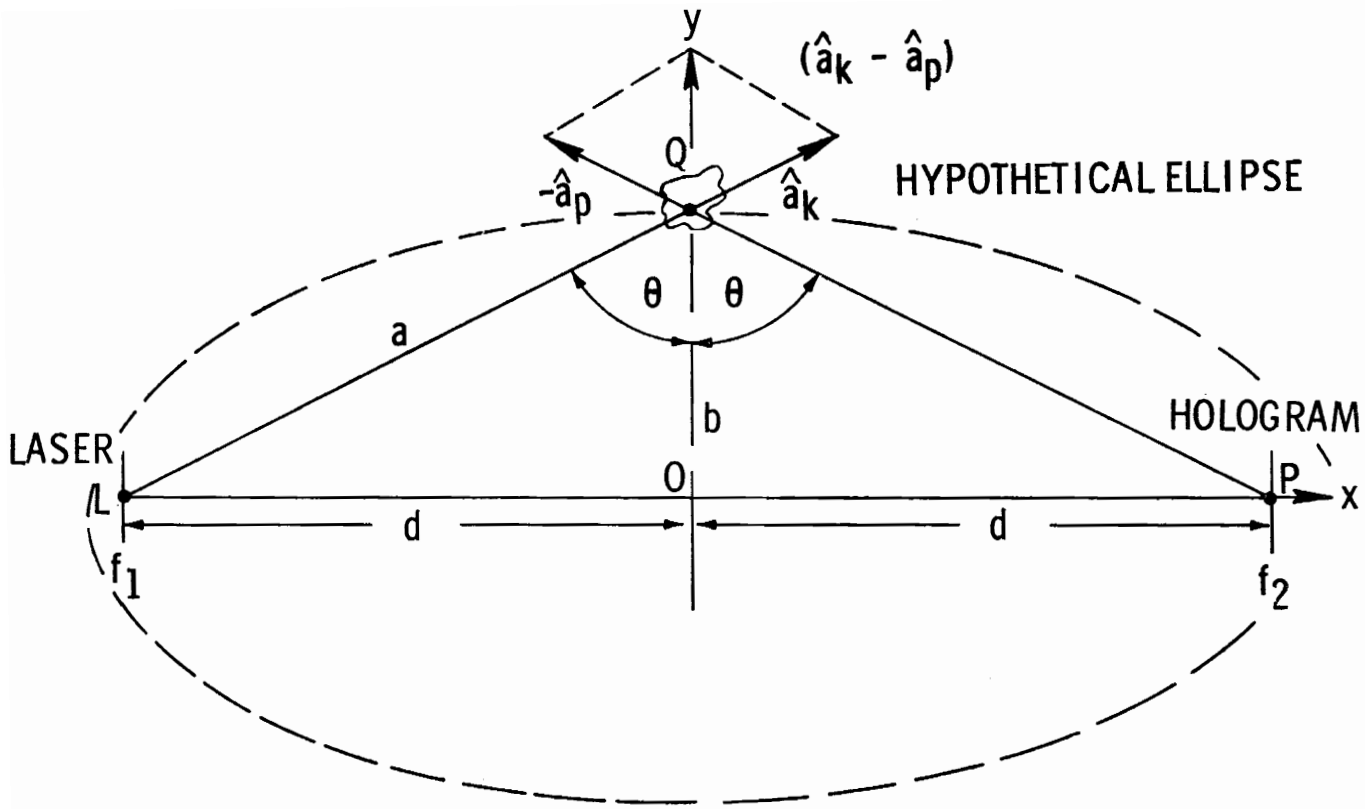

FIGURE 18. DIAGRAM FOR $\vec{V}_{||}$ COMPUTATION

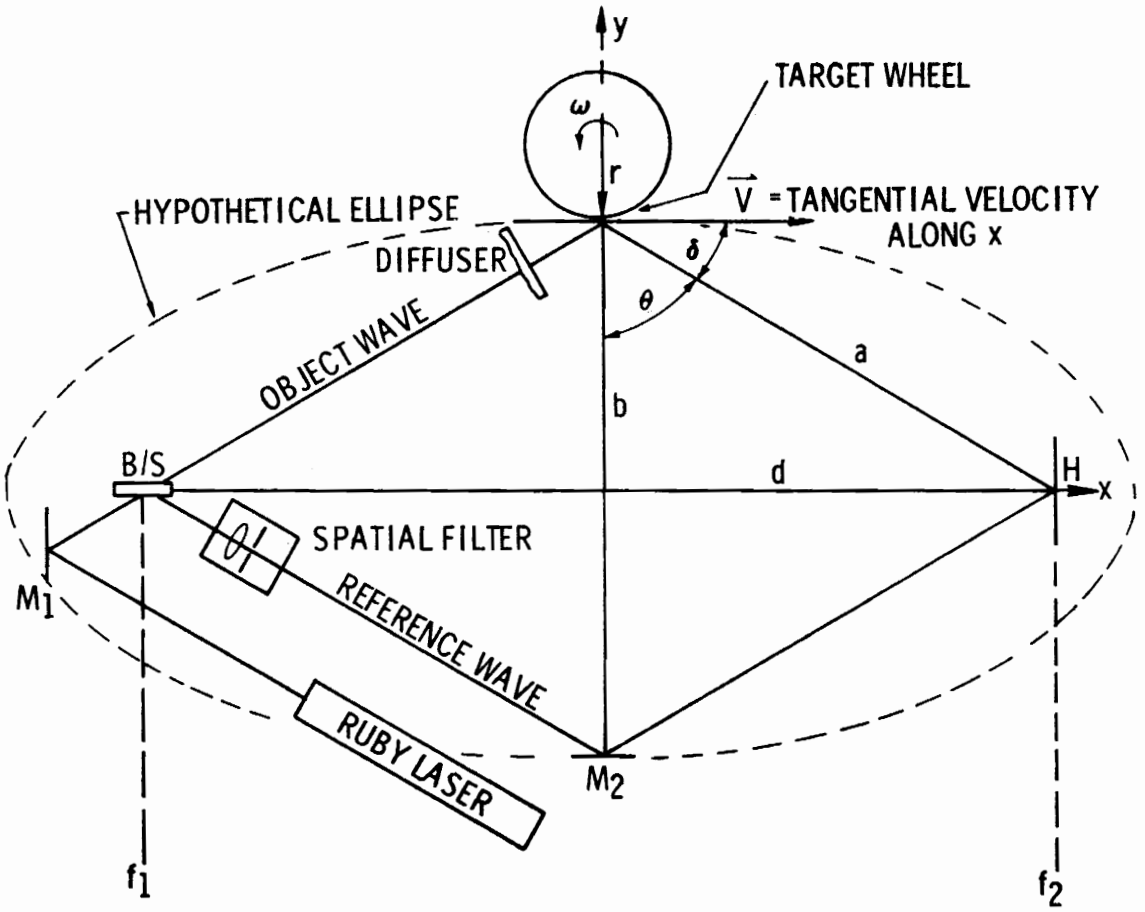

FIGURE 19. GENERAL CONFIGURATION

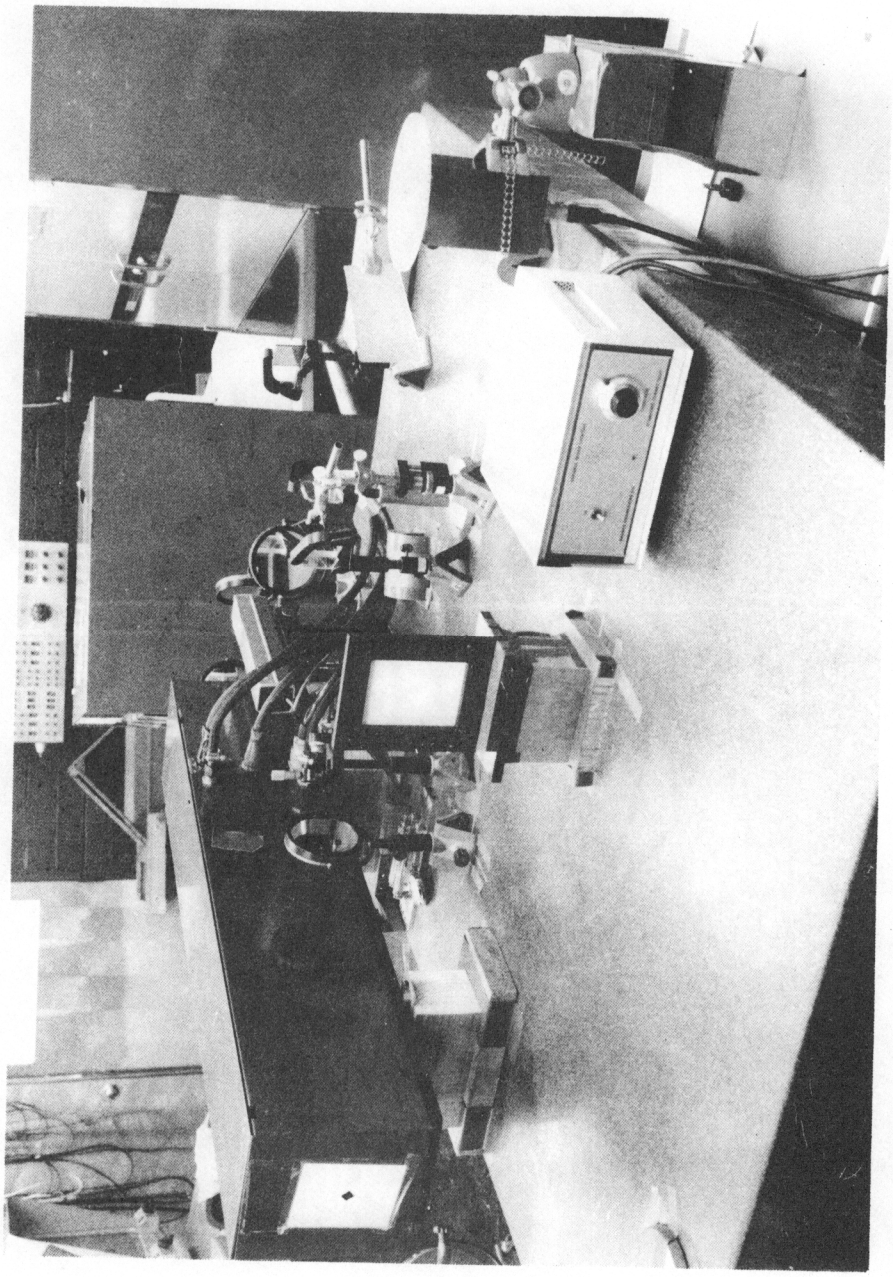

FIGURE 20. PHOTOGRAPH OF SYSTEM SHOWING WHEEL POSITION

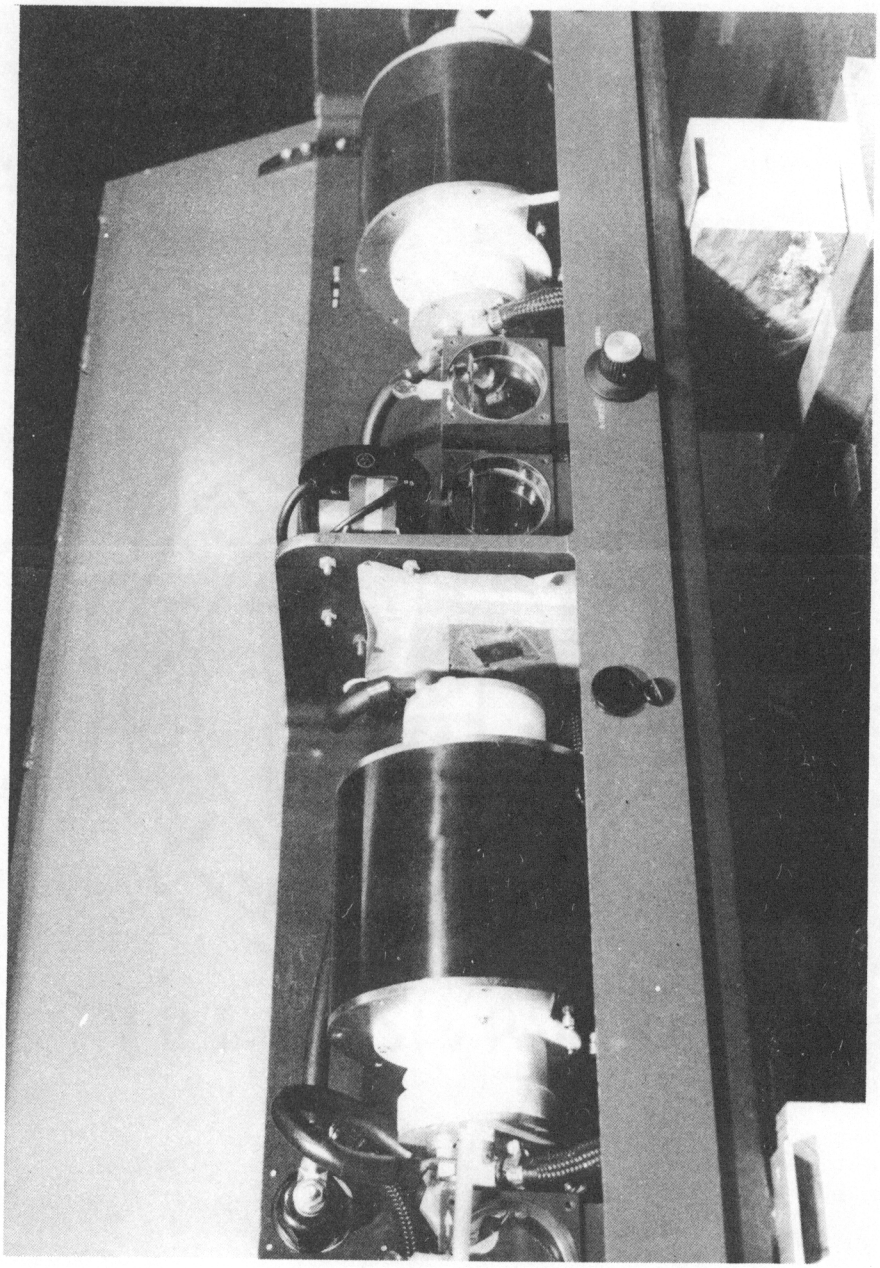

FIGURE 21. PHOTOGRAPH OF RUBY LASER SYSTEM

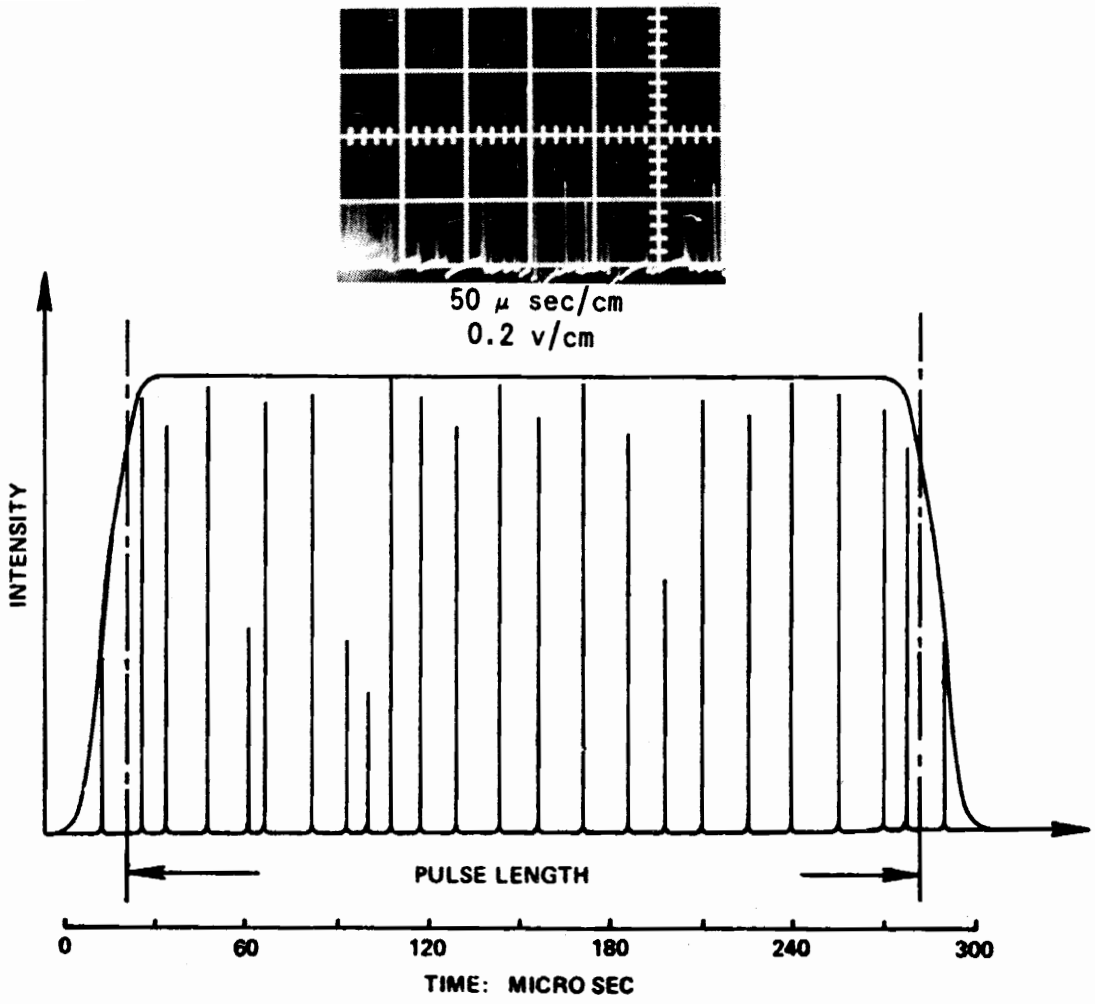

FIGURE 22. GRAPHICAL DESCRIPTION AND PHOTOGRAPH OF NORMAL MODE PULSE

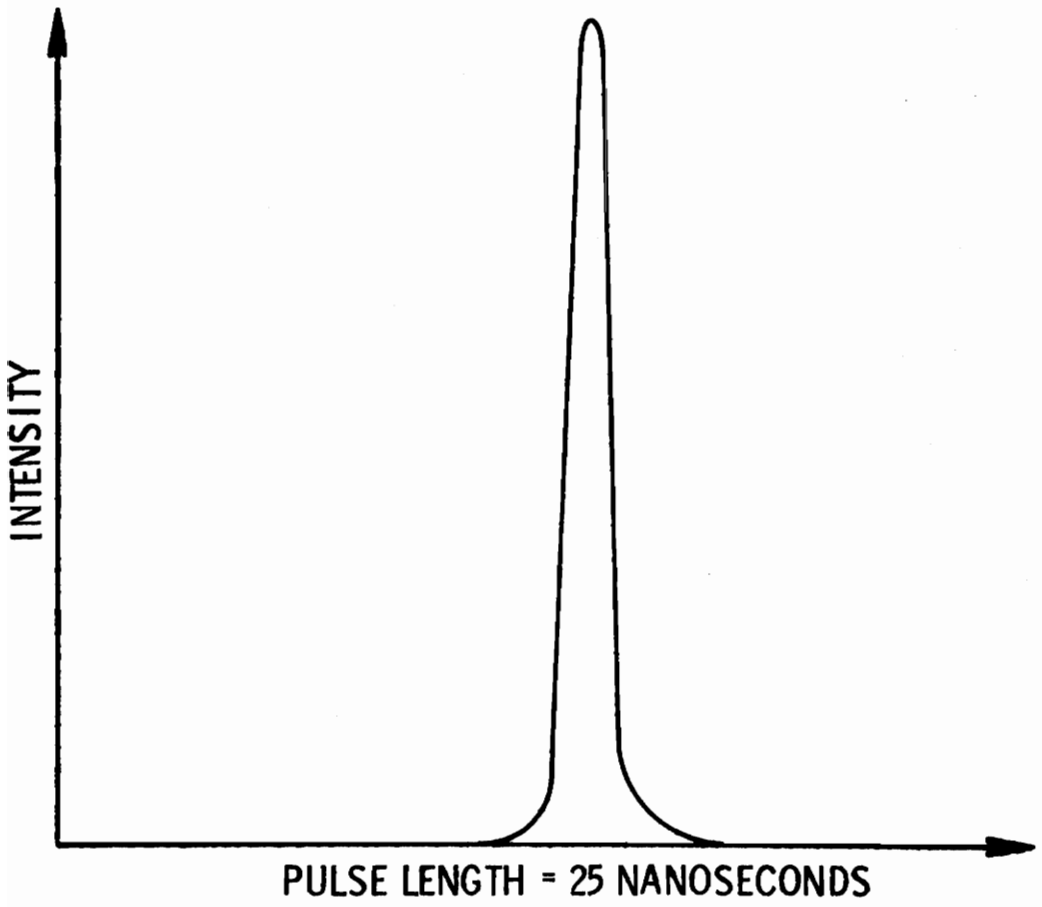

FIGURE 23. GRAPHICAL DESCRIPTION OF Q-SPOIL PULSE

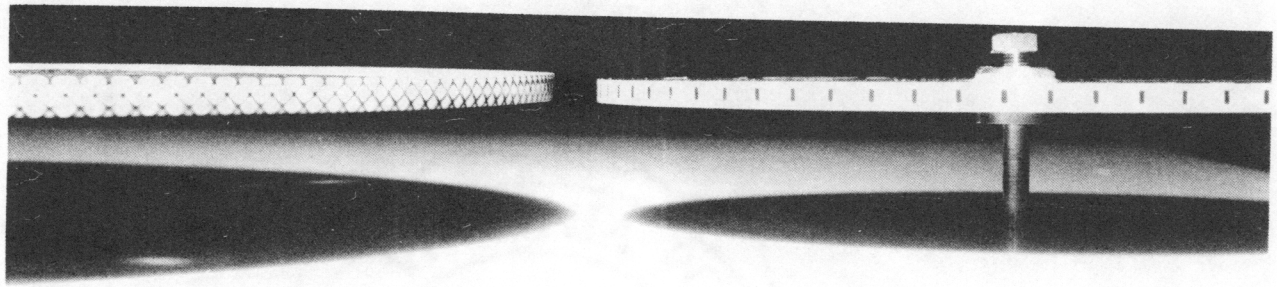

Close-Up View of Wheels' Edges

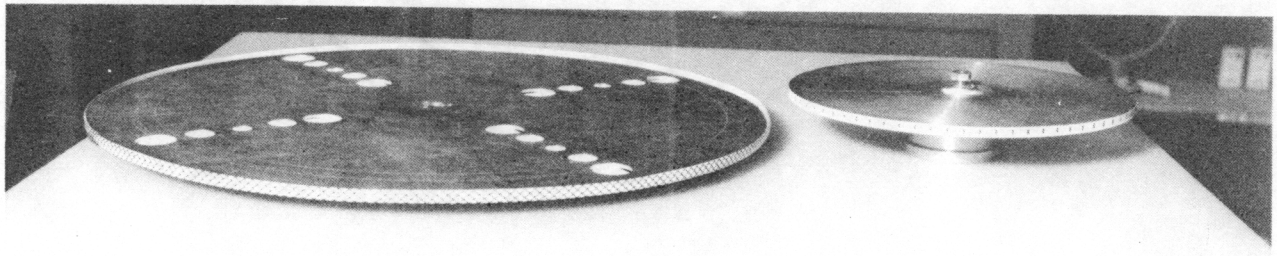

FIGURE 24. PHOTOGRAPHS OF TWO DIFFERENT RADII TARGET WHEELS

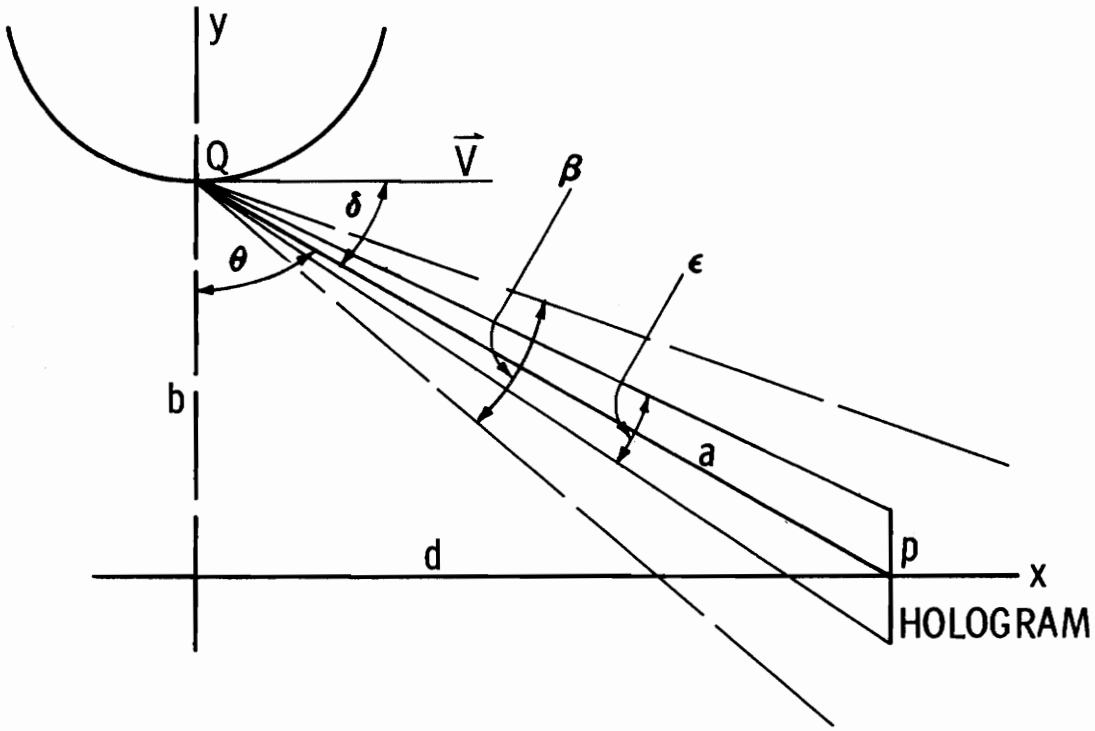

FIGURE 25. SCHEMATIC OF SCATTERED RADIATION

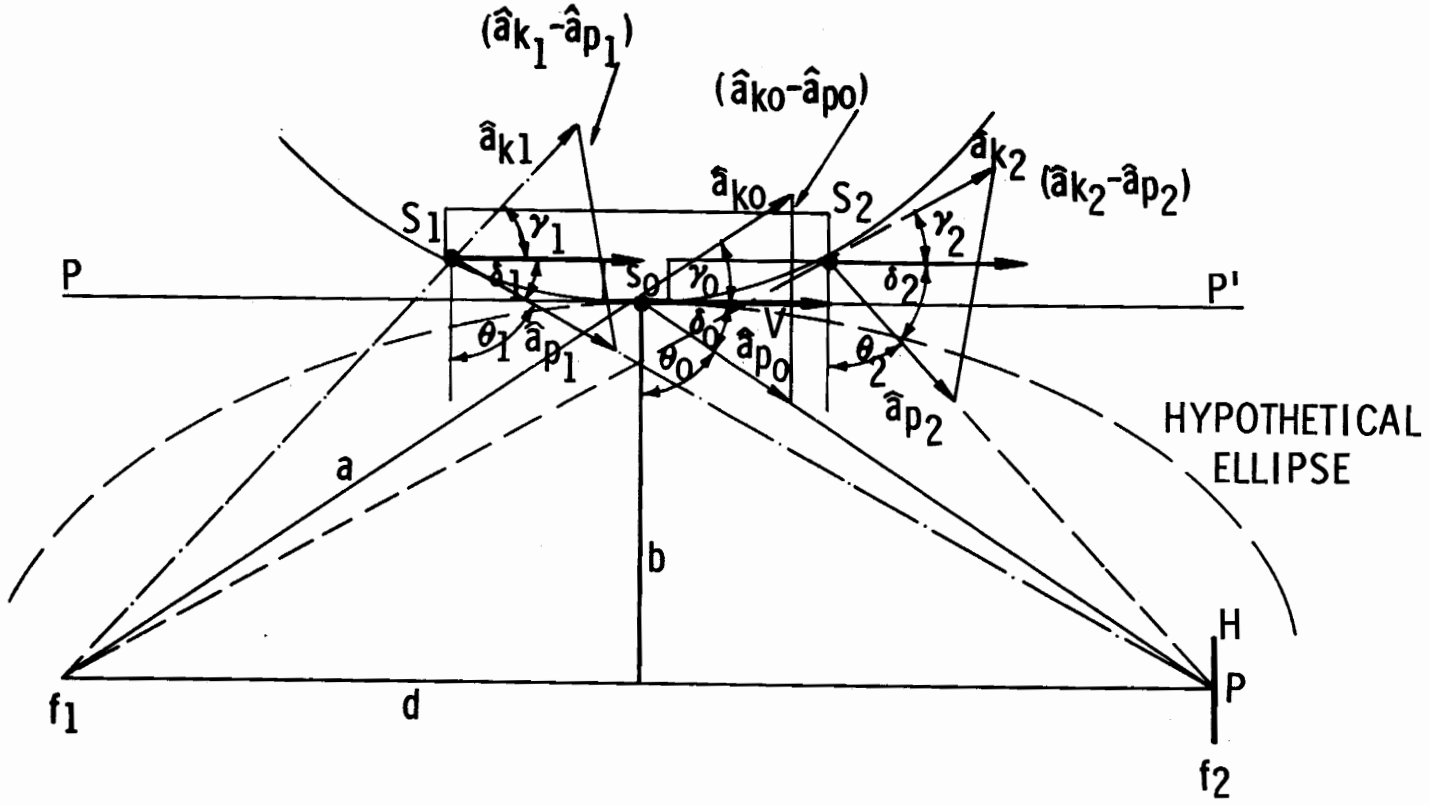

FIGURE 26. VARIATION OF SINC FUNCTION DUE TO TARGET GEOMETRY

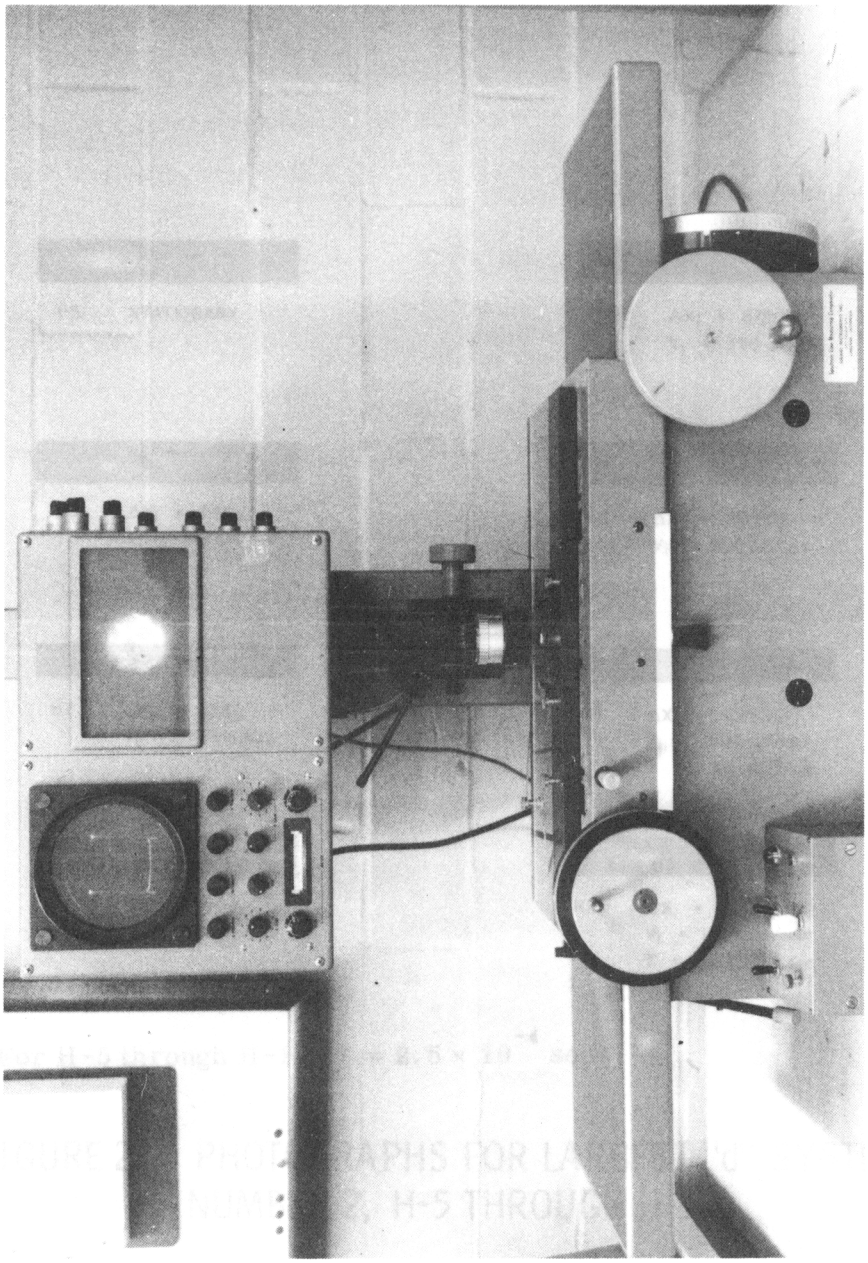

FIGURE 27. PHOTOGRAPH OF SPECTRUM LINE COMPARATOR

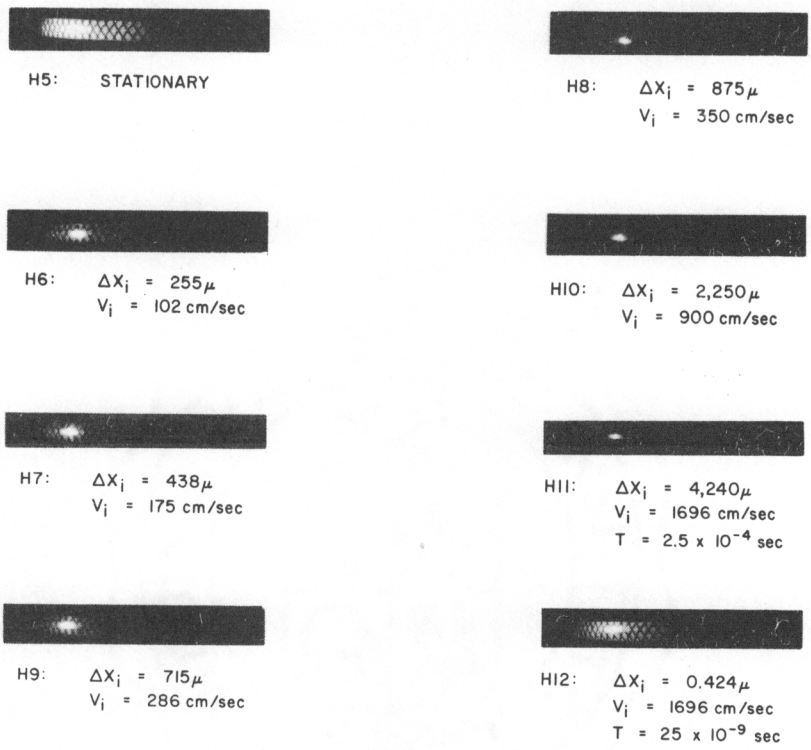

Note: For H-5 through H-11, $\tau = 2.5 \times 10^{-4}$ sec.

FIGURE 28. PHOTOGRAPHS FOR LARGEST "d" SYSTEM NUMBER 2, H-5 THROUGH H-12

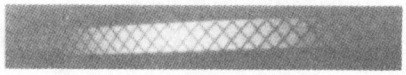

H1: STATIONARY

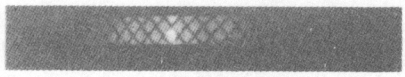

H2: $\Delta X_i = 128\mu$
$V_i = 52$ cm/sec

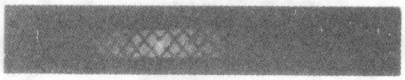

H3: $\Delta X_i = 257\mu$
$V_i = 102$ cm/sec

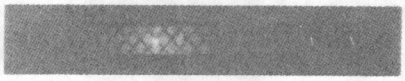

H4: $\Delta X_i = 715\mu$
$V_i = 286$ cm/sec

Note: $\tau = 2.5 \times 10^{-4}$ sec.

FIGURE 29. PHOTOGRAPHS FOR SMALLEST "d" SYSTEM NUMBER 1, H-1 THROUGH H-4

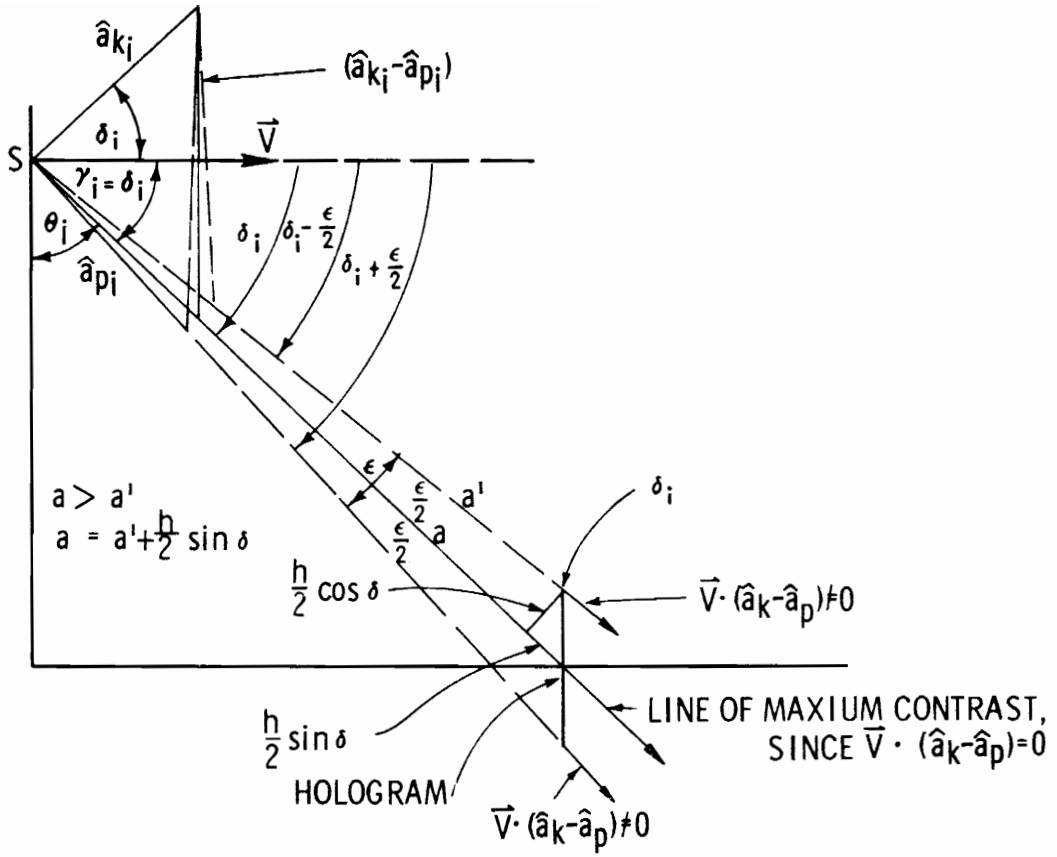

FIGURE 30. RELATION BETWEEN PARAMETERS a, ϵ, AND VARIATION OF SINC FUNCTION

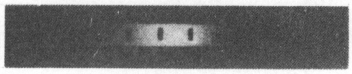

H19: STATIONARY

H20: $\Delta X_i = 4.4\mu$
$V_i = 1.7546 \times 10^{4}$ cm/sec
$T = 25 \times 10^{-9}$ sec

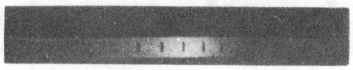

H21: STATIONARY

H22: $\Delta X_i = 4.4\mu$
$V_i = 1.76$ cm/sec
$T = 2.5 \times 10^{-4}$ sec

FIGURE 31. PHOTOGRAPHS FOR SYSTEMS NUMBERS 5 AND 6

REFERENCES

1. Born, M., and Wolf, E. Principles of Optics. New York and London: Pergamon Press, 1967, Third Edition.

2. Brooks, R. E., Heflinger, L. O., et. al. Holographic Photography of High-Speed Phenomena with Conventional and Q-Switched Ruby Laser." Applied Physics Letters, Vol. 7, No. 4, August, 1965.

3. Brooks, R. E., Heflinger, L. O., et. al. "Interferometry with a Holographically Reconstructed Comparison Beam." Applied Physics Letters, Vol. 7, No. 9, November, 1965.

4. Chau, Henry H. M., and Horman, Melvin H. "Demonstration of the Application of Wavefront Reconstruction to Interferometry." Applied Optics, Vol. 5, No. 7, July, 1966.

5. De Bitetto, D. J. On the Use of Moving Scatterers in Conventional Holography. Philips Laboratories, Briarcliff Manor, New York, January, 1966.

6. Dotson, William P., Jr. In Effect of Object Motion in Fraunhofer Holography with Application to Velocity Measurements. NASA TN 9637 report, Washington, D. C., November, 1969.

7. Dyes, W. A., Kellen, P. F., et. al. "Velocity Synchronized Fourier Transform Hologram Camera System." Applied Optics, Vol. 9, No. 5, May, 1970.

8. Falconer, David G. "Role of the Photographic Process in Holography." Photographic Science and Engineering, Vol. 10, No. 3, May-June, 1966.

9. Goodman, J. W., and Knight, G. R. "Effects of Film Nonlinearities on Wavefront-Reconstruction Images of Diffuse Objects." Journal of the Optical Society of America, Vol. 58, No. 9, September, 1968.

10. Forney, M. E., Matkin, J. H., et. al. Aerosol Size and Velocity Determination via Holography." The Review of Scientific Instruments, Vol. 40, No. 2, February, 1969.

11. Friesem, A. A., and Zelenka, J. S. "Effects of Film Nonlinearities in Holography." Applied Optics, Vol. 6, No. 10, October, 1967.

REFERENCES (Continued)

12. Goodman, J. W. "Temporal Filtering Properties of Holograms." Applied Optics, Vol. 6, No. 5, May, 1967.

13. Heflinger, L. O., Wuerker, R. F., et. al. "Holographic Interferometry." Journal of Applied Physics, Vol. 37, No. 2, February, 1966.

14. Hilderbrand, B. P. A General Analysis of Contour Holography. February, 1968, NASA Acquisition No. AD 828 931.

15. Horman, Melvin H. "An Application of Wavefront Reconstruction to Interferometry." Applied Optics, Vol. 4, No. 3, March, 1965.

16. Kurtz, Robert L. Multiple Image Storing System for High Speed Projectile Holography. August 1969, NASA Case No. MFS-20596.

17. Kurtz, R. L., and Norden, B. N. Hybrid Holographic System. U. S. Patent No. 3,535,014, November, 1970.

18. Kurtz, R. L., and Loh, H. Y. "A Holographic Technique for Recording a Hypervelocity Projectile with Front Surface Resolution." Applied Optics, Vol. 9, No. 5, May, 1970.

19. La Macchia, J. T., and Bjorkholm, J. E. "Resolution of Pulsed Laser Holograms." Applied Physics Letters, Vol. 12, No. 2, January, 1968.

20. Lehmann, Matt. Photography for Optical Measurements. Stanford University, Palo Atto, California, April, 1967.

21. Leith, Emmett N., and Upatnieks, Juris. "Reconstructed Wavefronts and Communication Theory." Journal of the Optical Society of America, Vol. 52, No. 10, October, 1962.

22. Leith, Emmett N., and Upatnieks, Juris. "Wavefront Reconstruction with Diffused Illumination and Three-Dimensional Objects." Optical Society of America. Vol. 54, No. 11, November, 1964.

23. Leith, E. N., Upatnieks, J., et. al. "Hologram Visual Displays." Journal of the Society of Motion Picture and Television Engineers, Vol. 75, No. 4, April, 1966.

24. Long, Leslie T., and Parks, John A. "Simple Flash Holography." Applied Optics, Vol. 8, No. 5, May, 1969.

REFERENCES (Concluded)

25. Neumann, Don B. "Holography of Moving Scenes." Journal of the Optical Society of America, Vol. 58, No. 4, April, 1968.

26. Ramberg, E. G. "The Hologram — Properties and Applications." RCA Review, December, 1966.

27. Reynolds, G. O., and DeVelis, J. B. "Hologram Coherence Effects." IEEE Transactions on Antennas and Propagation, Vol. AP-15, No. 1, January, 1967.

28. Rogers, G. L. The Design of Experiments for Recording and Reconstructing Three-Dimensional Objects in Coherent Light (Holography)." Journal of Scientific Instruments, Vol. 43, 1966.

29. Smith, Howard M. Principles of Holography, New York: Wiley Intersciences, 1969.

30. Staselko, D. I., Smirnov, A. G., et. al. Production of High-Quality Holograms of Three-Dimensional Diffuse Objects with the Use of Single-Made Ruby Lasers, March, 1968, Acquisition No. VDC 535.317.1.

31. Stroke, George W. A Reformulated General Theory of Holography, Presented at Symposium of Modern Optics Polytechnic Institute of Brooklyn, March 22-24, 1967.

32. Mees, Kenneth. The Theory of the Photographic Process, New York: The Macmillan Company, 1954.

BIBLIOGRAPHY

Brooks, R. E., Heflinger, et. al. "Holographic Photography of High-Speed Phenomena with Conventional and Q-Switched Ruby Lasers." Applied Physics Letters, Vol. 7, No. 4, August, 1965.

Caulfield, H. J., Lu, Sun, et. al. "Biasing for Single-Exposure and Multiple-Exposure Holography." Letters to the Editor, Applied Optics, Vol. 7, July, 1968.

Collier, Robert J. "Holography and Integral Photography." Physics Today, Vol. 12, July, 1968.

Frecska, Sandor A. "Characteristics of the Agfa-Gevaert Type 10E70 Holographic Film." Applied Optics, Vol. 7, No. 11, November, 1968.

Friesem, A. A., and Zelenka, J. S. "Effects of Film Nonlinearities in Holography. Applied Optics, Vol. 6, No. 10, October, 1967.

Goodman, J. W., Miles, R. B., et. al. "Comparative Noise Performance of Photographic Emulsions in Holographic and Conventional Imagery." Journal of the Optical Society of America, Vol. 58, No. 3, May, 1968.

Goodman, J. W. Film-Grain Noise in Holography. Presented at Symposium on Modern Optics — Polytechnic Institute of Brooklyn, March 22-24, 1967.

Mau, Allan E., and Young, Willard A. "An Electronic Shutter for Holographic Applications." Applied Optics, Vol. 7, No. 7, July, 1968.

Lurie, M. "Effects of Partial Coherence on Holography with Diffuse Illumination." Journal of the Optical Society of America, Vol. 56, No. 10, October, 1966.

Paques, H., and Smigielski, P. Holography. NASA TN-8506, August, 1966.

Pistol kors, A. A. "Resolving Power of a Hologram." Soviet Physics Doklady, Vol. 12, No. 1, July, 1967.

Redman, J. D. "Holographic Velocity Measurement." Journal of Scientific Instruments, Vol. 44, 1967.

BIBLIOGRAPHY (Concluded)

Siebert, L. D. "Front-Lighted Pulse Laser Holography." Applied Physics Letters, Vol. 11, No. 10, November, 1967.

Trolinger, J. D., Farmer, W. M., et. al. "Multiple Exposure Holography of Time Varying Three-Dimensional Fields." Applied Optics, Vol. 7, August, 1968.

APPENDIX. THE ROLE OF PHOTOGRAPHY IN THE HOLOGRAPHIC PROCESS

One of the most important elements in the holographic process is the photographic emulsion or the various recording media in which the interference pattern is stored. A replica of this interference pattern produced by the scattered wave from the object and the coherent reference wave must exist as detectable changes in some physical medium to constitute a hologram. In most cases the interference pattern is recorded in the medium in one of two forms: (1) an optical density pattern in which the material is absorptive and the hologram recorded is a density grating that diffracts light by modulating the intensity of the reconstruction beam (this is the most commonly used in Fresnel or Fraunhofer types of holography, although its diffraction efficiency is ≤ 4 percent), or (2) as a phase-shift pattern, in which the material is nonabsorptive or phase only, and the hologram has a uniform optical density. The phase variation of the recording media diffracts light just as a phase grating. For phase-only materials, the required phase shift of the reconstruction wave is provided through the local variations in the thickness and or the refractive index of the recording medium.

Among the various recording media used for the holographic recordings are (8):

1. Photographic Emulsions. These emulsions are basically absorptive media. However, they can be bleached with ammonia, after proper development, and the phase-only term will remain.

2. Photochromic Materials. These have the economic advantage that they can be erased and used again and again. The materials contain absorptive color centers and most of them are sensitive only in the shorter wavelength region of the visible spectrum and in the ultraviolet. These usually have high resolution capabilities and low scattering noise; yet, they have low sensitivity.

3. Photopolymer Materials. These include photosensitive resist and other organic materials that have the property of changing from monomer to polymer because of exposure to light. After exposure, the materials show either a differential index of refraction or a differential solubility to a solvent. Therefore, holograms recorded on these materials are phase-only holograms. With certain materials, holograms can be recorded without the need for chemical development and fixing; therefore, this process has the advantage of real-time holography.

4. Thermoplastic Materials. These materials respond to an electrostatic force and form a phase image from the charge-induced deformation. These are said to have high sensitivity and low scattering noise.

5. Dichromate Sensitized Gelatin. These are materials that are believed to be sensitized by a process of reducing the dichromat ion Cr^{+6} to Cr^{+3} by exposure to light to form a complex that hardens the gelatin. A phase image is formed by dissolving the unhardened gelatin.

6. Electrooptical Crystals. The first crystal used for hologram storage was lithium niobate. A suitably intense beam from an argon laser

produces refractive index changes in the crystal. Erasure of the hologram is achieved by heating the crystal to 170° C and the crystal can be reused.

Table A-I provides a summary of the recording media used in holography.

Since photographic emulsions are the most commonly used recording medium for holography, we will now discuss this medium in some detail.

Probably the two main properties that made a photographic material suitable for holography are its color sensitivity and its resolving power. In order to record the laser radiation, the photographic emulsion must, of course, be sensitive to the laser's particular monochromatic radiation. The two most important laser lines are 6328Å (HeNe) and 6943Å (ruby); then, since most panchromatic materials have already passed through their maximum sensitivity at these lines, special sensitizers must be used. Because of the mechanical rigidity requirements of holography, the base used is usually a glass plate. Two readily available sources for holography are: Kodak 649F spectroscopic plates with a resolution >3000 lines/mm and the Agfa Gavaert line, which supplies a range of especially sensitized emulsions that allow exposures of a fraction of a second.

The medium used in the present experiment was the Agfa Gavaert plate 10-E-75 that is especially sensitized for the ruby line, 6943Å. A plot of its sensitivity is shown in Figure A-1.

The resolving power of emulsions can be explained in the following way. The distance on the hologram between a line of high density and one of

low density corresponds to the difference in path length between the reference beam and the object beam of $\lambda/2$.

If Φ is the angle between the reference beam and object beam when they are incident on the photographic plate, the distance between two dark lines is given by

$$d = \frac{\lambda}{2 \sin \Phi/2} \quad ,$$

where λ is the wavelength of the incident radiation. The results of this in terms of 1/d, i.e., in lines per millimeter, are given in Table A-II for $3 \text{ deg} \leq \Phi/2 \leq 50 \text{ deg}$.

As stated before, the photographic emulsion is an absorptive medium. When the material is exposed to light, developable centers are formed on the silver halide grains inside the gelatin emulsion. In the development process, silver grains are formed from these centers. The portion of the emulsion that receives more exposure will have more silver grains developed. After completion of the fixing process, which removes the unexposed sensitive silver halide in the emulsion, a negative black- and white-image remains. The development process can be considered as a posterior amplification of the inherent photosensitivity. The larger the grains, the greater the amplification but the lower the resolution. Holography usually requires high resolution and, hence, relatively low amplification.

Usually in conventional photography the exposure characteristics of the photographic emulsion are discussed in terms of a curve called the

Huerter-Driffield (H-D) curve, which is a plot of the optical density versus the common log of the exposure. A typical plot of the H-D curve is given in Figure A-2. In conventional photography this characteristic curve contains all the necessary information on its response to exposure. This curve is constructed by exposing the film to a stepped function of exposure and plotting the resulting densities against these steps. The densities are measured with a densitometer calibrated to read logarithm to base 10 of opacity or reciprocal transmittance. The linear portion of this H-D curve is often called the range for correct tone reproduction. Staying on the linear portion of this curve allows an interpretation of the effect of the photographed gamma on the holographic process. In Figure A-2, this gamma is the slope of the linear portion of this curve. For the case of Fresnel and Fraunhofer holography, gamma (γ) appears as a parameter affecting the contrast of the reconstructed image.

We note here that this gamma (γ) is the gamma described in equation (3.11) of Chapter III, Section 1. For a given material, the value of gamma can be controlled by changing the type of developer and the time of development. We point out here that all the holograms developed in the present experiment were carefully processed as follows:

Developer	D-19
Development time	5 min
Stop bath	0.5 min
Fixer	4 min

Wash	15 min
Photo-flow	0.5 min
Chemical temperature	68° F
Density	0.8

All photographs of the hologram image were processed just as carefully.

Characteristic curves contain much useful information in the case of certain holographic exposures; yet, still another curve exists that is quite useful. Recently the amplitude transmission curves have been preferred because where not the local density but the local amplitude transmission is the more important consideration. A typical plot of this amplitude transmission factor is plotted against energy in ergs/cm^2 for a 10-E-75 Agfa Gavaert plate. The amplitude transmission factor is defined as the ratio between the amplitudes of a monochromatic plane wave after and before passing through the photographic emulsion. Now the intensity transmission that was useful in the H-D curve is related to the transmission amplitude factor by

$$T = T_a T_a^* = |T_a|^2 \quad .$$

Therefore, since

$$T = (It)^{-\gamma} \quad ,$$

$$T_a = (It)^{-\gamma/2} \quad .$$

We refer to Figure A-3 and derive an expression used in equation (3.72a) in Chapter III, Section 3, that is used repeatedly in the theory:

$$T_a = T_o - k_f \mathcal{E} \ .$$

From the m formula for the slope of a straight line,

$$m = \tan \epsilon = \frac{y_2 - y_1}{x_2 - x_1} \ ,$$

and Figure A-3 we may write

$$\frac{k_f}{1} = \tan \epsilon = \frac{T_o - T_a}{\mathcal{E}}$$

as

$$k_f \mathcal{E} = T_o - T_a$$

or

$$T_a = T_o - k_f \mathcal{E} \ ,$$

where k_f is the slope of the linear region of the curve and is determined by the film type and development time.

A little more should be said concerning the reciprocity of an emulsion. For a density of, say 0.8, an exposure of approximately 20 to 50 ergs/cm^2 will suffice for non-Q-spoiled pulses. For a Q-spoiled pulse (in the nanosecond range), reciprocity losses are such that to achieve the density of 0.8, the energy density for the exposure must be multiplied by a factor of approximately 2 to 4. It is sufficient to say that very short nanosecond-type pulses are much less efficient in their ability to expose the grains of emulsions.

Figure A-4 presents a photograph of an actual hologram such as resulted from the experimental work done for this project.

TABLE A-I. PROPERTIES OF RECORDING MEDIA

Recording Medium	Typical Resolution (lines/mm)	Typical Exposure Required (ergs/cm^2)	Absorptive (A) or Phase Only (P)
Photographic Emulsions	>2000	20 - 10^3	A and P
Photochromic Materials	>2000	10^5 - 10^7	A
Photopolymer Materials	>1000	10^4 - 10^6	P
Thermo-Plastic Materials	>1000	10 - 100	P
Dichromate Sensitized Gelatin	>2000	10^5	P
Electrooptical Crystals	>4000	10^9	P

TABLE A-II. MINIMUM FILM RESOLUTION (lines/mm)

ANGLE	LASER EMISSION WAVELENGTH				
	3473 Å	4880 Å	5145 Å	6328 Å	6943 Å
2°	100	72	68	60	50
4°	201	143	136	120	101
6°	302	215	204	170	151
8°	400	285	270	220	200
10°	501	357	338	290	251
15°	746	531	503	409	373
20°	987	702	667	580	493
25°	1217	866	822	668	609
30°	1439	1024	972	790	720
40°	1851	1317	1250	1016	926
50°	2206	1570	1489	1210	1103

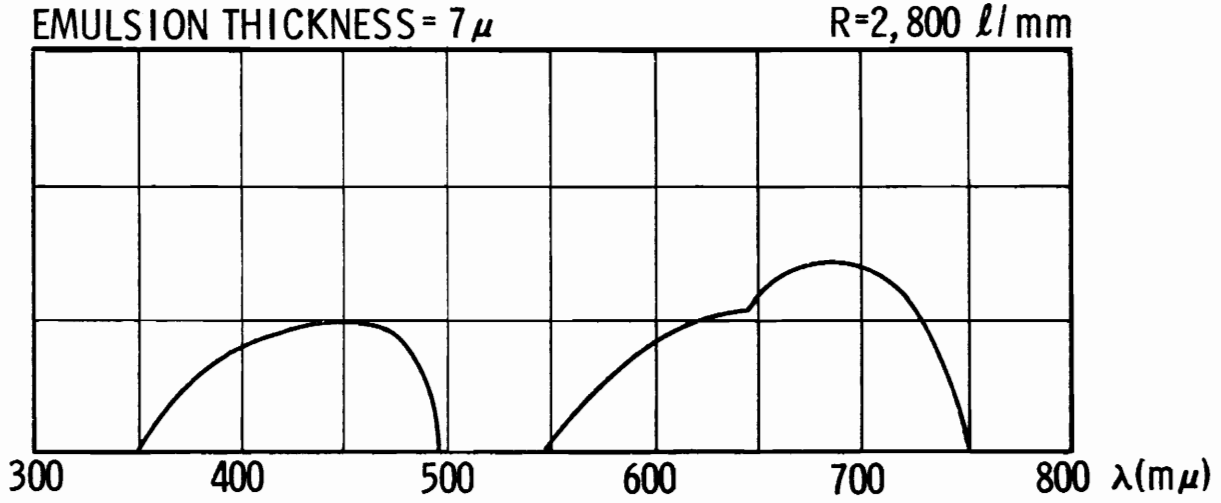

FIGURE A-1. SPECTROGRAM FOR ARTIFICIAL LIGHT (3,2000° K), SCIENTIA 10-E-75

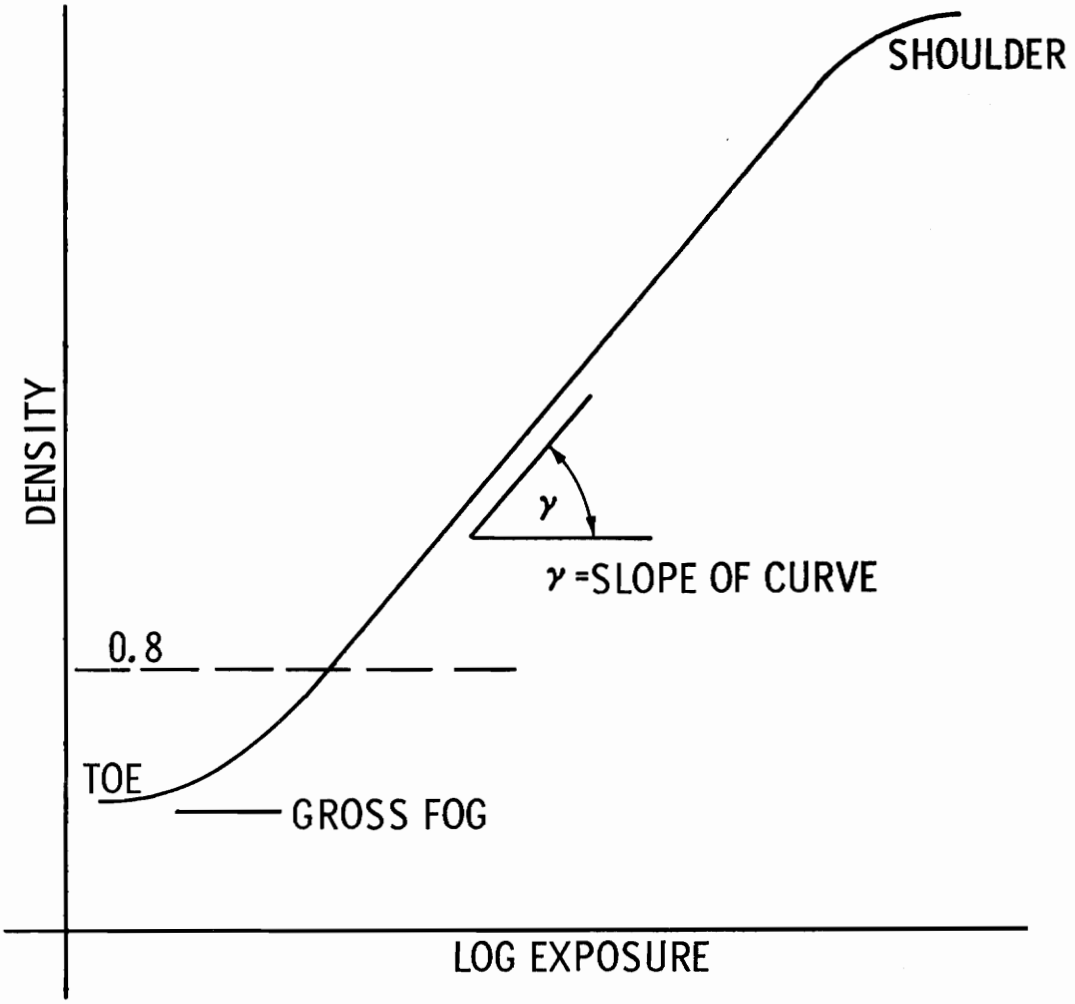

FIGURE A-2. CHARACTERISTIC CURVE

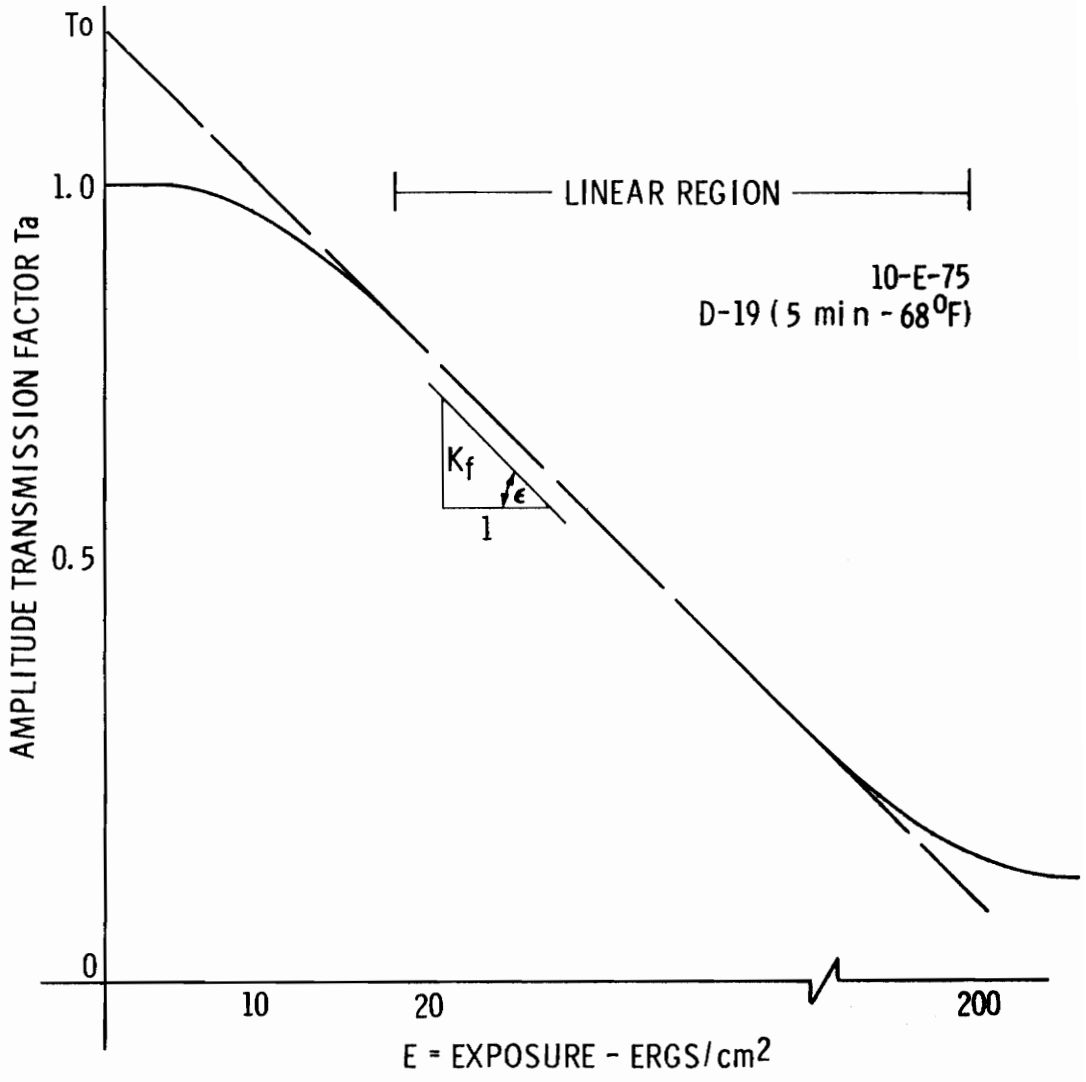

FIGURE A-3. 10-E-75 AMPLITUDE TRANSMISSION CURVE

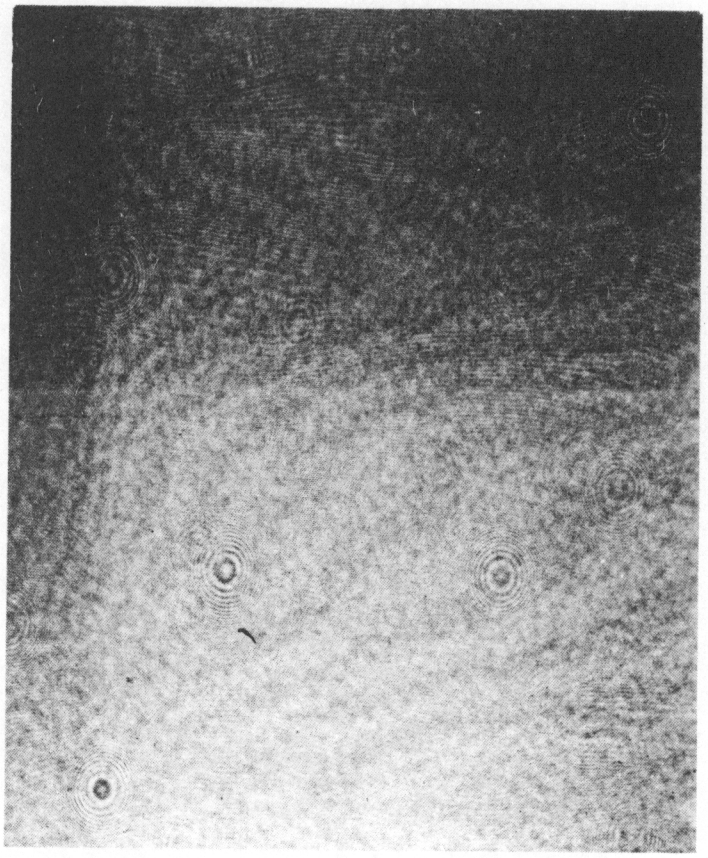

FIGURE A-4. PHOTOGRAPH OF HOLOGRAM

VITA

Robert L. Kurtz was born on May 21, 1933, in Rustburg, Virginia. He was graduated from E. C. Glass High School, Lynchburg, Virginia, in 1951. He attended Lynchburg College, Lynchburg, Virginia, from 1956 through 1960, where he graduated cum laude with a B.S. degree in physics. In June, 1960, he accepted a position with the United States Civil Service, and worked with the Army Ballistics Missile Agency, Huntsville, Alabama, and the Naval Research Laboratory, Washington, D. C. For the past eight years he has been associated with the National Aeronautics and Space Administration, George C. Marshall Space Flight Center, Huntsville.

He received the Master of Science degree from the Virginia Polytechnic Institute in 1968 and fulfilled requirements for the Doctor of Philosophy degree at Virginia Polytechnic Institute and State University while on leave from NASA from January, 1967, to September, 1970.

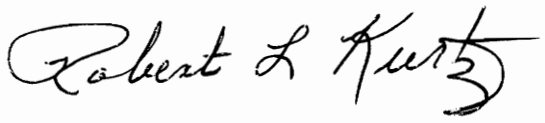

A HOLOGRAPHIC SYSTEM THAT RECORDS FRONT-SURFACE DETAIL OF A SCENE MOVING AT HIGH VELOCITY

By Robert L. Kurtz

ABSTRACT

It is known that any motion of the scene during the exposure of a hologram results in a spatial modulation of the recorded fringe contrast. On reconstruction this produces a spatial amplitude modulation of the reconstructed wavefront that tends to blur out the image. This paper discusses a novel holographic technique that uses an elliptical orientation for the holographic arrangement. It is shown that the degree of image degradation is not only a function of exposure time but also of the system used. The form of the functional system dependence is given, as well as the results of several systems tested, which verify this dependence. It is further demonstrated that the velocity of the target or the exposure time alone is inconsequential by itself and the important parameter is the total motion of the target $\Delta X = VT$. Using the resolution of front-surface detail from a target with a velocity of 17,546 cm/sec, we are able to predict an upper limit on target velocity for resolution of front-surface detail for a given system.